INFORMATION TO USERS

This dissertation was produced from a microfilm copy of the original document. While the most advanced technological means to photograph and reproduce this document have been used, the quality is heavily dependent upon the quality of the original submitted.

The following explanation of techniques is provided to help you understand markings or patterns which may appear on this reproduction.

1. The sign or "target" for pages apparently lacking from the document photographed is "Missing Page(s)". If it was possible to obtain the missing page(s) or section, they are spliced into the film along with adjacent pages. This may have necessitated cutting thru an image and duplicating adjacent pages to insure you complete continuity.

2. When an image on the film is obliterated with a large round black mark, it is an indication that the photographer suspected that the copy may have moved during exposure and thus cause a blurred image. You will find a good image of the page in the adjacent frame.

3. When a map, drawing or chart, etc., was part of the material being photographed the photographer followed a definite method in "sectioning" the material. It is customary to begin photoing at the upper left hand corner of a large sheet and to continue photoing from left to right in equal sections with a small overlap. If necessary, sectioning is continued again — beginning below the first row and continuing on until complete.

4. The majority of users indicate that the textual content is of greatest value, however, a somewhat higher quality reproduction could be made from "photographs" if essential to the understanding of the dissertation. Silver prints of "photographs" may be ordered at additional charge by writing the Order Department, giving the catalog number, title, author and specific pages you wish reproduced.

University Microfilms

300 North Zeeb Road
Ann Arbor, Michigan 48106

A Xerox Education Company

73-6815

DAVIDSON, Jr., John Albert, 1944-
$\bar{P}P$ ANNIHILATIONS INTO FOUR CHARGED MESONS AT 1.6 TO 2.2 GEV/C.

The University of Michigan, Ph.D., 1972
Physics, high energy

University Microfilms, A XEROX Company, Ann Arbor, Michigan

$\bar{P}P$ ANNIHILATIONS INTO FOUR CHARGED MESONS AT 1.6 TO 2.2 GEV/C

by

John Albert Davidson, Jr.

A dissertation submitted in partial fulfillment
of the requirements for the degree of
Doctor of Philosophy
(Physics)
in The University of Michigan
1972

Doctoral Committee:

Professor Jay Wehrley Chapman, Chairman
Professor Guenther H. Elste
Professor Oliver E. Overseth
Professor Byron P. Roe
Professor Marc H. Ross

PLEASE NOTE:

Some pages may have

indistinct print.

Filmed as received.

University Microfilms, A Xerox Education Company

ACKNOWLEDGEMENTS

The author is indebted to a host of people who have contributed much to his growth and development in general, and this research effort in particular. It is possible to mention but a few:

Professor Jay W. Chapman for showing what can be accomplished with enthusiasm and determination, for serving as my committee chairman and providing willing assistance when needed, and for giving me the freedom to pursue the larger questions.

Professor Byron P. Roe for serving on my doctoral committee and for his helpful suggestions and comments on the physics of the analysis.

Professor Marc Ross for serving on my doctoral committee and for contributing to the development of my weltanschauung.

Professor Oliver E. Overseth for serving on my doctoral committee and for his willingness to be helpful when possible.

Professor Guenther H. Elste for serving on my doctoral committee.

Dr J. Lys for his patient and cogent comments concerning the analysis of the experiment and for reading the initial manuscript.

Dr. R. Green for entensive collaboration throughout the experiment, for his efforts in writing SHERLOCK, and for being a friend.

Dr. H. Ring for his confidence at a critical point.

My colleagues M. Church, R. Kiang, J. Koschik, K. Bartley, C. Arnold, and J. Cooper for their generous help.

The scanning, programming, and technical staff, including J. Allen, L. Dintsch, B. Eby, J. Fisch, L. Peterson, I. Russo, and V. French.

The Bubble Chamber Group, specifically Professor D. Sinclair as Director of the Group, and Professor J. Vander Velde as proposer of the $\bar{p}p$ experiment.

Dr. K. Rao, D. Baycura, and B. Matteson for their needed support when the going got rough.

My parents for their encouragement and perseverance.

TABLE OF CONTENTS

ACKNOWLEDGEMENTS ii

LIST OF TABLES vi

LIST OF FIGURES vii

Chapter

I. THE EXPERIMENT 1

1.1 Introduction 1

1.2 The Beam 3

1.3 The Four Prong Event Measurement . . 3

1.4 Event Reconstruction and Fitting . . 4

1.5 Four prong Topological Cross Sections . 5

II. THE REACTION $\bar{p}p \rightarrow \pi^-\pi^-\pi^+\pi^+$ 11

2.1 Introduction 11

2.2 Reaction Cross Sections 13

2.3 Mass Distributions 16

2.4 Resonance Production 45

2.5 Angular Distributions 58

2.6 Spin Density Matrix Elements . . . 62

2.7 Rho-Omega Interference 100

III. THE REACTION $\bar{p}p \rightarrow \pi^-\pi^+K^-K^+$ 108

3.1 Introduction 108

3.2 Cross Sections for $2\pi 2K$ 111

3.3 Mass Distributions 111

3.4 Sub-Channel Percentages 124

3.5 Angular Distributions 131

IV. THE REACTION $\bar{p}p \rightarrow K^-K^-K^+K^+$ 138

4.1 Introduction 138

4.2 Reaction Cross Section 138

4.3 Mass Distributions 140

4.4 Angular Distributions 140

V. SUMMARY 146

LIST OF REFERENCES 149

LIST OF TABLES

Table		Page
1.5-1	Four prong topological cross sections for this experiment	8
1.5-2	Four prong topological cross sections from earlier experiments	9
2.2-1	Four pion cross sections for this experiment .	17
2.2-2	Four pion cross sections from earlier experiments	18
2.4-1	Results of maximum likelihood fits to all 4π events using hypotheses (1) thru (9) . . .	51
2.4-2	The χ^2 values from Monte Carlo distributions for hypotheses (1) thru (9).	53
2.4-3	Results of maximum likelihood fits for various momenta sets	54
2.4-4	Results of maximum likelihood fits and χ^2 values with the inclusion of the Goldhaber parameter	56
2.4-5	Comparison of maximum likelihood fits with previous experiments	57
2.6-1	Results of (S,P) wave fits for the $\pi^+\pi^-$ matrix elements in the Gottfried-Jackson and Helicity frames for various mass cuts	65
2.6-2	The χ^2 values for (S,P) wave fits . . .	66
2.6-3	The β and γ parameters and χ^2 values for (S,P,D) wave fits to the f mass region . .	99
2.7-1	The χ^2 values for least square fits for ρ-ω interference using the formulation by S. Flatté	104
3.2-1	The $\pi^-\pi^+K^-K^+$ cross sections	112
3.4-1	Results of maximum likelihood fitting in percent of $2\pi 2K$ cross section for various momenta sets .	126
3.4-2	Results of maximum likelihood fits to all $2\pi 2K$ events using hypotheses (a) thru (f) . . .	127
3.4-3	The χ^2 values for Momte Carlo generated distributions for fits (a) thru (f) . . .	129

LIST OF FIGURES

Figure		page
1.5-1	Four prong topological cross sections . .	10
2.1-1	Confidence level distribution for 4π events .	12
2.1-2	Confidence level(4π) versus CL(5π). . .	14
2.1-3	Confidence level(4π) versus CL(5π) expanded .	15
2.2-1	Four pion cross sections as a function of $\bar{p}$ momentum	19
2.3-1	The $\pi^{\mp}\pi^{\mp}$ mass distribution	20
2.3-2	The $\pi^{+}\pi^{-}$ mass distribution	21
2.3-3	The $\pi^{+}\pi^{-}\pi^{\mp}$ mass distribution	22
2.3-4	The $\pi^{+}\pi^{-}$ mass distribution when the recoil $\pi^{+}\pi^{-}$ is in the ρ mass range	23
2.3-5	The $\pi^{+}\pi^{-}$ mass distribution when the recoil $\pi^{+}\pi^{-}$ is in the f mass range	24
2.3-6	The $\rho^{\circ}\pi^{\mp}$ mass distribution	25
2.3-7	The $\pi^{+}\pi^{-}$ mass spectrum for 1.63 and 1.77 GeV/c momenta sets	27
2.3-8	The $\pi^{\mp}\pi^{\mp}$ mass spectrum for 1.83 and 1.88 GeV/c	28
2.3-9	The $\pi^{\mp}\pi^{\mp}$ mass spectrum for 1.95 and 2.20 GeV/c	29
2.3-10	The $\pi^{+}\pi^{-}$ mass spectrum for 1.63 and 1.77 GeV/c momenta sets	30
2.3-11	The $\pi^{+}\pi^{-}$ mass spectrum for 1.83 and 1.88 GeV/c	31
2.3-12	The $\pi^{+}\pi^{-}$ mass spectrum for 1.95 and 2.20 GeV/c	32
2.3-13	The $\pi^{+}\pi^{-}\pi^{\mp}$ spectrum for 1.63 and 1.77 GeV/c .	33
2.3-14	The $\pi^{+}\pi^{-}\pi^{\mp}$ spectrum for 1.83 and 1.88 GeV/c .	34
2.3-15	The $\pi^{+}\pi^{-}\pi^{\mp}$ spectrum for 1.95 and 2.20 GeV/c .	35
2.3-16	The $\pi^{+}\pi^{-}$ spectrum with recoil ρ meson for the 1.63 and 1.77 GeV/c momenta sets . .	36

LIST OF FIGURES (CONTINUED)

Figure		Page
2.3-17	The $\pi^+\pi^-$ mass spectrum with recoil ρ meson for 1.83 and 1.88 GeV/c	37
2.3-18	The $\pi^+\pi^-$ mass spectrum with recoil ρ meson for 1.95 and 2.20 GeV/c	38
2.3-19	The $\pi^+\pi^-$ mass spectrum with recoil f meson for 1.63 and 1.77 GeV/c	39
2.3-20	The $\pi^+\pi^-$ mass spectrum with recoil f meson for 1.83 and 1.88 GeV/c	40
2.3-21	The $\pi^+\pi^-$ mass spectrum with recoil f meson for 1.95 and 2.20 GeV/c	41
2.3-22	The $\rho^\circ\pi^\mp$ mass spectrum for 1.63 and 1.77 GeV/c momenta sets	42
2.3-23	The $\rho^\circ\pi^\mp$ mass spectrum for 1.83 and 1.88 GeV/c	43
2.3-24	The $\rho^\circ\pi^\mp$ mass spectrum for 1.95 and 2.20 GeV/c	44
2.5-1	The angular distribution of pions in the Center of Momentum frame	59
2.5-2	The Forward-Backward ratio versus pion momentum in the CM	60
2.5-3	The Polar-Equatorial ratio versus pion momentum in the CM	61
2.6-1	The $\cos(\theta)$ spectrum in GJ frame for $\pi^+\pi^-$ mass <668 MeV	67
2.6-2	The φ spectrum in the GJ frame with $\pi^+\pi^-$ mass <668 MeV	68
2.6-3	The $\cos(\theta)$ spectrum in GJ frame with $\pi^+\pi^-$ mass in ρ region	69
2.6-4	The φ spectrum in the GJ frame with $\pi^+\pi^-$ mass in ρ region	70
2.6-5	The $\cos(\theta)$ spectrum in GJ frame with $\pi^+\pi^-$ mass between 810 and 1154 MeV	71
2.6-6	The φ spectrum in the GJ frame with $\pi^+\pi^-$ mass between 810 and 1154 MeV	72

LIST OF FIGURES (CONTINUED)

Figure		page
2.6-7	The $\cos(\theta)$ spectrum in GJ frame with $\pi^+\pi^-$ mass in the f region	73
2.6-8	The φ spectrum in GJ frame with the $\pi^+\pi^-$ mass in the f region	74
2.6-9	The $\cos(\theta)$ spectrum in GJ frame with $\pi^+\pi^-$ mass > 1332 MeV	75
2.6-10	The φ spectrum in GJ frame with the $\pi^+\pi^-$ mass > 1332 MeV	76
2.6-11	The $\cos(\theta)$ spectrum in the Helicity frame with the $\pi^+\pi^-$ mass < 668 MeV	77
2.6-12	The φ spectrum in Helicity frame with $\pi^+\pi^-$ mass < 668 MeV	78
2.6-13	The $\cos(\theta)$ spectrum in Helicity frame with $\pi^+\pi^-$ mass in ρ region	79
2.6-14	The φ spectrum in Helicity frame with $\pi^+\pi^-$ mass in ρ region	80
2.6-15	The $\cos(\theta)$ spectrum in Helicity frame with $\pi^+\pi^-$ mass between 810 and 1154 MeV	81
2.6-16	The φ spectrum in Helicity frame with $\pi^+\pi^-$ mass between 810 and 1154 MeV	82
2.6-17	The $\cos(\theta)$ spectrum in Helicity frame with $\pi^+\pi^-$ mass in f region	83
2.6-18	The φ spectrum in Helicity frame with $\pi^+\pi^-$ mass in f region	84
2.6-19	The $\cos(\theta)$ spectrum in Helicity frame with $\pi^+\pi^-$ mass > 1332 MeV	85
2.6-20	The φ spectrum in Helicity frame with $\pi^+\pi^-$ mass > 1332 MeV	86
2.6-21	The $(\rho_{00}-\rho_{11})$ parameter as a function of $\pi^+\pi^-$ mass in GJ and Helicity frames	87
2.6-22	$\mathrm{Re}(\rho_{10})$ versus $\pi^+\pi^-$ mass in GJ and Helicity frames	88
2.6-23	The ρ_{1-1} parameter versus $\pi^+\pi^-$ mass in GJ and Helicity frames	89

LIST OF FIGURES (CONTINUED)

Figure		Page
2.6-24	$Re(\rho_{00}^{int})$ versus $\pi^+\pi^-$ mass in GJ and Helicity frames	90
2.6-25	The $Re(\rho_{10}^{int})$ parameter versus $\pi^+\pi^-$ mass in GJ and Helicity frames	91
2.6-26	The $(\rho_{00}-\rho_{11})$ parameter in the ρ mass region versus the negative of the squared momentum transfer (-t)	93
2.6-27	$Re(\rho_{10})$ in the ρ mass region versus (-t)	94
2.6-28	The ρ_{1-1} parameter in the ρ mass region versus (-t)	95
2.6-29	$Re(\rho_{00}^{int})$ in the ρ mass region versus (-t)	96
2.6-30	$Re(\rho_{10}^{int})$ in the ρ mass region versus (-t)	97
2.7-1	The $\pi^+\pi^-$ mass spectrum with fits (a) and (b) to ρ-ω interference	102
2.7-2	The subset of the $\pi^+\pi^-$ mass spectrum having (-t) between 0.2 and 0.3 $(GeV/c)^2$ with ρ-ω interference fits (a) and (d)	107
3.1-1	Confidence level distribution for $2\pi 2K$ events	110
3.2-1	The $\pi^-\pi^+K^-K^+$ cross section versus $\bar{p}$ momentum	113
3.3-1	The $\pi^{\mp}K^{\mp}$ mass spectrum	115
3.3-2	The $\pi^-\pi^+$ mass spectrum for the $2\pi 2K$ final state	116
3.3-3	The $\pi^{\mp}K^{\pm}$ mass spectrum	117
3.3-4	The K^-K^+ mass spectrum	118
3.3-5	The $\pi^-\pi^+K^{\mp}$ mass spectrum	119
3.3-6	The $\pi^{\mp}K^-K^+$ mass spectrum	120
3.3-7	The $\pi^{\mp}K^{\mp}$ mass spectrum with recoil πK in the K^* region	121
3.3-8	The $\pi^-\pi^+K^{\mp}$ mass spectrum with Breit-Wigner fit	122

LIST OF FIGURES (CONCLUDED)

Figure		Page
3.5-1	The cos(θ) distribution of $\pi^{\mp}$ from the $2\pi 2K$ final state in CM frame	132
3.5-2	The cos(θ) distribution of $K^{\mp}$ from the $2\pi 2K$ final state in the CM frame	133
3.5-3	The cos(θ) distribution of $\pi^{-}K^{-}$ combinations for $2\pi 2K$ final state in CM frame	134
3.5-4	The cos(θ) distribution of $\pi^{-}K^{+}$ combinations for $2\pi 2K$ final state in CM frame	135
3.5-5	The cos(θ) distribution of $\pi^{+}\pi^{-}$ combinations for the $2\pi 2K$ final state in the CM frame . .	136
4.1-1	The confidence level distribution for the $K^{-}K^{-}K^{+}K^{+}$ events	139
4.3-1	The $K^{\mp}K^{\mp}$ mass spectrum for 4K events . . .	141
4.3-2	The $K^{+}K^{-}$ mass spectrum for 4K events . . .	142
4.3-3	The $K^{-}K^{+}K^{\mp}$ mass spectrum for 4K events . . .	143
4.4-1	The cos(θ) distribution of $K^{\mp}$ in CM frame . .	144
4.4-2	The cos(θ) distribution of $K^{+}K^{+}$ combinations in CM frame	145

Chapter I

THE EXPERIMENT

1.1 Introduction

Ever since the discovery of antiprotons by Chamberlain, Segrè, Wiegand, and Ypsilantis in 1955, $\bar{p}p$ interactions have been used to study the properties of elementary particles. Much effort has been expended in an attempt to understand $\bar{p}p$ annihilations into mesons. Most of this experimental work has been done with hydrogen bubble chambers.

The film used in this experiment was taken in the Argonne National Laboratory 30-inch MURA hydrogen bubble chamber. A total of approximately 150,000 exposures were made at six antiproton beam momenta(total invariant mass): 1.63(2300), 1.77(2349), 1.83(2371), 1.88(2388), 1.95(2413), and 2.20 GeV/c (2500 MeV).

Several earlier studies have been made with this film. Large-angle elastic scattering having momentum transfer squared greater than $|t| = 0.3(\text{GeV/c})^2$ was the first reaction to be analyzed(J. Lys, et al.,1968; D. Falconer, 1969). Another experiment measured the cross sections for the reaction $\bar{p}p \rightarrow \pi^-\pi^+$ and K^-K^+(J. Chapman, et al., 1968). A third study of annihilations into K_1 mesons has also been completed(H. Ring, 1970).

The data for this experiment comes from a fourth scan in which four-prong events were measured. A four-prong is an event that has four fast visible tracks leaving the $\bar{p}p$ interaction point. It includes by necessity, 2-prong Vee

events in which the Vee is located very close to the origin, as well as 2-prong e^-e^+ events having a fast e^-e^+ pair. An important motivation for this experiment was the continuing search to find the channels that produce enhancements in the total $\bar{p}p$ cross section. These are seen at 2345 MeV and 2380 MeV with a width of 140 MeV(R. Abrams, et al., 1967). A CERN missing mass experiment also saw enhancements at 2200 and 2380 MeV (G. Chikovani, et al., 1966).

From our sample of four prongs, events which fit the reaction $\bar{p}p \rightarrow \pi^-\pi^-\pi^+\pi^+\pi^\circ$ have been investigated (R. Green, 1972). This report concerns the events which fit the following four-constraint reactions:

$$\bar{p}p \rightarrow \pi^-\pi^-\pi^+\pi^+,$$
$$\bar{p}p \rightarrow \pi^-\pi^+K^-K^+,$$
$$\bar{p}p \rightarrow K^-K^-K^+K^+.$$

Cross sections are determined. Mass distributions and resonance production are examined and compared to earlier experiments. The maximum-likelihood method is used to find the percentages of the quasi two and three body states. Fits are done to determine the spin-density matrix elements for the ρ and f mesons in both the Gottfried-Jackson and the Helicity frames. In the four pion channel ρ-ω interference is observed. A study is done to determine the parameters which characterize this interference.

1.2 The Beam

The antiprotons were produced by targeting the internal proton beam of the Zero-Gradient Synchrotron onto a movable copper target. The Argonne seven-degree beam selected and transported the antiprotons with the desired momentum to the bubble chamber. Since the details of the beam transport system have been described in earlier reports (D. Falconer, 1969; H. Ring, 1970) only a general description will be given. The beam was approximately 490 feet long; it had four bending magnets and two separators along with the appropriate mass slits, collimators and quadrupole pairs to define and focus the particles.

The length of the beam as well as its two stages of separation reduced the contamination of other particles to a low level. An estimate of the contamination has been made by measuring the length of delta rays produced by a sample of beam tracks.* It indicated that the pion contamination was $0.4 \pm 0.3\%$. The maximum spread in beam momentum $\Delta P/P$ was 1.4%.

1.3 The Four-Prong Event Measurement

The film was scanned and measured in one pass. Film plane measuring machines were used to digitize the events. All scanned events** having nominal beam tracks visible in at least three views were measured. The machines were linked directly

---

* This study was done by R. Kiang and J. Lys.

**Accurate momentum measurement was obtained by insisting all tracks be > 3 cm; the measuring machines had a linear magnification ~1.9 over chamber size.

to a Computer Control Company DDP-24.* A magnetic tape was generated which had the track coordinates along with the necessary bookkeeping information. This output was next processed through SCANAL# followed by TPGEN. These programs produced an appropriately formatted tape for input to the geometry program, as well as a list of events and detailed accounting information.

1.4 Event Reconstruction and Fitting

TVGP (Three-View Geometry Program)** was used to reconstruct the events in space, i.e. the (x,y,z) location of a track was found from (x',y') measurements in three views. Fits were done for each of the outgoing tracks assuming that it had either a pion, kaon or proton mass. For each mass hypothesis the momentum, azimuth, dip and their errors were calculated.

This information was used by SQUAW to fit the final states consistent with the known conservation laws. Each track was given a particular mass interpretation. SQUAW then determined if it were possible to conserve four-momentum within the errors in the reconstructed quantities. The goodness of the fit was indicated by a χ^2 which was also computed by SQUAW.

---

*This system was the result of the efforts of J. Chapman.

#SCANAL was written by J. Koschik.

**The programs TVGP and SQUAW are described elsewhere(T. Day, 1967; D. Falconer, 1969). They were were written by T. Day and and others at Berkeley and introduced at Michigan by J. Chapman.

Programs were run on the SQUAW output tapes to condense and format the data into a more useable form. Tapes were written for each momentum set. Duplicates were removed by checking for events having the same roll, frame and vertex. Finally, tapes were written to separate the various channels for further analysis. A total of 49,732 events had been processed and of this number 46,423 were successfully reconstructed and fitted.

1.5 Four-Prong Topological Cross Sections

The topological cross section was calculated from the total $\bar{p}p$ cross section (R. Abrams, et al., 1967), the density of the hydrogen (D. Falconer, 1969), the beam track length through the chamber, and the number of four prongs at each momentum set. The number of protons per cm^3 used in the calculation was:

$$\rho = (2 \text{ targets/molecule}) \cdot (6.0225 \cdot 10^{23} \text{ molecules/mole}) \cdot (1 \text{ mole}/2.016 \text{ grams}) \cdot (0.0622 \pm 0.0004 \text{ grams/cm}^3)$$
$$= 3.716 \pm 0.024 \cdot 10^{22} \text{ protons/cm}^3.$$

The shape of the MURA chamber is a right cylinder 38 cm high with a radius of 38 cm. The area of the chamber illuminated by flash rings is roughly circular with a minimum radius of 29.5 cm. In order to reduce the errors introduced by events near the boundary of the visible region, the fiducial volume for the four prong cross section determination was fixed to be a right cylinder with a radius of 28.0 cm.

The average track length through the fiducial volume was determined by using the measured events. It was assumed those events represented an unbiased sample of all the beam tracks.* From the coordinates of the event, the radius of the beam in the chamber's magnetic field, and its slope at the interaction point, the geometrical path length and the standard error in the mean were calculated for all the measured events at each momentum set.

Two rolls of film (each having approximately 1200 frames and 14,000 beam tracks) were selected at each of the momentum sets. They were independently scanned; a list was made of the four prong events and their quadrant locations. All disagreements between the scan and the events that had been initially measured were resolved by a final scan of the film.

Using a random-miss model (D. Falconer, 1969) the double-scan efficiency for each roll was found. The efficiencies ranged from 0.9976 to 0.9999 with an average of 0.9990. These values were used to correct for missed events.

The topological cross section for each roll was determined by the following formula:

$$\sigma = \frac{\sigma' \cdot N}{E \cdot T \cdot F \cdot (1 - \exp\{-\sigma' \rho L\})}$$

where,

σ' = $\bar{p}p$ total cross section

N = number of four prong events,

T = average number of tracks/frame (H. Ring, 1970),

F = number of frames,

*The tracks were weighted to remove the bias which favors longer path lengths.

ρ = protons/cm^3,

L = average path length

E = double scan efficiency.

The dependence on σ' is minimal; expanding the exponential, σ is approximately equal to $N/(E \cdot T \cdot F \cdot \rho \cdot L)$. In principle of course σ' is not needed. The results are presented in Table 1.5-1. These values as well as the cross sections from previous experiments are shown in Figure 1.5-1. The values from earlier experiments are also listed in Table 1.5-2.

Table 1.5-1. Topological cross sections σ(4-prong) calculated for the six momentum sets. P = incident $\bar{p}$ momentum; N = number of four prongs scanned; σ' = $\bar{p}p$ total cross section; L = average path length.

P (GeV/c)	N	σ' (mb)	L (cm)	σ(4-prong)* (mb)
1.63	1382	97.57±0.07	52.56±0.06	29.8±0.8
1.77	1491	95.32±0.07	52.99±0.05	27.1±0.7
1.83	1282	94.14±0.07	53.15±0.05	27.4±0.8
1.88	1393	92.75±0.07	53.49±0.04	25.8±0.7
1.95	1441	91.36±0.07	53.45±0.05	25.5±0.7
2.20	1333	86.31±0.07	53.77±0.04	23.1±0.6

*The errors are statistical only. There is also a systematic error of 0.5% due to the systematic error in σ'.

Table 1.5-2. Four prong topological cross sections from previous experiments.

Reference	$\bar{p}$ Momentum (GeV/c)	σ(4 prong) (mb)	
(Kalbfleish, G., et al., 1969)	1.11	32.6	±0.5
	1.33	31.0	±0.2
	1.52	28.8	±0.3
(Donald, R., et al., 1968)	1.20	31.6	±1.0
(Cooper, W., et al., 1968)	1.23	31.2	±0.8
	1.27	30.0	±1.0
	1.32	29.4	±0.6
	1.37	28.9	±0.8
	1.43	30.1	±0.7
	1.49	27.7	±1.0
	1.54	28.0	±0.5
	1.63	27.7	±1.0
(Parker, D., 1971)	1.51	27.8	±0.4
	1.65	26.8	±0.4
	1.80	25.8	±0.4
	1.95	24.7	±0.4
	2.15	24.9	±0.7
	2.45	23.2	±0.6
	2.60	22.7	±0.7
	2.75	22.0	±0.7
	2.90	21.8	±0.7
(Button, J., et al., 1962)	1.61	25.0	±2.2
(Ferbel, T., et al., 1966)	3.28	22.9	±0.9
	3.66	21.6	±0.9
(Bockman, K., et al., 1966)	5.7	18.2	±0.4
(Alles-Borelli, V., et al., 1967)	5.7	17.3	±0.7
(Kitagaki, T., et al., 1968)	6.9	18.7	±1.0
(Ferbel, T., et al., 1968)	6.94	16.6	±1.5
(Borecka, I., et al., 1971)	12.0	15.8	±0.7

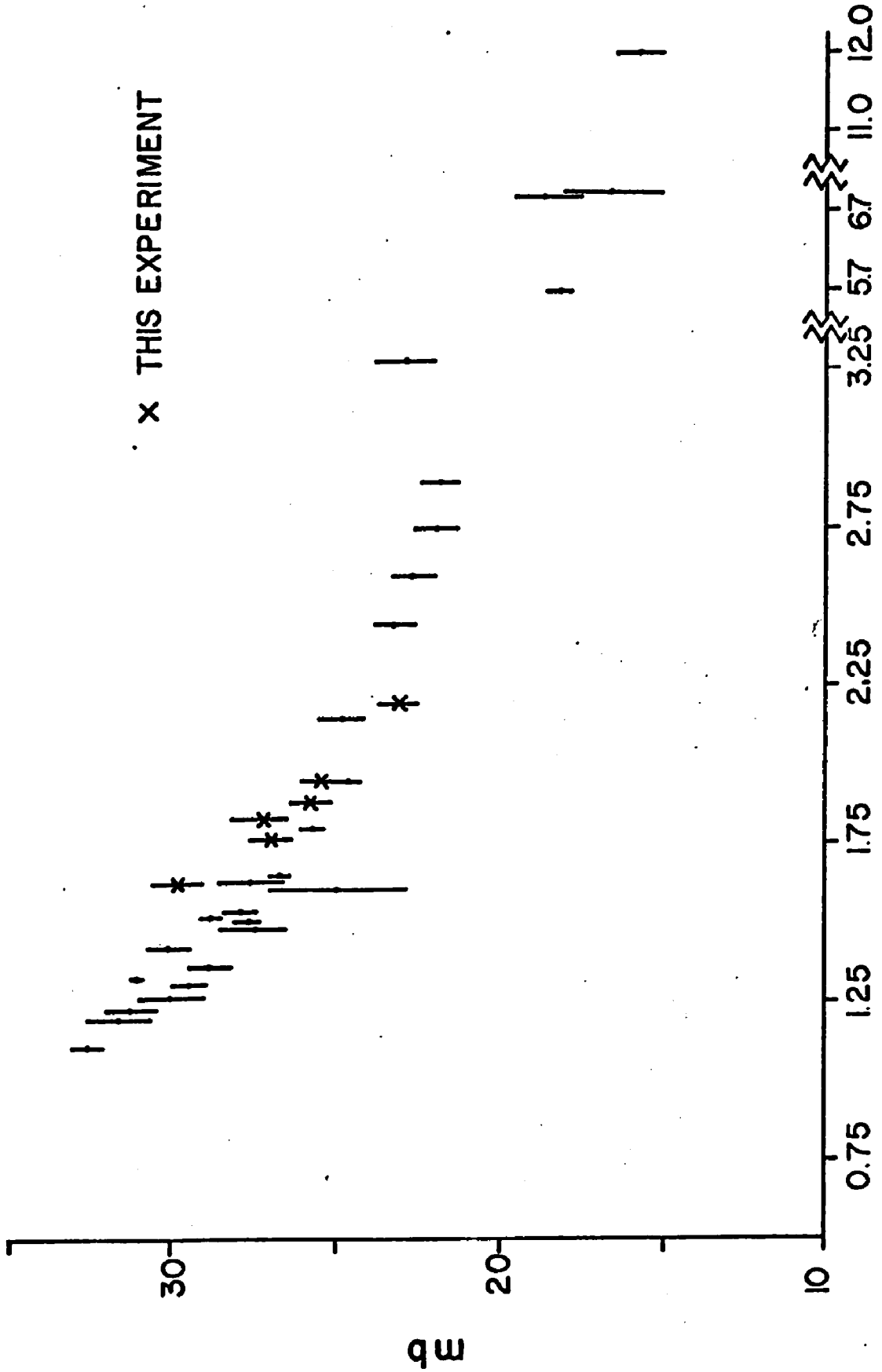


Figure 1.5-1. The four-prong topological cross section as a function of $\bar{p}$ momentum.

Chapter II

THE REACTION $\bar{p}p \rightarrow \pi^-\pi^-\pi^+\pi^+$

2.1 Introduction

The $\bar{p}p$ annihilation into four charged pions has been the subject of many previous studies.* These investigations, as well as this report, find properties in the four pion channel which do not change radically as the $\bar{p}$ momentum changes from 0.9 to 5.7 GeV/c. The cross section σ decreases from the order of 4 mb at 1.0 GeV/c $\bar{p}$ momentum to 0.8 mb at 5.7 GeV/c. Both the ρ and the f mesons are very noticeably produced. Quasi two and three body resonance production accounts for a large part of the channel. Nonresonant phase space production is significantly less important. Angular distributions show a marked asymmetry which increases with increasing beam momentum. An effect which we call "charge inertia" is observed in the center of momentum (CM) frame wherein pions prefer to follow the direction of the nucleon of like charge. Finally, ρ-ω interference has been observed both in this experiment and in a study from 1.26 to 1.65 GeV/c (W. Allison, et al., 1970).

From the 46,423 four prong events a total of 3,821 fitted the four pion final state with two or more constraints. The confidence level (CL) distribution of these events is shown in Figure 2.1-1. Ideally, this distribution should be flat.

*See, for instance, at 0.94 GeV/c(R. Burns, et al., 1971); at 1.2 GeV/c (R. Donald, et al., 1968); at 3.7 GeV/c (T. Ferbel, et al., 1966), and at 5.7 GeV/c (A. Accensi, et al., 1966).

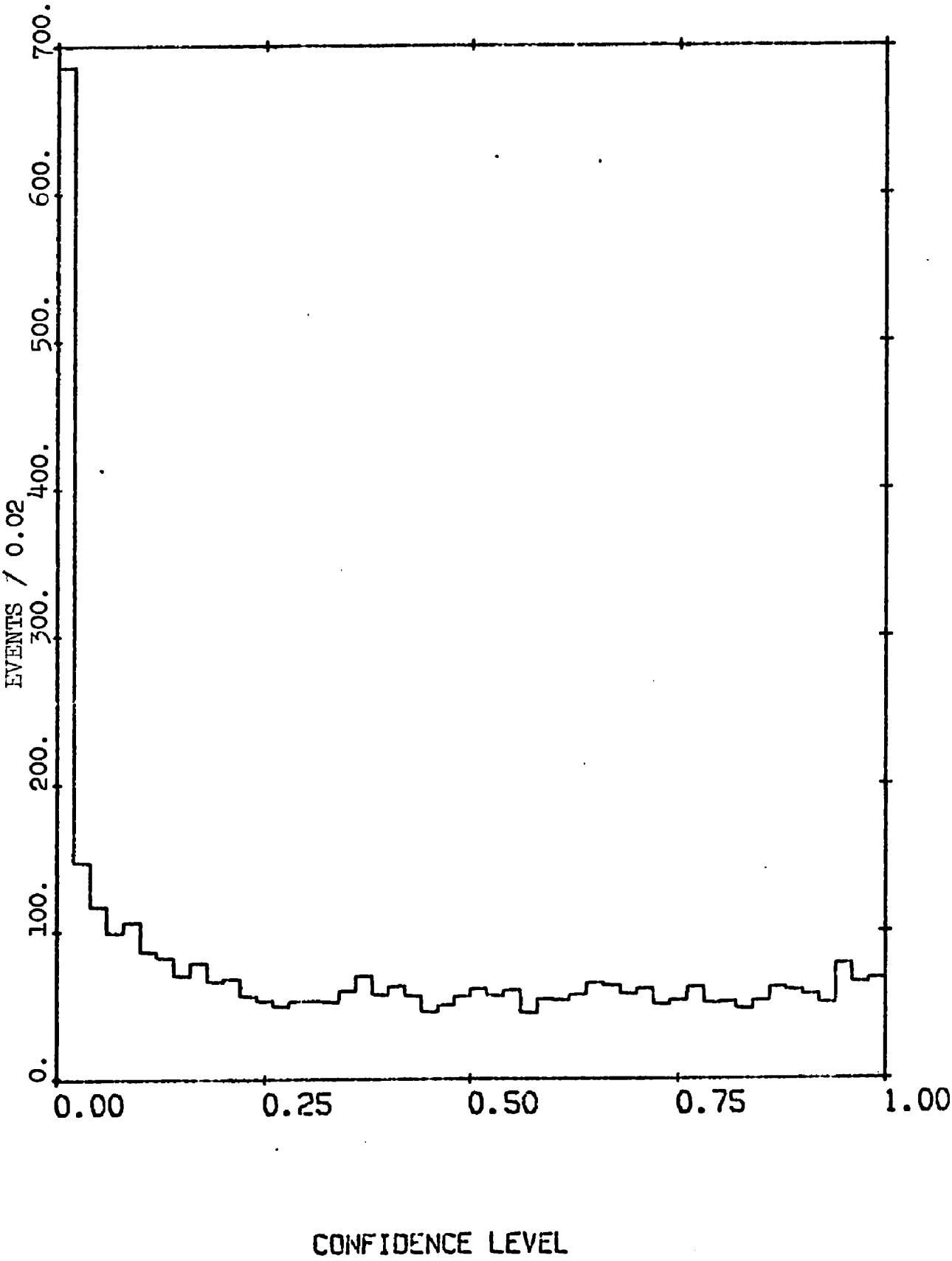


Figure 2.1-1. Confidence level distribution of four pion events with number of constraints ≥ 2.

However, the spectrum is highly peaked at very low CL. This is a reflection of two factors. First, errors due to measuring are non-gaussian; they have long tails. This leads to an excess of events at low CL. Secondly, the contamination from other channels is expected to be more important at low CL. For the 686 events with CL(4π) between 0.00 and 0.02, 126 events were ambiguous with $\pi^-\pi^+K^-K^+$. Only four events were resolved by bubble density (see Chapter III) to be $2\pi 2K$; nine events remained ambiguous. The $\pi^-\pi^+\pi^\circ K^-K^+$ ($K^-K^-K^+K^+$) channel had 26 (5) fits ambiguous with 4π. None of these were consistent with bubble density. For an estimate of the contamination due to $\pi^-\pi^-\pi^+\pi^+\pi^\circ$, we made a scatterplot of CL(4π) versus CL(5π), Figures 2.1-2 and 3. Assuming a flat CL distribution for the 5π events, we estimate 238 are $\pi^-\pi^-\pi^+\pi^+\pi^\circ$. Thus, out of 686 low CL events, we assign 242 events to be from other channels.

In order to reduce this contamination the following criteria were applied:

(i) The 4π fit must have at least two constraints.

(ii) The confidence level must be $\geq 2\%$.

When these cuts are made on the data, 3135 events remain.

2.2 Reaction Cross Sections

The cross section was calculated from the ratio of the four pion events to the total number of events.

$$\sigma(4\pi) = \sigma(4 \text{ prong}) \cdot N \cdot (1.14)/N_{4 \text{ pr}}$$

where,

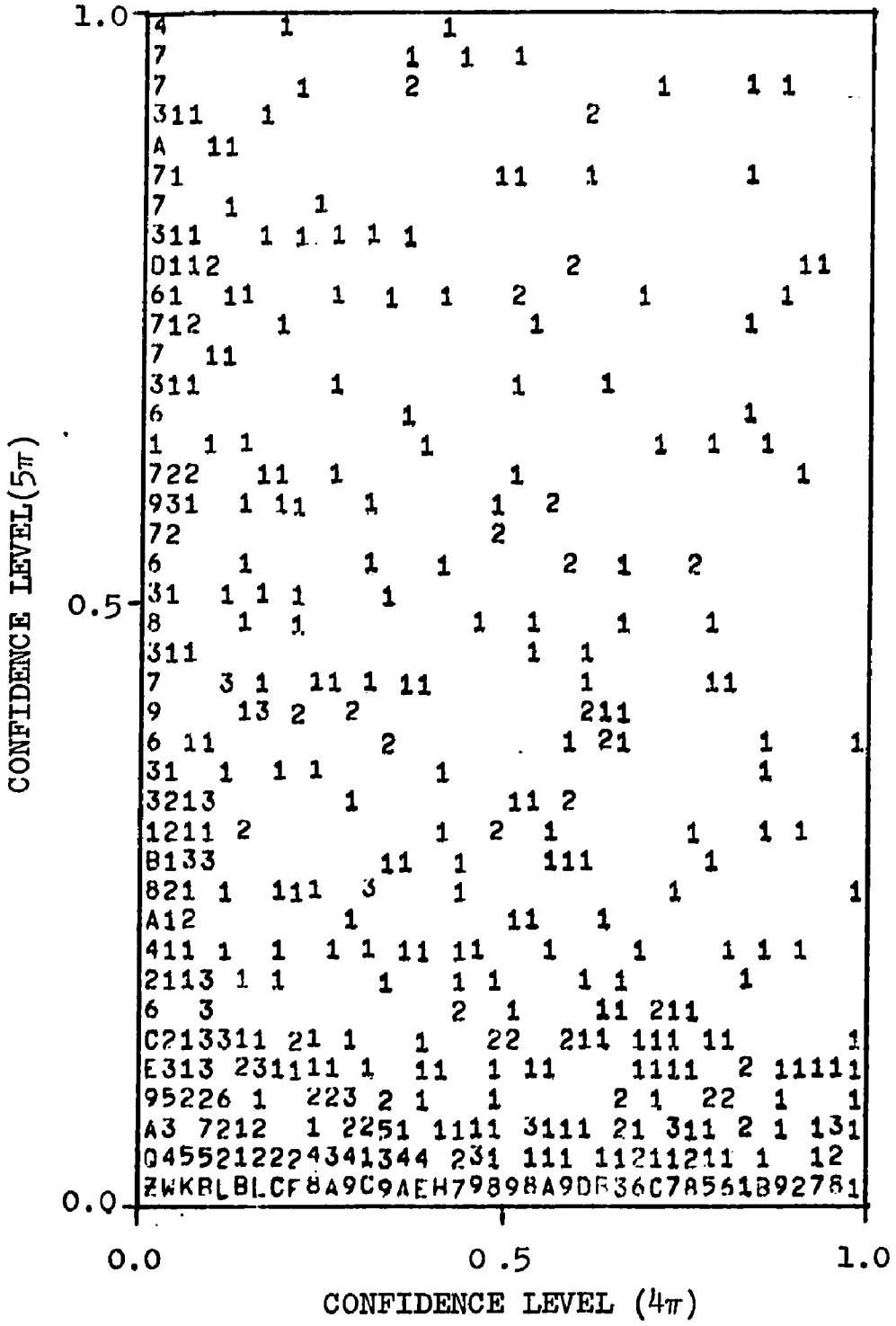


Figure 2.1-2. Confidence level of 4π fit versus confidence level of 5π fit for ambiguous events.

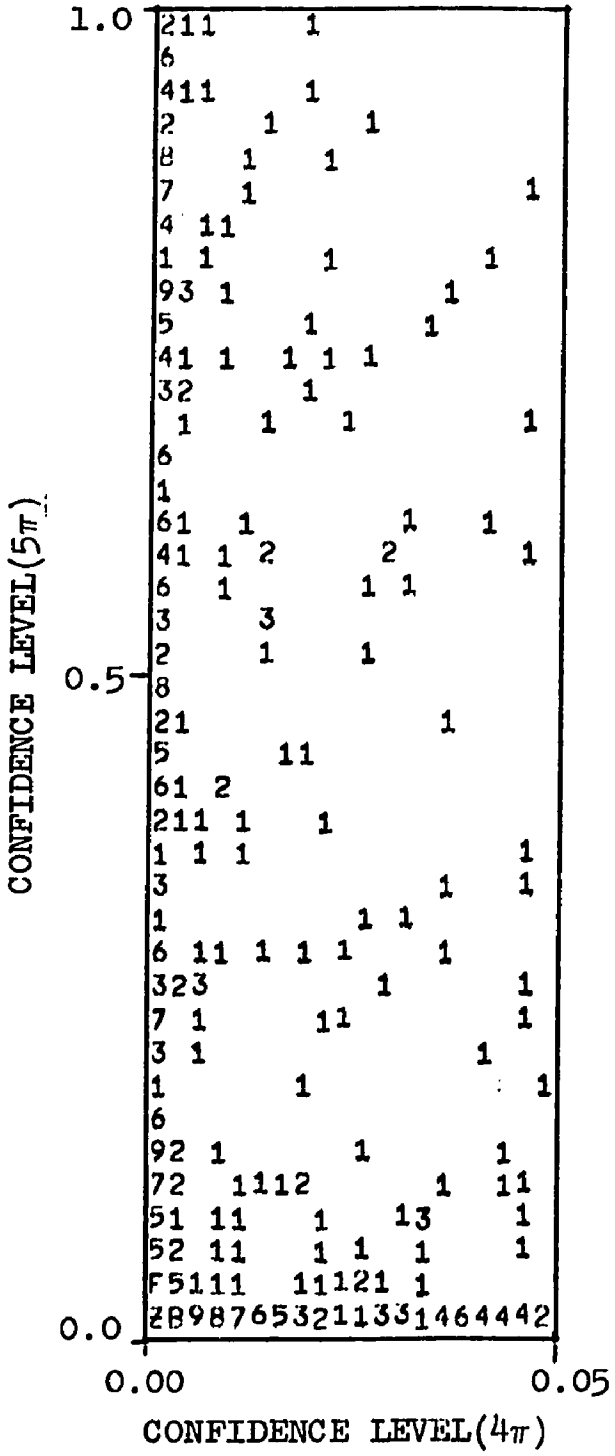


Figure 2.1-3. Confidence level 4π versus CL(5π) with an expanded scale.

N = number of 4π events,

N_4 = number of 4 prongs.

The factor 1.14 is to correct for the CL cut.* Table 2.2-1 gives the results. Figure 2.2-1 shows the $\sigma(4\pi)$ points that have been measured thus far. The previous data points are listed in Table 2.2-2.

2.3 Mass Distributions

The invariant mass distributions of interest for all momenta sets combined are presented in Figures 2.3-1 thru 2.3-6. They show the following mass projections:

(2.3-1) $M(\pi^{\pm}\pi^{\pm})$,

(2.3-2) $M(\pi^{-}\pi^{+})$,

(2.3-3) $M(\pi^{-}\pi^{+}\pi^{\pm})$,

(2.3-4) $M(\pi^{-}\pi^{+})$ other $\pi^{-}\pi^{+}$ in ρ region,

(2.3-5) $M(\pi^{-}\pi^{+})$ other $\pi^{-}\pi^{+}$ in f region,

(2.3-6) $M(\pi^{-}\pi^{+}\pi^{\pm})$ with $M(\pi^{-}\pi^{+})$ in ρ region,

where,

ρ region is $668 \leq M(\pi^{-}\pi^{+}) \leq 810$ MeV,

f region is $1154 \leq M(\pi^{-}\pi^{+}) \leq 1332$ MeV.

The positions and widths of the resonances were determined by doing a least squares fit to the $\pi^{-}\pi^{+}$ mass spectrum using resonance production and phase space. The resonances were parameterized by the simple Breit-Wigner form:

*The estimated 444 four pion events are in the 0.00 to 0.02 CL bin (444 = 686 - 242). The correction factor is then (3135 + 444)/3135.

Table 2.2-1. Four pion cross sections $\sigma(4\pi)$ as a function of $\bar{p}$ momentum P. N = number of 4π events; $N_{4\ pr}$ = number of four prongs; σ(4 prong) = four prong cross section.

P (GeV/c)	N	$N_{4\ pr}$	σ(4 prong) (mb)	$\sigma(4\pi)$ (mb)
1.63	569	7187	29.8 ±0.8	2.69 ±0.14
1.77	603	8251	27.1 ±0.7	2.26 ±0.11
1.83	570	7885	27.4 ±0.8	2.26 ±0.12
1.88	577	8391	25.8 ±0.7	2.02 ±0.10
1.95	494	8085	25.5 ±0.7	1.78 ±0.10
2.20	322	6624	23.1 ±0.6	1.28 ±0.08

Table 2.2-2. Four pion cross sections from previous experiments.

Reference	$\bar{P}$ Momentum (GeV/c)	σ(4 prong) (mb)
(Lab. de Phys. Nucl., 1969)	0.70	6.7 ±0.3
(Burns, R., et al., 1971)	0.94	3.6 ±0.4
(Strand, R., 1972)	1.11	3.4 ±0.2
	1.33	2.8 ±0.1
	1.52	2.2 ±0.1
(Donald, R., et al., 1968)	1.20	2.9 ±0.2
(Parker, D., 1971)	1.51	2.32 ±0.09
	1.65	2.26 ±0.08
	1.80	2.05 ±0.07
	1.95	1.78 ±0.08
	2.15	1.62 ±0.09
	2.45	1.24 ±0.08
	2.60	0.96 ±0.07
	2.75	0.97 ±0.07
	2.90	0.88 ±0.07
(Button, J., et al., 1962)	1.61	1.4 ±0.3
(Clayton, J., et al., 1970)	2.5	1.35 ±0.10
(Ferbel, T., et al., 1966)	3.28	0.8 ±0.1
(Bockman, K., et al., 1966)	5.7	0.11 ±0.03
(Accensi, A., et al., 1966)	5.7	0.173±0.016
(Alles-Borelli, V., et al., 1967)	5.7	0.173±0.016
(Ferbel, T., et al., 1968)	6.94	0.054±0.020

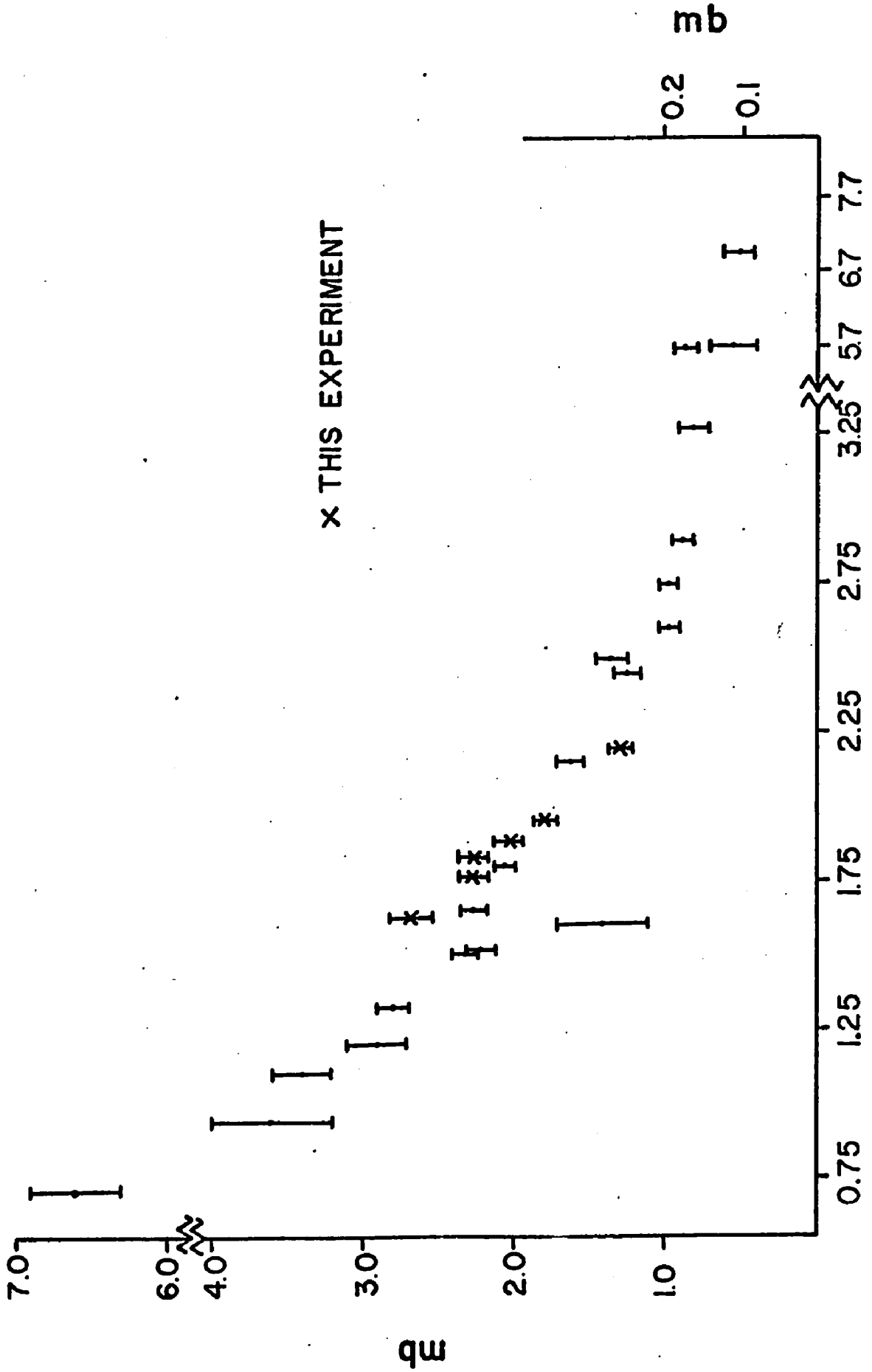


Figure 2.2-1. The $\pi^-\pi^-\pi^+\pi^+$ cross section as a function of p momentum.

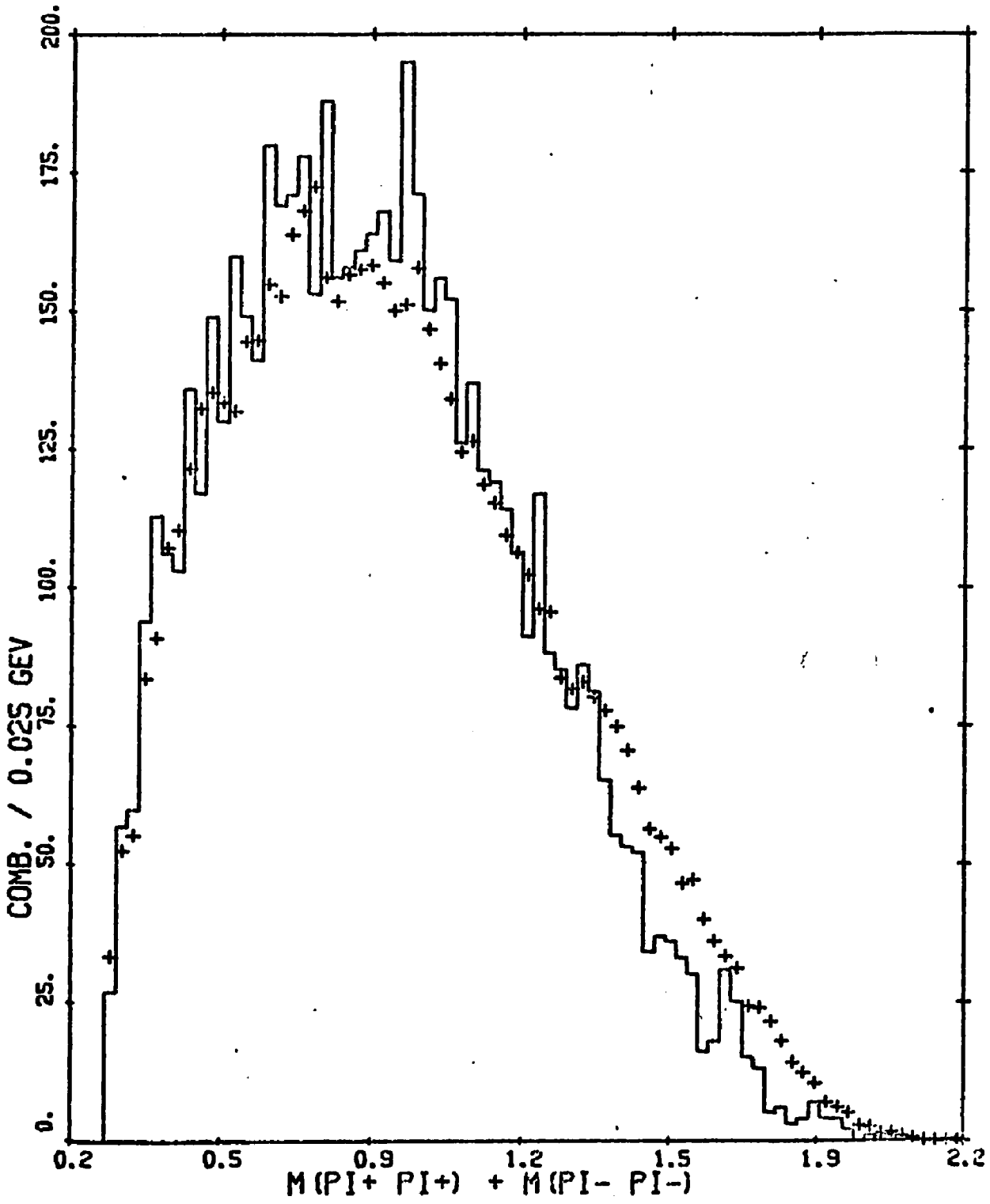


Figure 2.3-1. Mass distribution of $\pi^{\pm}\pi^{\pm}$. (2 combinations/event)

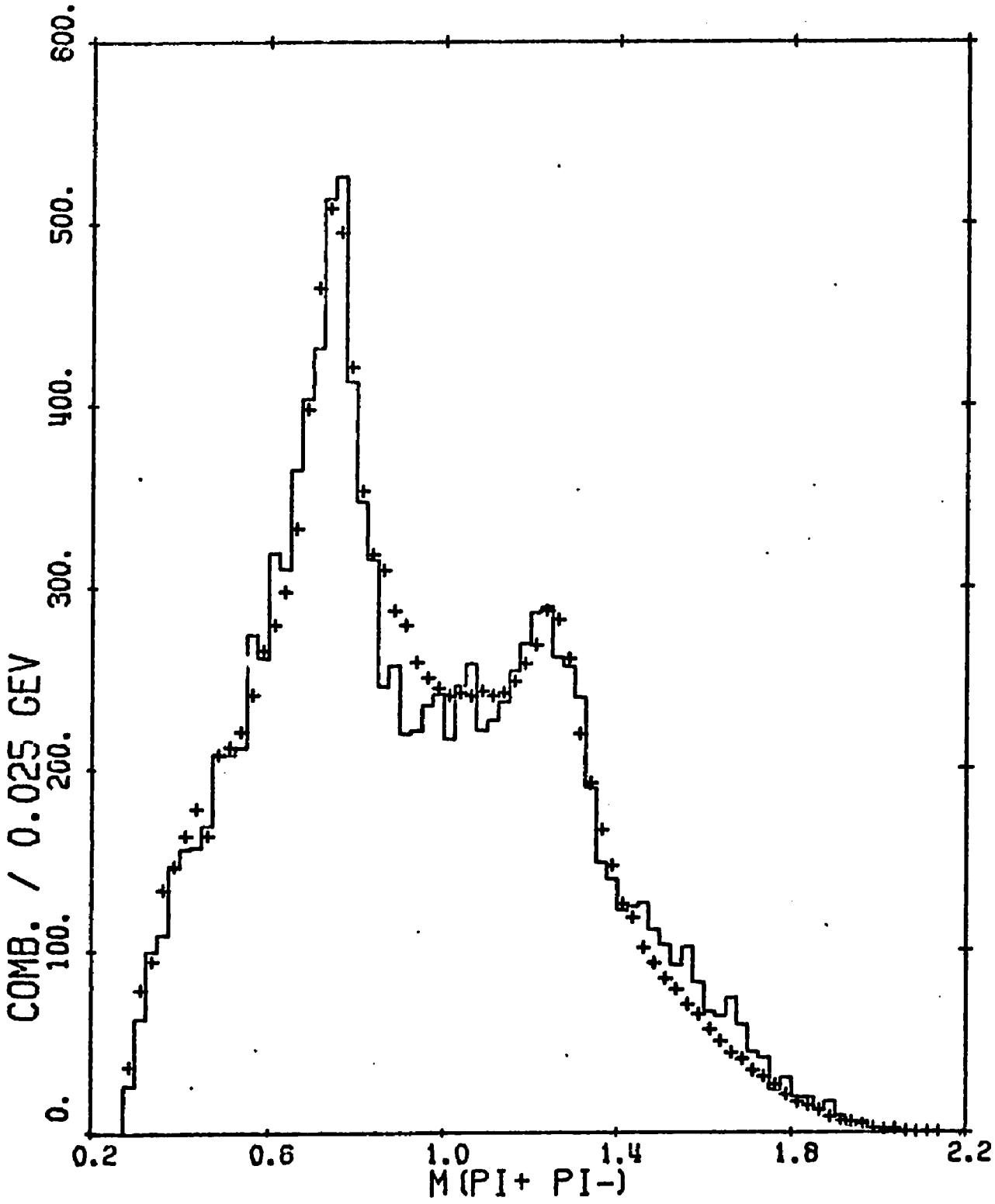


Figure 2.3-2. The $\pi^+\pi^-$ invariant mass spectrum. (4 combinations/event)

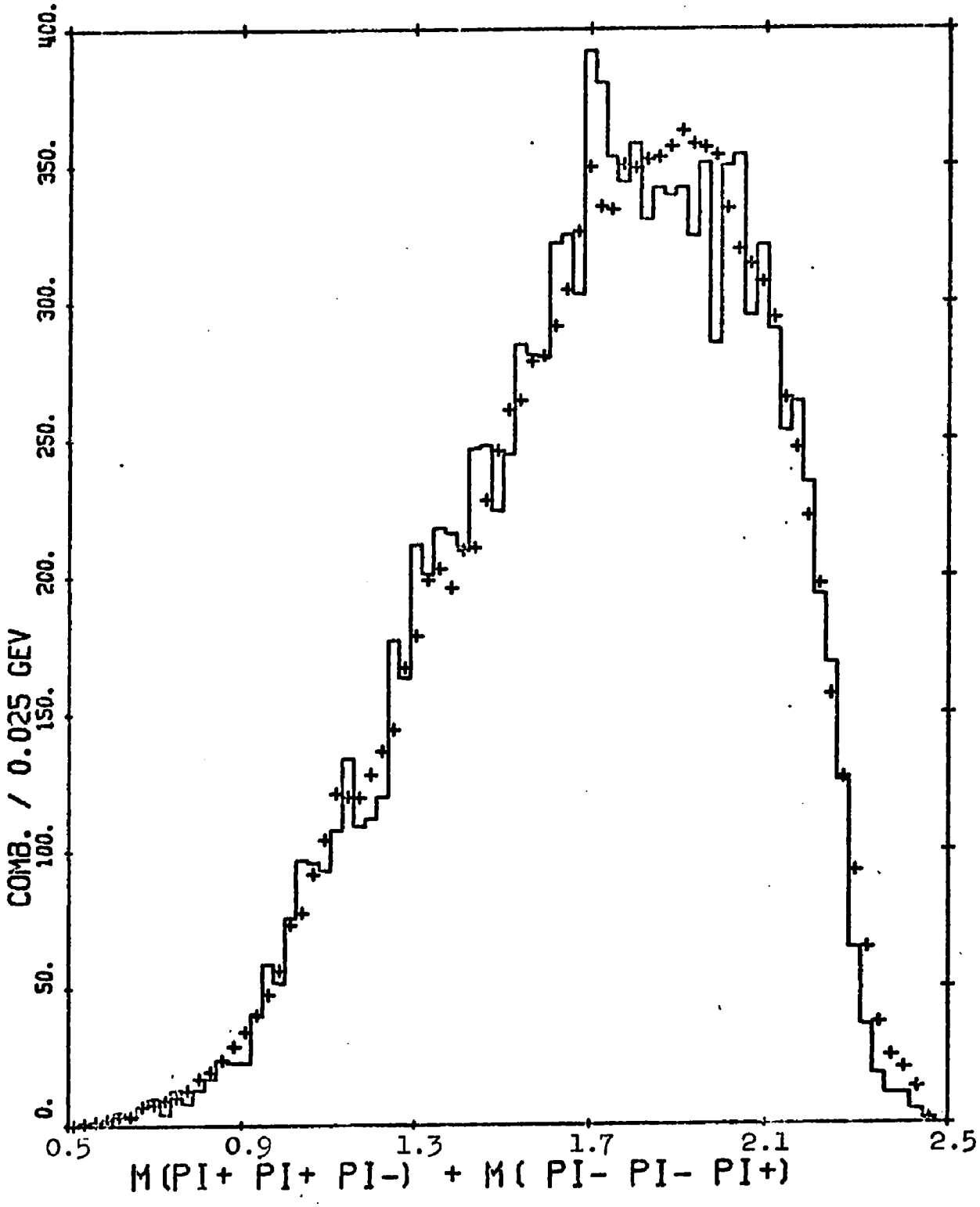


Figure 2.3-3. Mass distribution of $\pi^+\pi^-\pi^\pm$ combinations. (4 combinations/event)

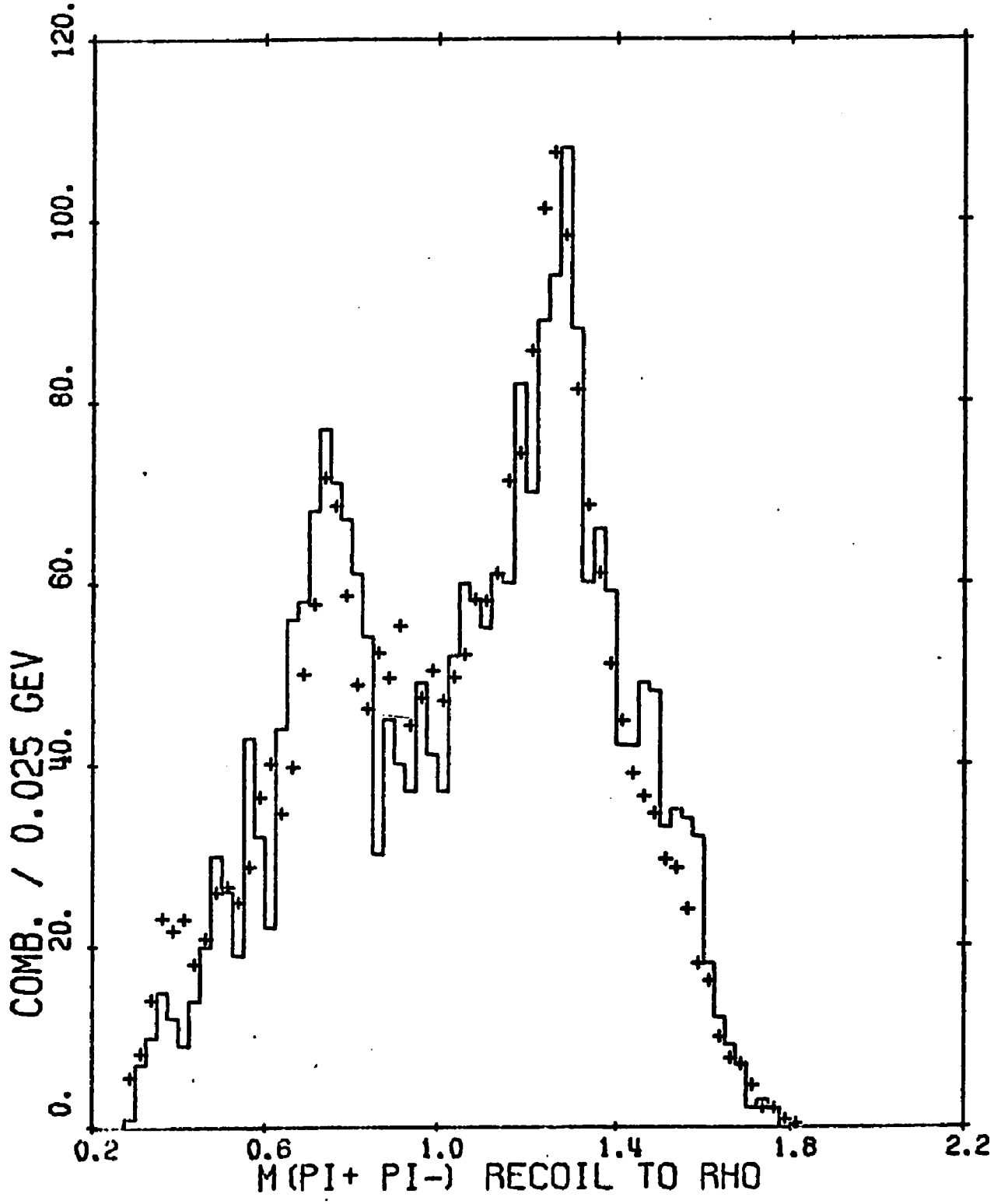


Figure 2.3-4. Mass spectrum of $\pi^+\pi^-$ combinations when recoil $\pi\pi$ is in the ρ mass region, 668 to 810 MeV.

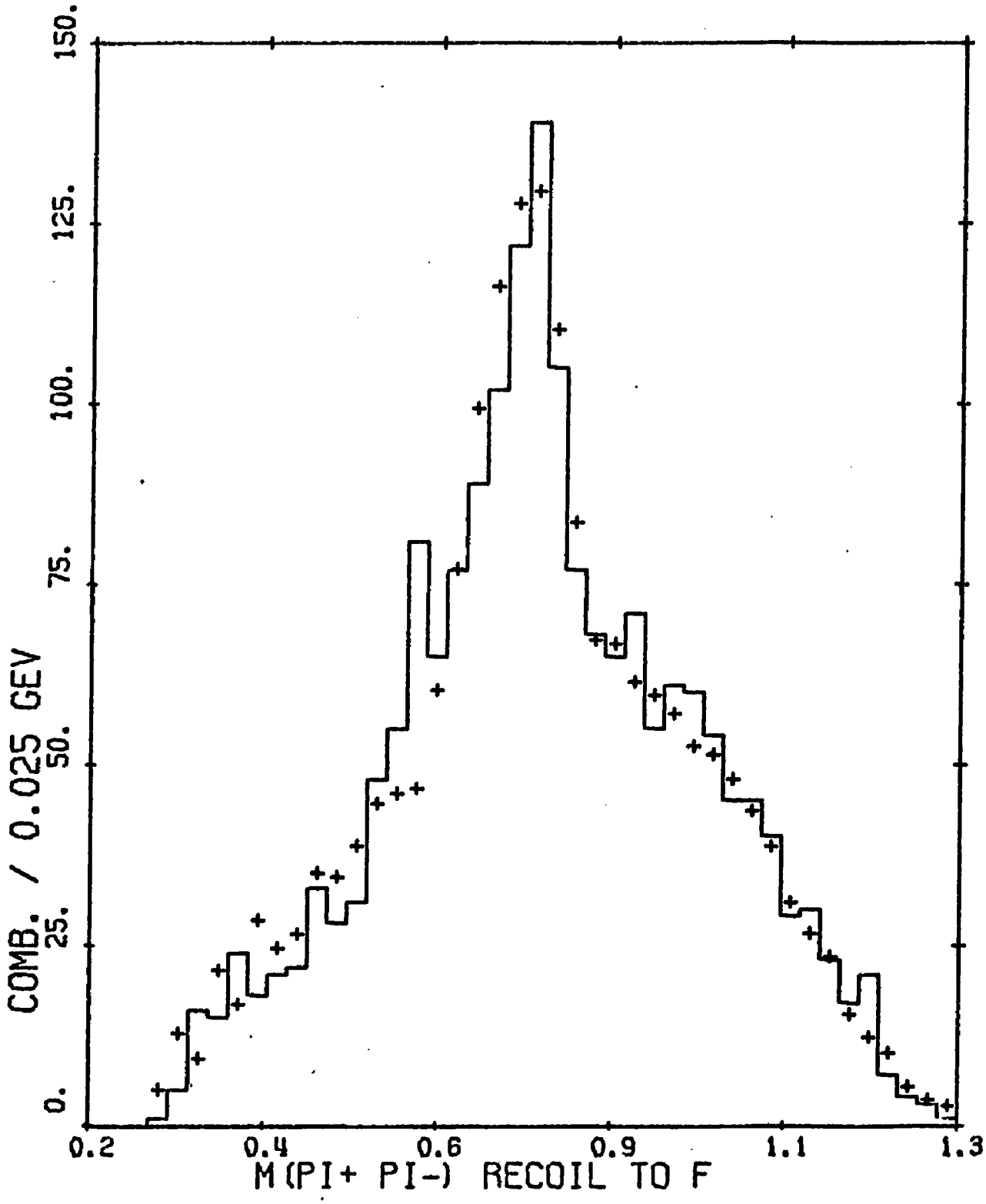


Figure 2.3-5. Effective mass spectrum of $\pi^+\pi^-$ combinations when recoil $\pi\pi$ is in f mass region, 1154 to 1332 MeV.

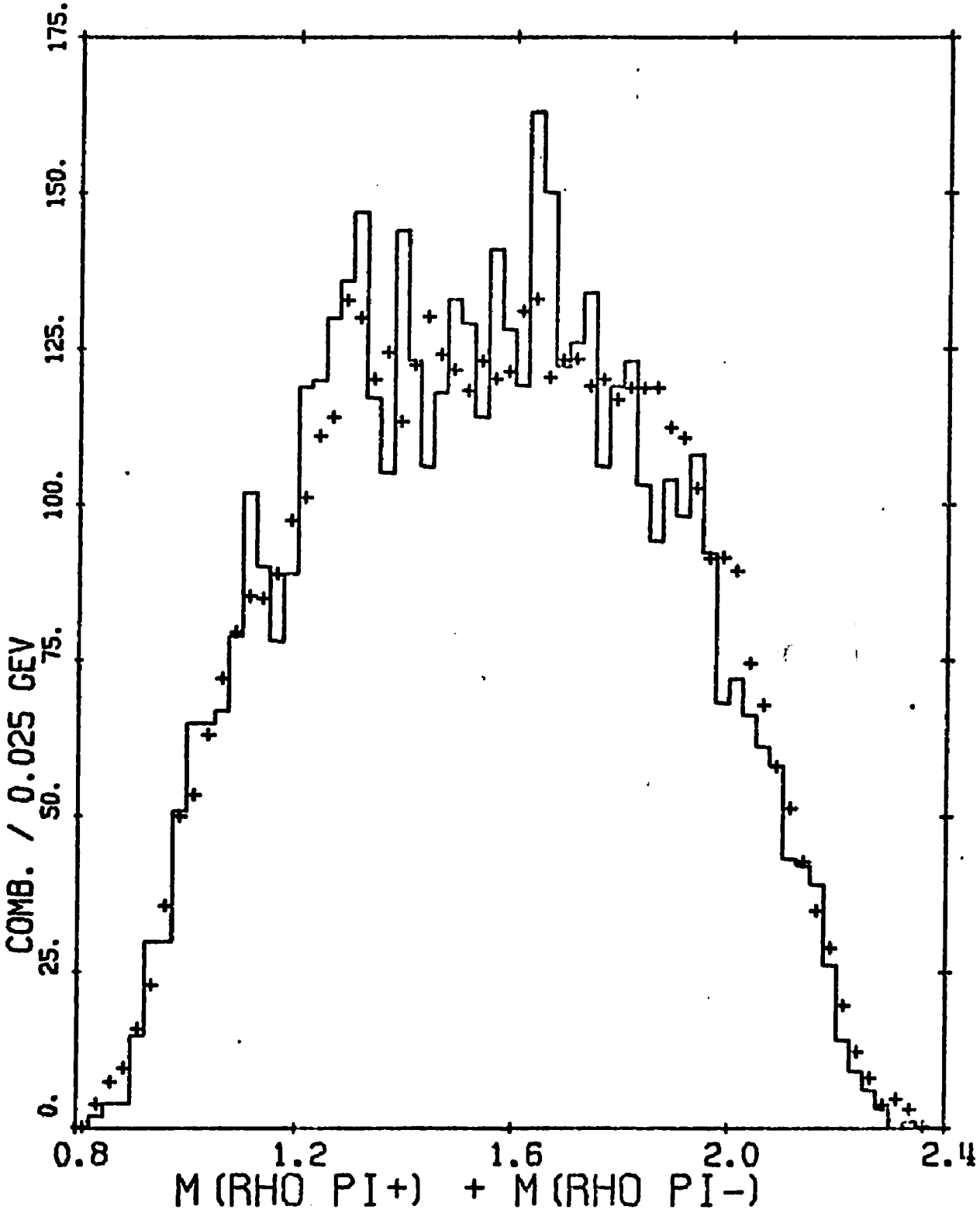


Figure 2.3-6. Invariant mass spectrum of $\rho^{\circ}\ \pi^{\pm}$ combinations.

$$(\Gamma/2)^2/\{(M-M_o)^2+ (\Gamma/2)^2\}$$

where,

M_o = central mass of the resonance,

Γ = full width at half maximum (FWHM) of the resonance.

The following values were found:

$$M_\rho = 740 \pm 3 \text{ MeV}, \ \Gamma_\rho = 142 \pm 5 \text{ MeV};$$
$$M_f = 1243 \pm 5 \text{ MeV}, \ \Gamma_f = 177 \pm 7 \text{ MeV};$$
$$M_S{}^* = 1051 \pm 8 \text{ MeV}, \ \Gamma_S{}^* = 76 \pm 18 \text{ MeV}.^{\#}$$

When the S^* was not included in the fit, the f meson fitted a mass of 1232 ±5 and a width of 191 ±8 MeV.

The $\pi^\pm\pi^\pm$ spectrum has essentially a phase space distribution. However, there is a significant number of events missing in the high mass region (see section 2.4). As in earlier experiments, the $\pi^-\pi^+$ spectrum shows copious ρ and f production along with possibly a small amount of S^*. The $\pi^-\pi^+\pi^\pm$ distribution is essentially phase space with an excess of events in the A_2 mass region around 1300 MeV, as well as, in the $A_3(1640)$ region. The remaining distributions give indications of quasi two body production.

Figures 2.3-7 thru 2.3-24 show how the invariant mass spectra vary with $\bar{p}$ momentum. To improve the statistics the momentum sets have been combined in pairs 1.63 and 1.77, 1.83 and 1.88, 1.95 and 2.20 GeV/c. The distributions generated by Monte Carlo simulations to be discussed in the next section are indicated with plus signs.

From the literature the S^* resonance has a mass of 1062 MeV and a width of 86 MeV (Review of Particle Properties, 1971).

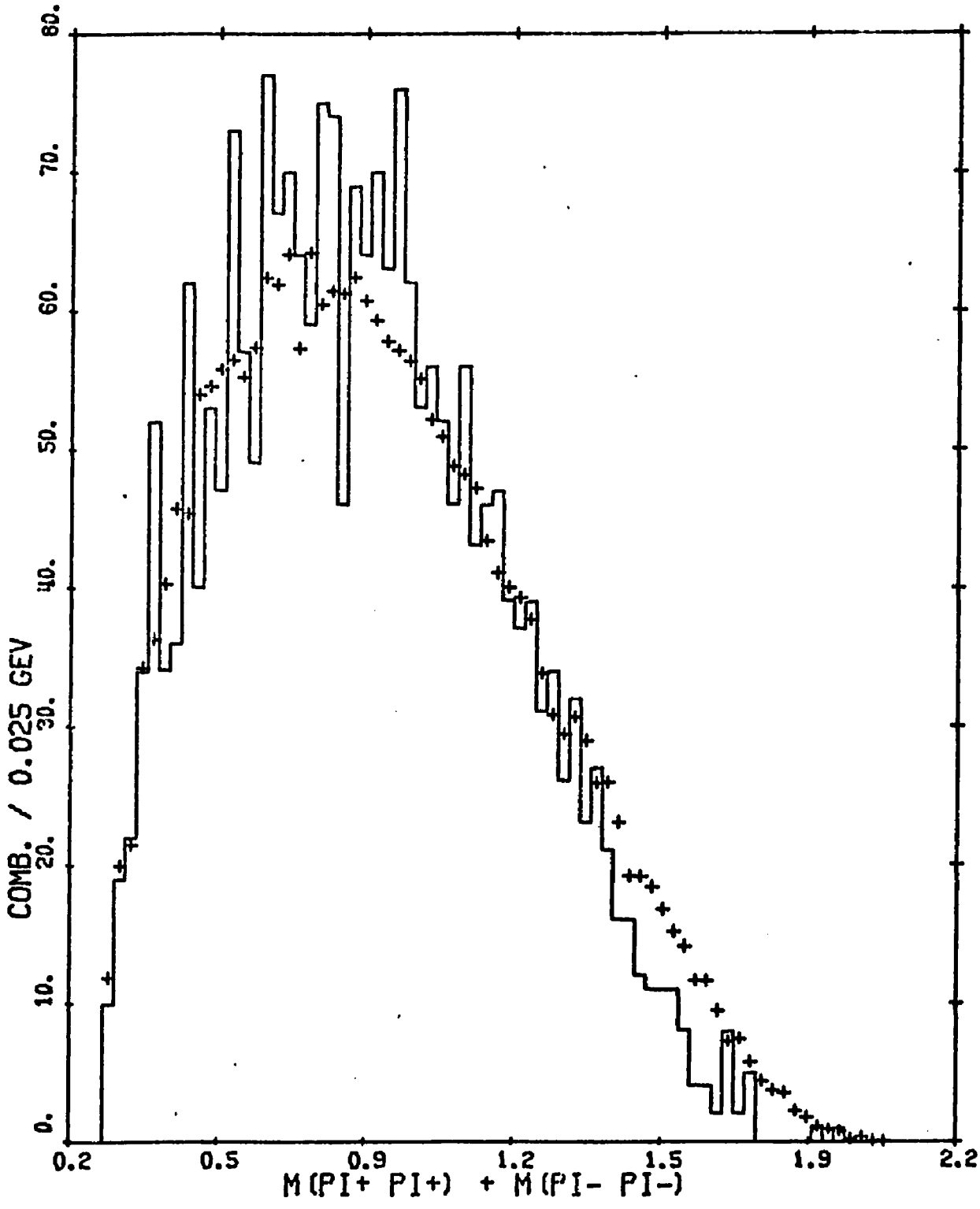


Figure 2.3-7. The $\pi^{\pm}\pi^{\pm}$ mass spectrum for 1.63 and 1.77 GeV/c momenta sets. (2 combinations/event)

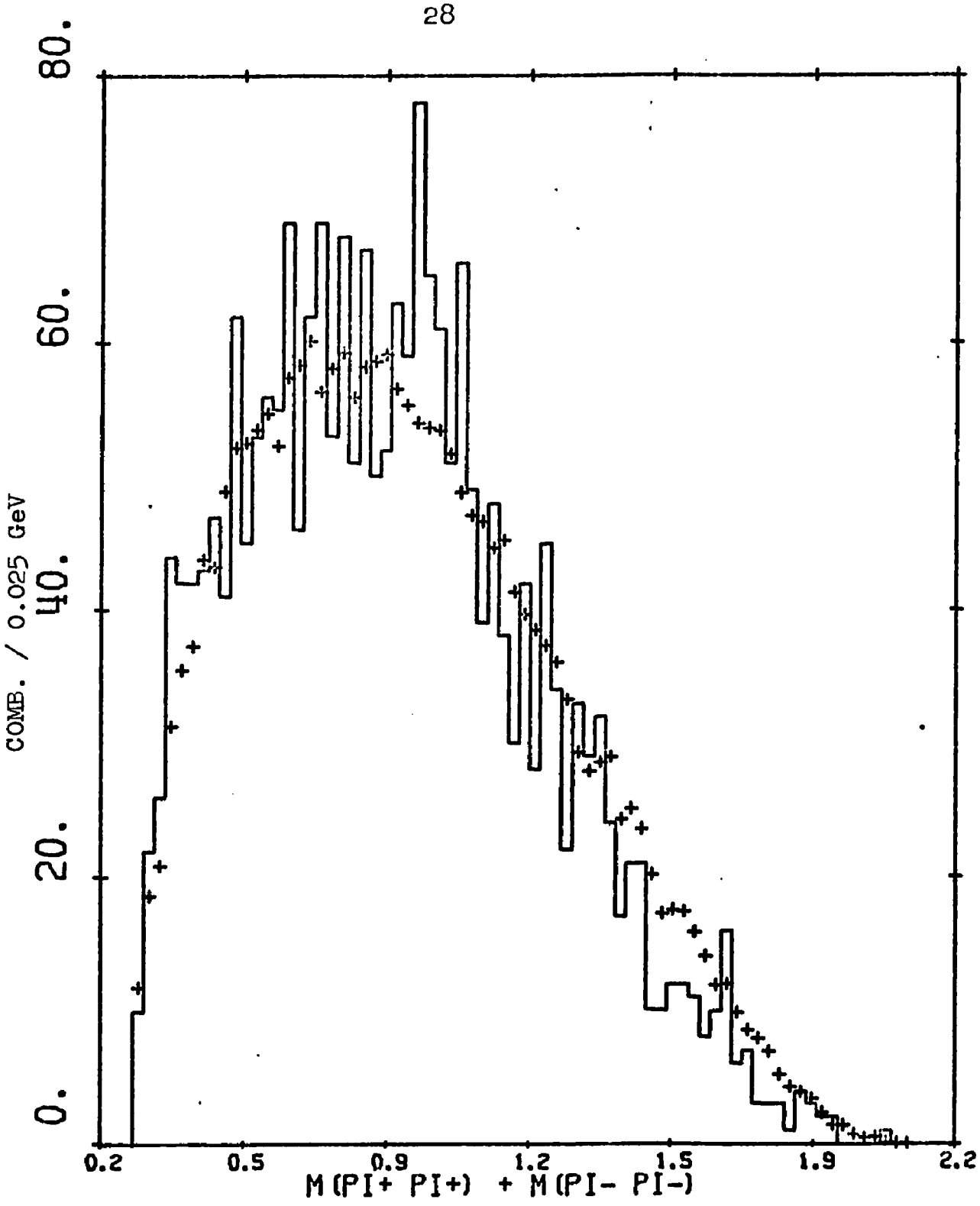


Figure 2.3-8. The $\pi^{\pm}\pi^{\pm}$ mass spectrum for 1.83 and 1.88 GeV/c momenta sets. (2 combinations/event)

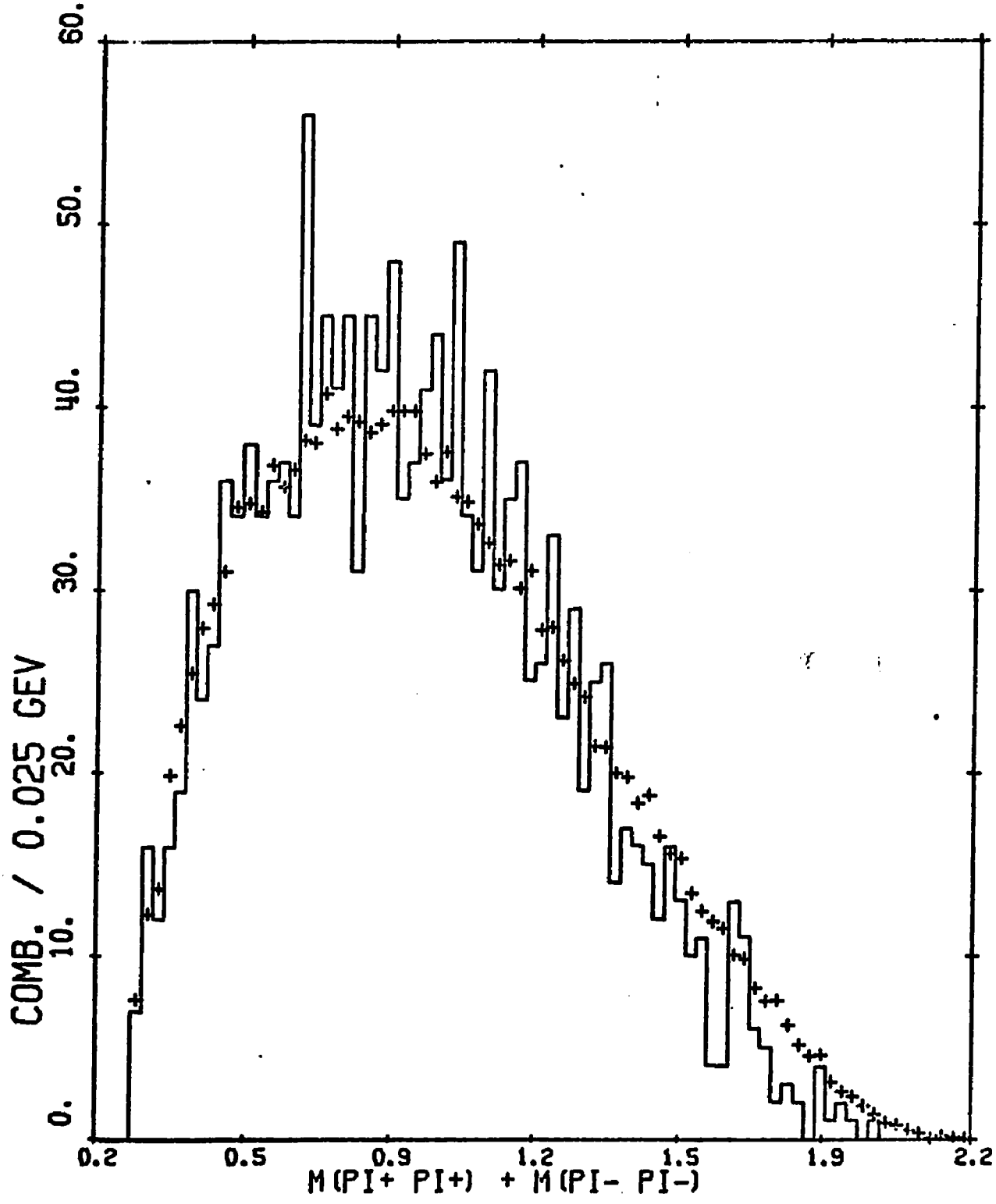


Figure 2.3-9. The $\pi^{\pm}\pi^{\pm}$ mass spectrum for 1.95 and 2.20 GeV/c momenta sets. (2 combinations/event)

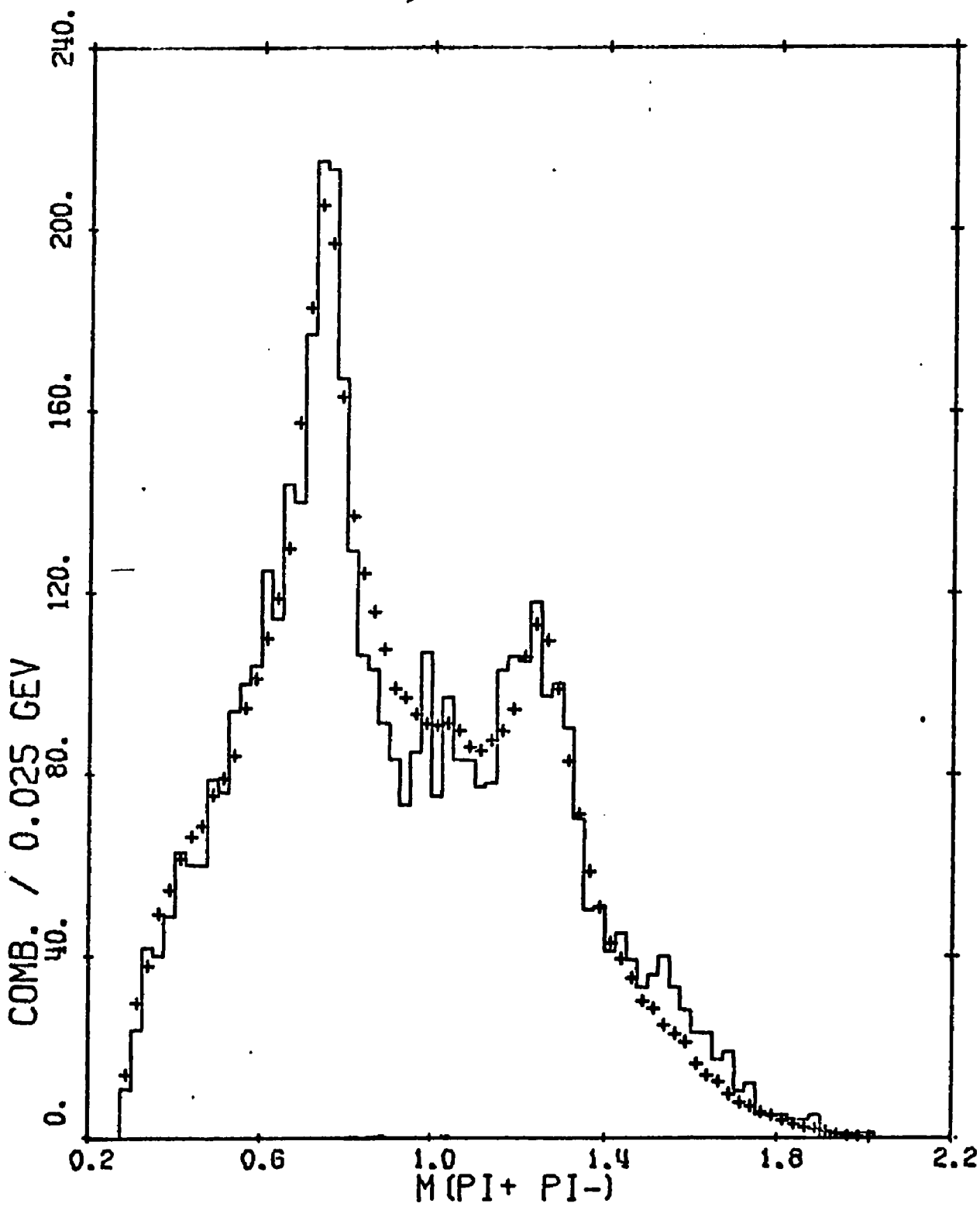


Figure 2.3-10. The $\pi^+\pi^-$ mass spectrum for 1.63 and 1.77 GeV/c momenta sets. (4 combinations/event)

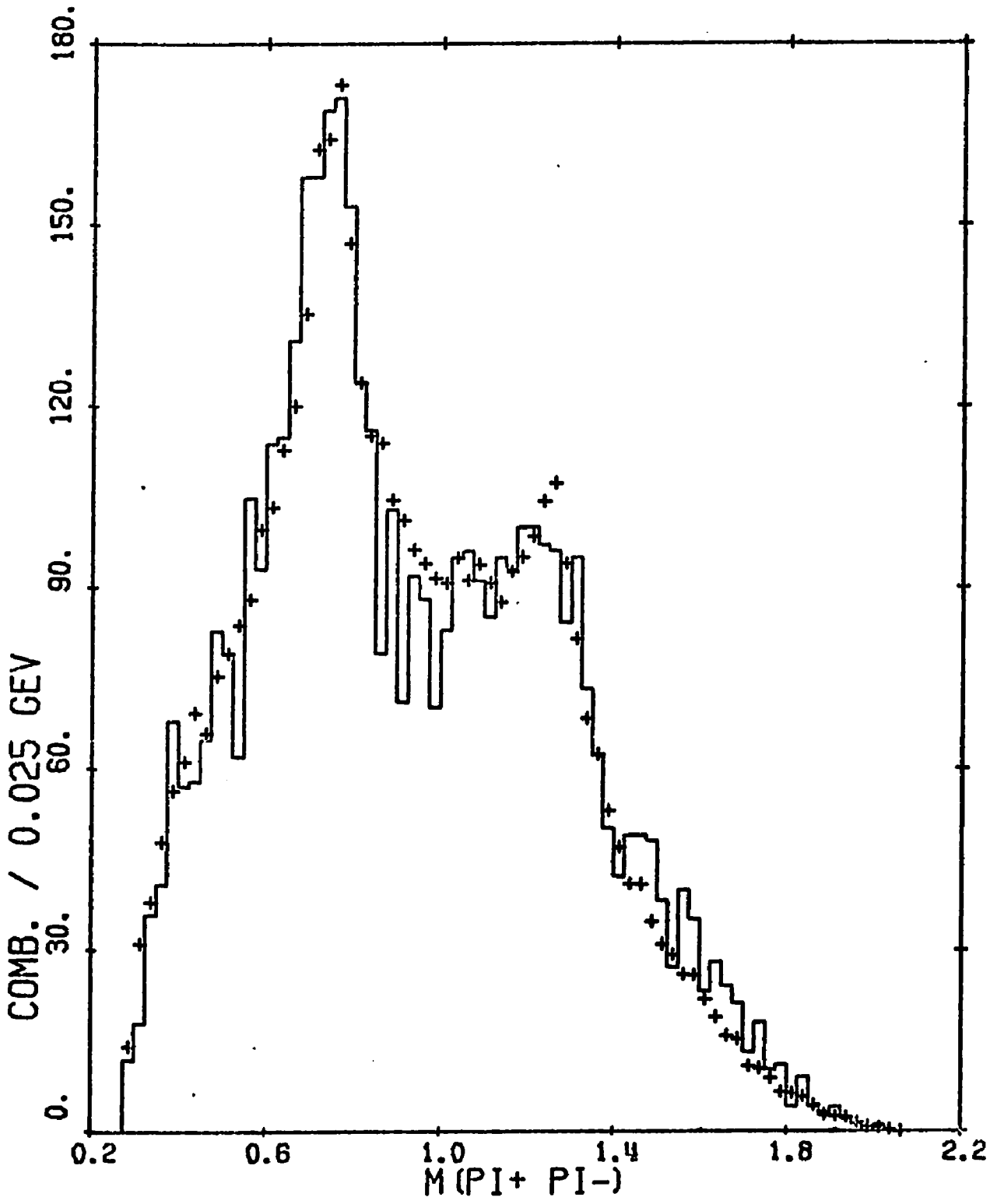


Figure 2.3-11. The $\pi^+\pi^-$ mass spectrum for 1.83 and 1.88 momenta sets. (4 combinations/event)

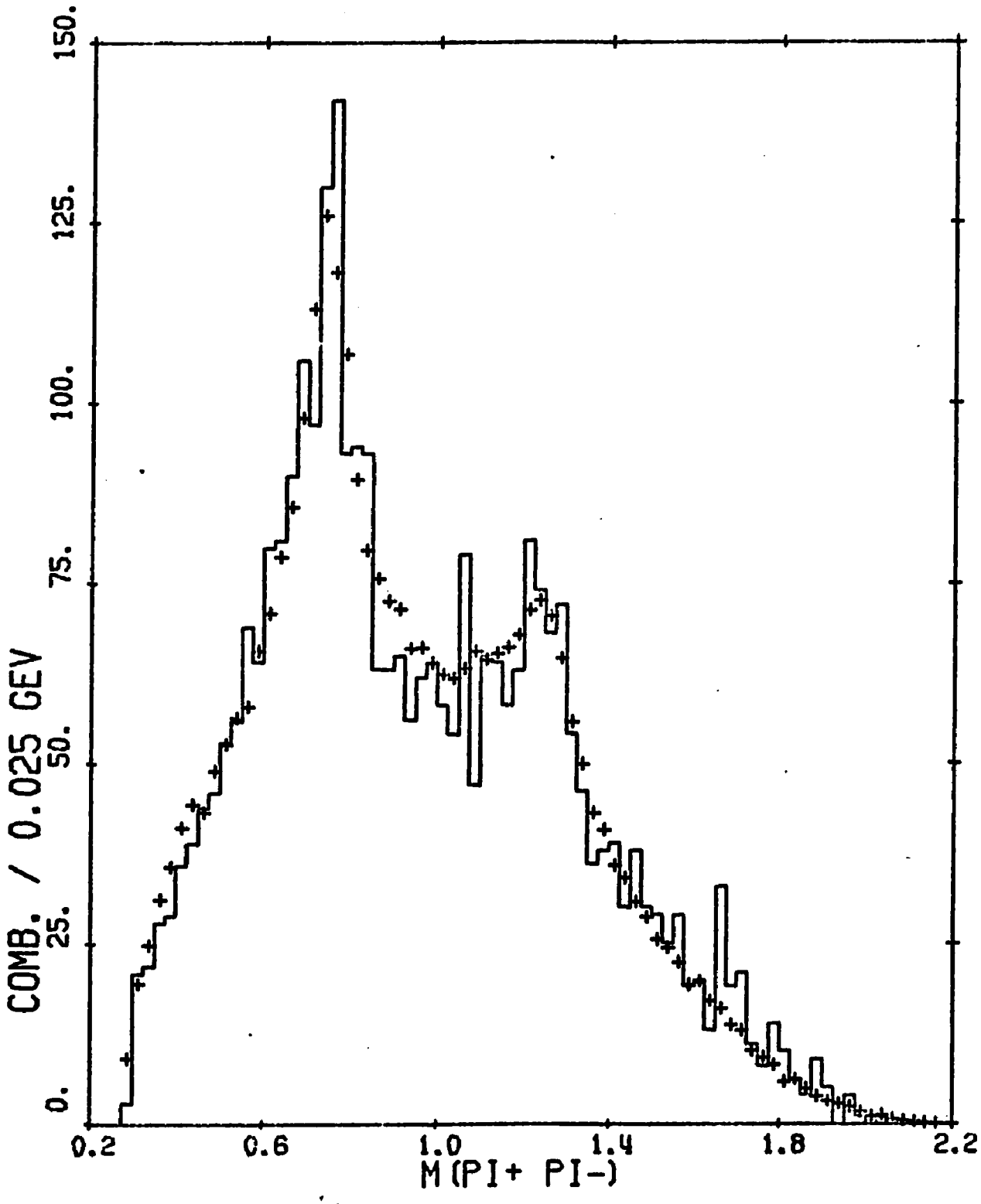


Figure 2.3-12. The $\pi^+\pi^-$ mass spectrum for 1.95 and 2.20 momenta sets. (4 combinations/event)

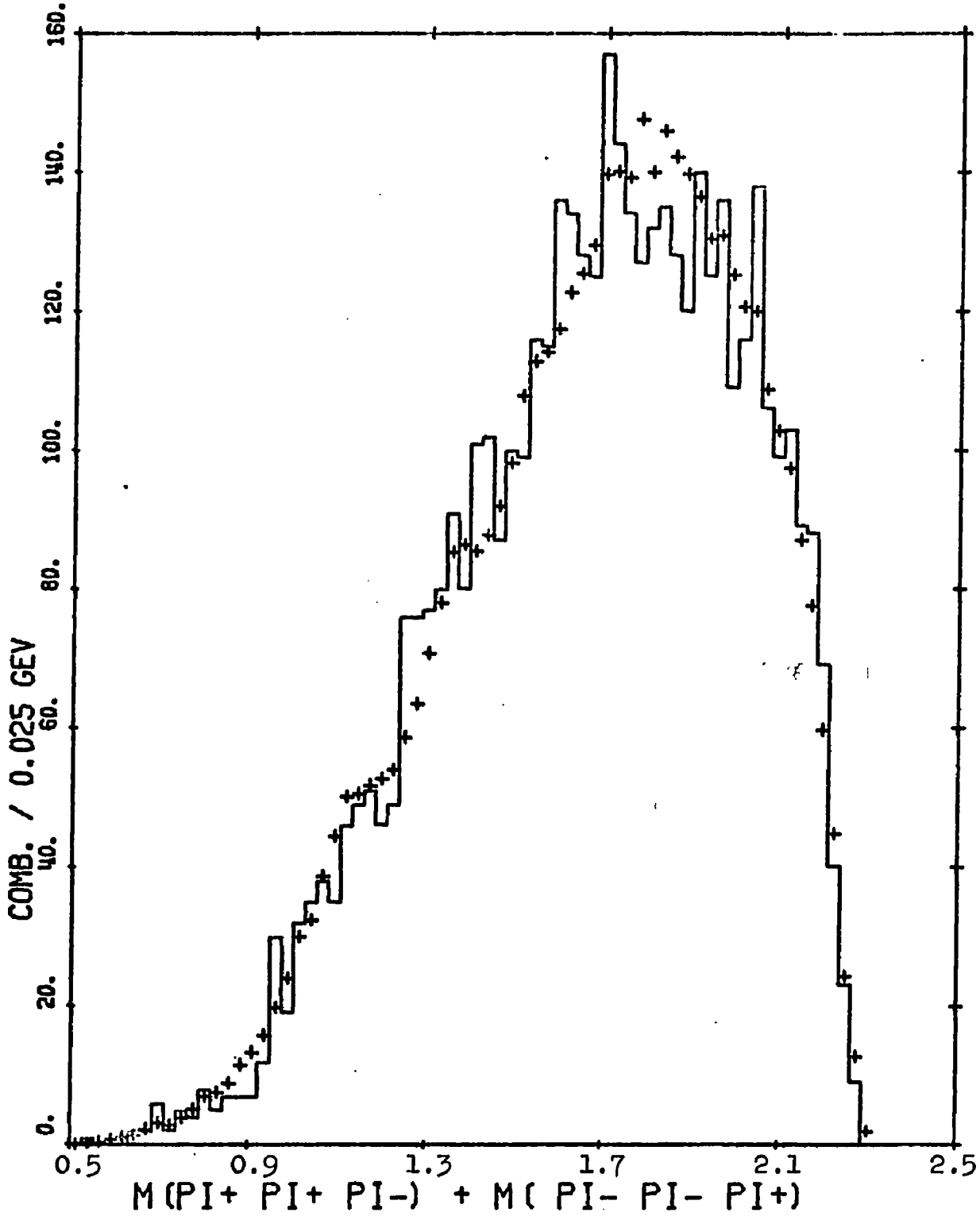


Figure 2.3-13. Mass spectrum of $\pi^+\pi^-\pi^\pm$ combinations for momenta sets 1.63 and 1.77 GeV/c. (4 combinations/event)

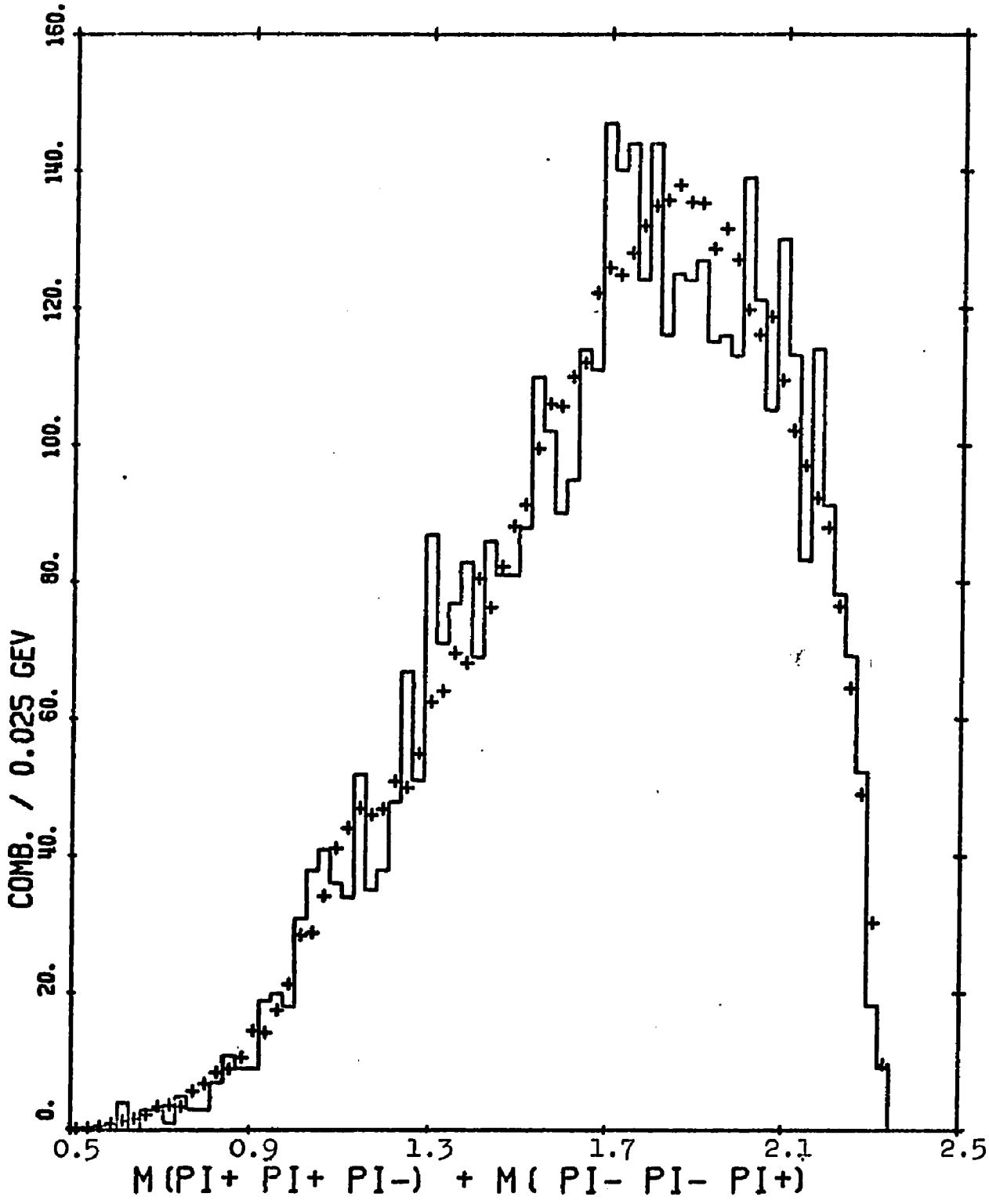


Figure 2.3-14. Mass spectrum of $\pi^+\pi^-\pi^\pm$ combinations for momenta sets 1.83 and 1.88 GeV/c. (4 combinations/event)

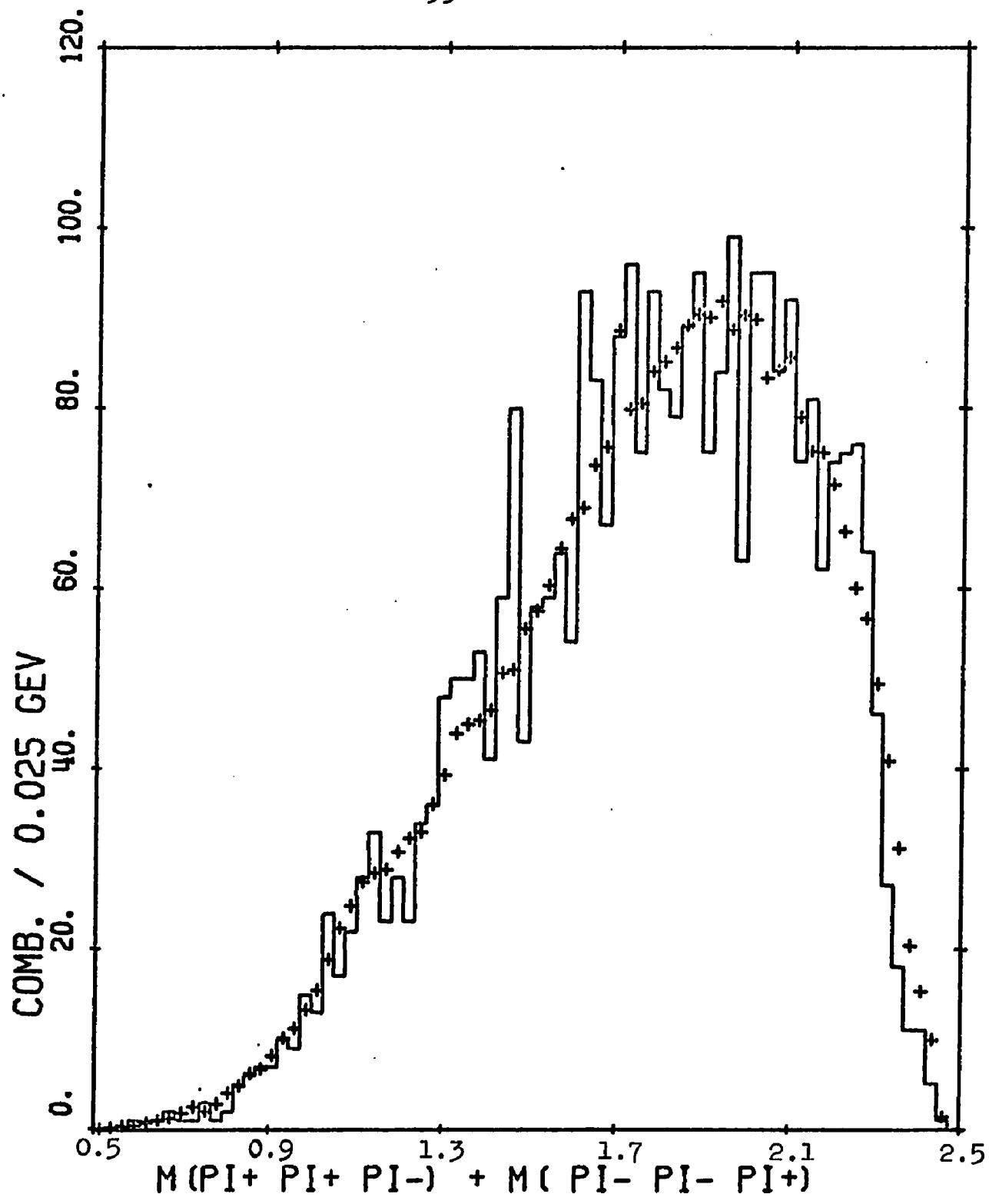


Figure 2.3-15. Mass spectrum of $\pi^+\pi^-\pi^\pm$ combinations for momenta sets 1.95 and 2.20 GeV/c. (4 combinations/ event)

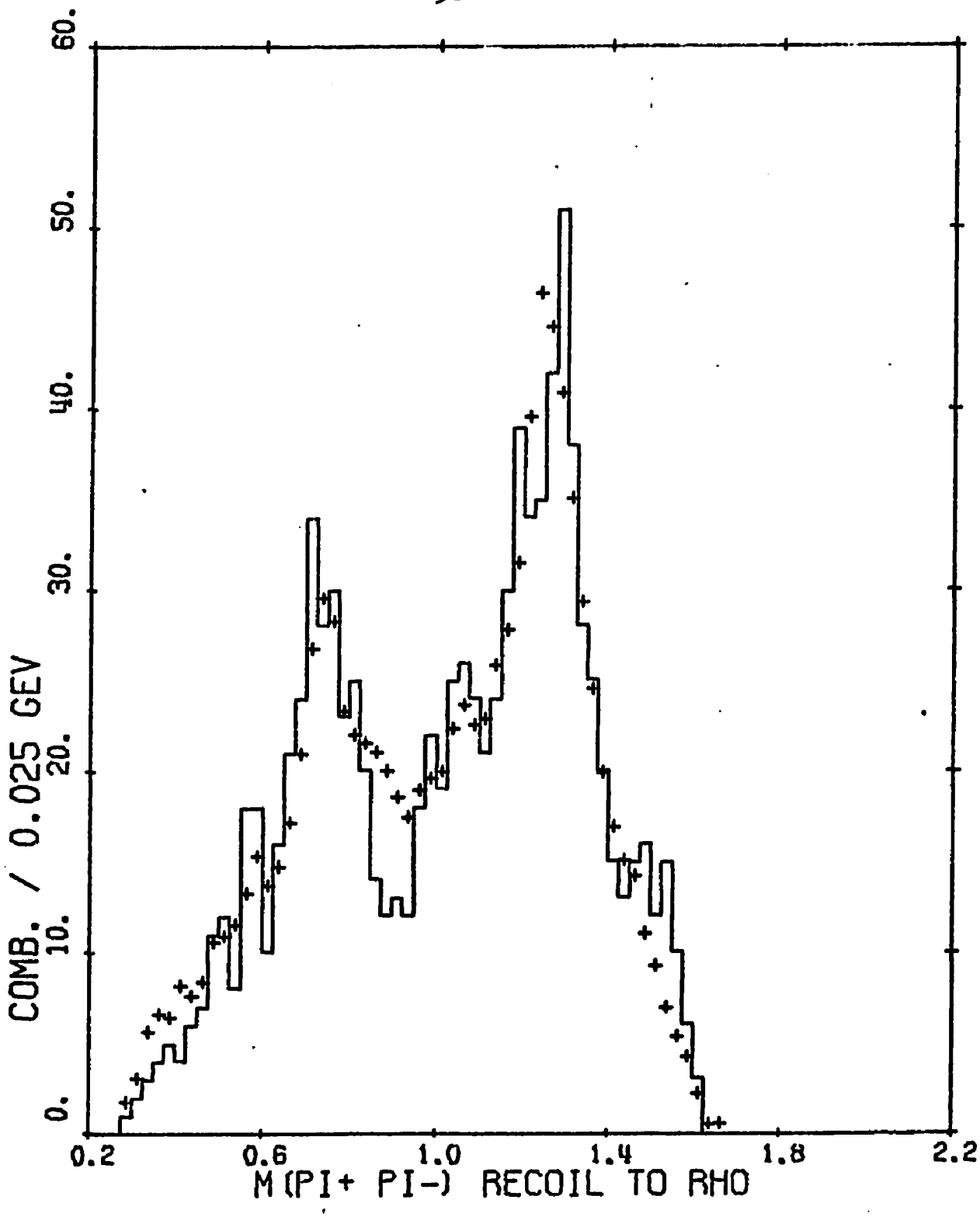


Figure 2.3-16. Mass spectrum of $\pi^+\pi^-$ combinations associated with the ρ meson for momenta sets 1.63 and 1.77 GeV/c.

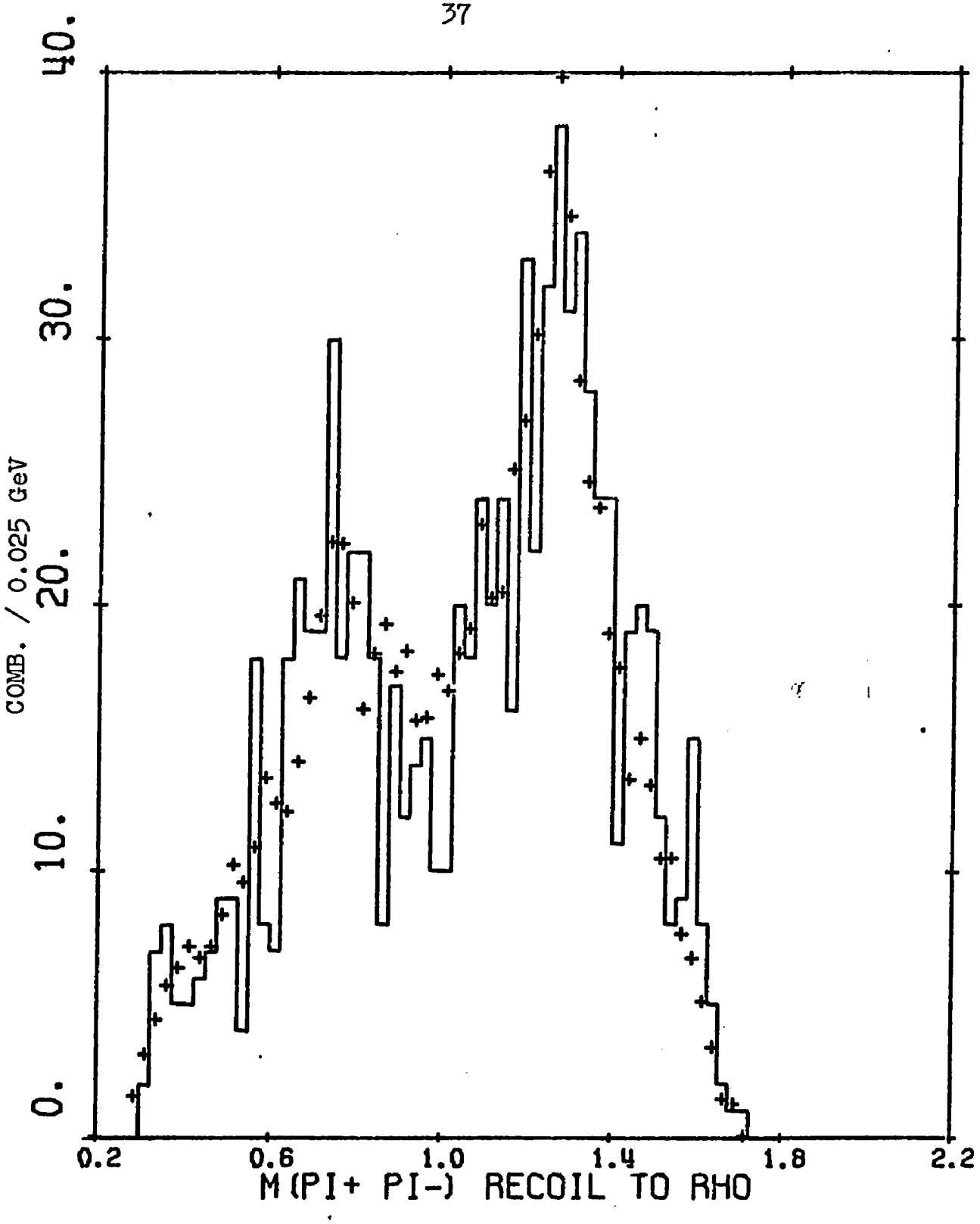


Figure 2.3-17. Mass spectrum of $\pi^+\pi^-$ combinations associated with the ρ meson for momenta sets 1.83 and 1.88 GeV/c.

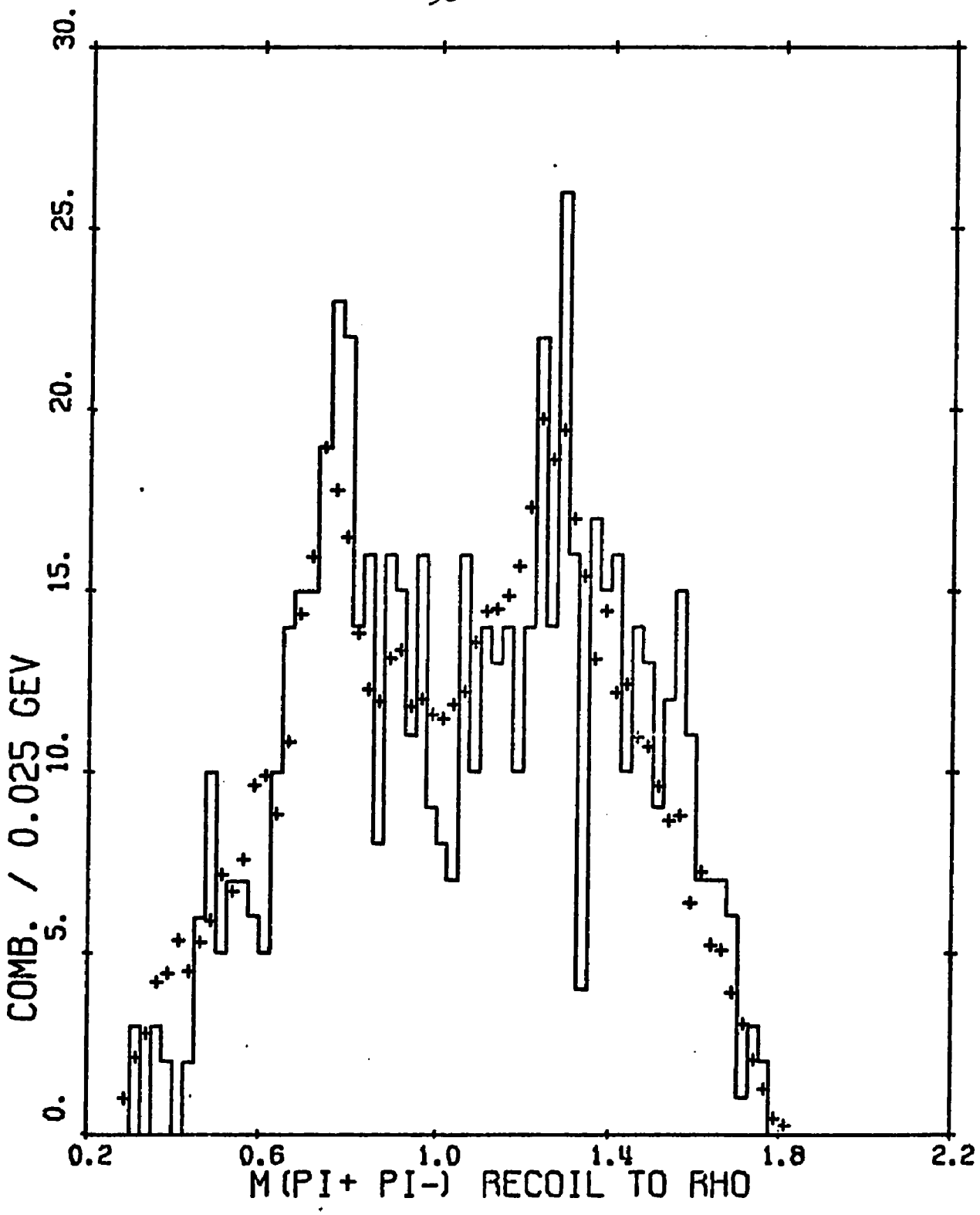


Figure 2.3-18. Mass spectrum of $\pi^+\pi^-$ combinations associated with the ρ meson for momenta sets 1.95 and 2.20 GeV/c.

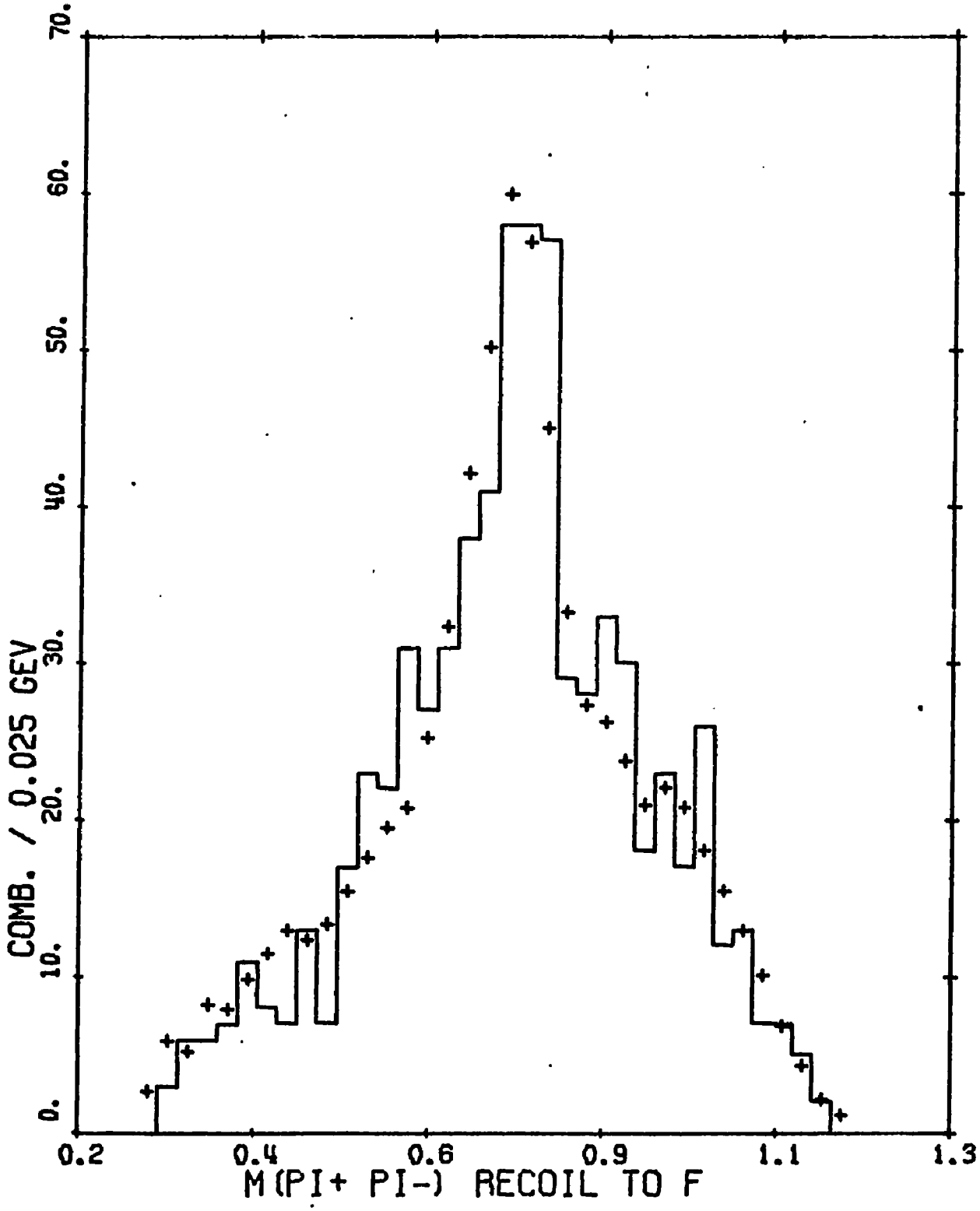


Figure 2.3-19. Effective mass spectrum of $\pi^+\pi^-$ combinations associated with the f meson for momenta sets 1.63 and 1.77 GeV/c.

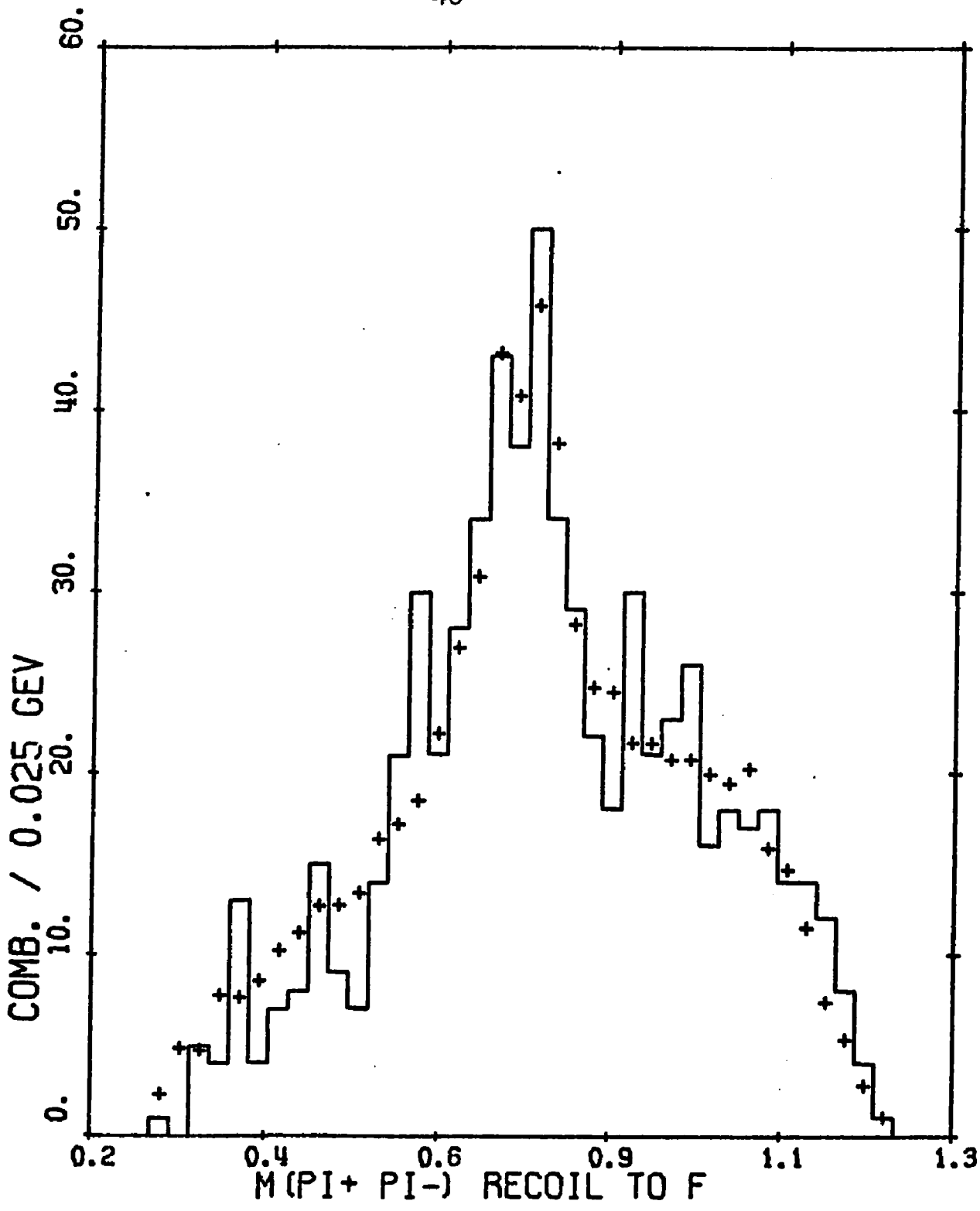


Figure 2.3-20. Mass spectrum for $\pi^+\pi^-$ combinations associated with the f meson for momenta sets 1.83 and 1.88 GeV/c.

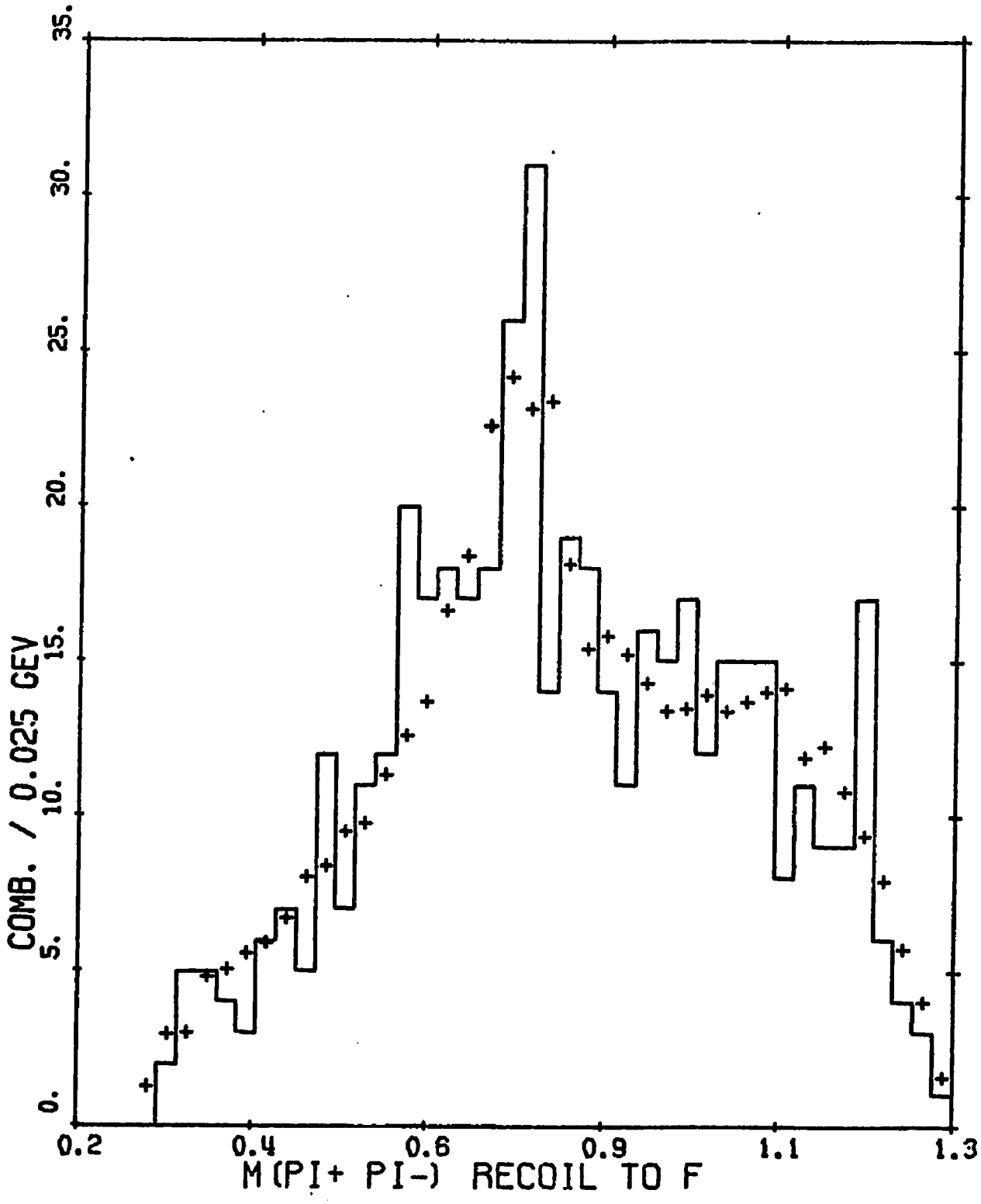


Figure 2.3-21. Mass spectrum for $\pi^+\pi^-$ combinations associated with the f meson for momenta sets 1.95 and 2.20 GeV/c.

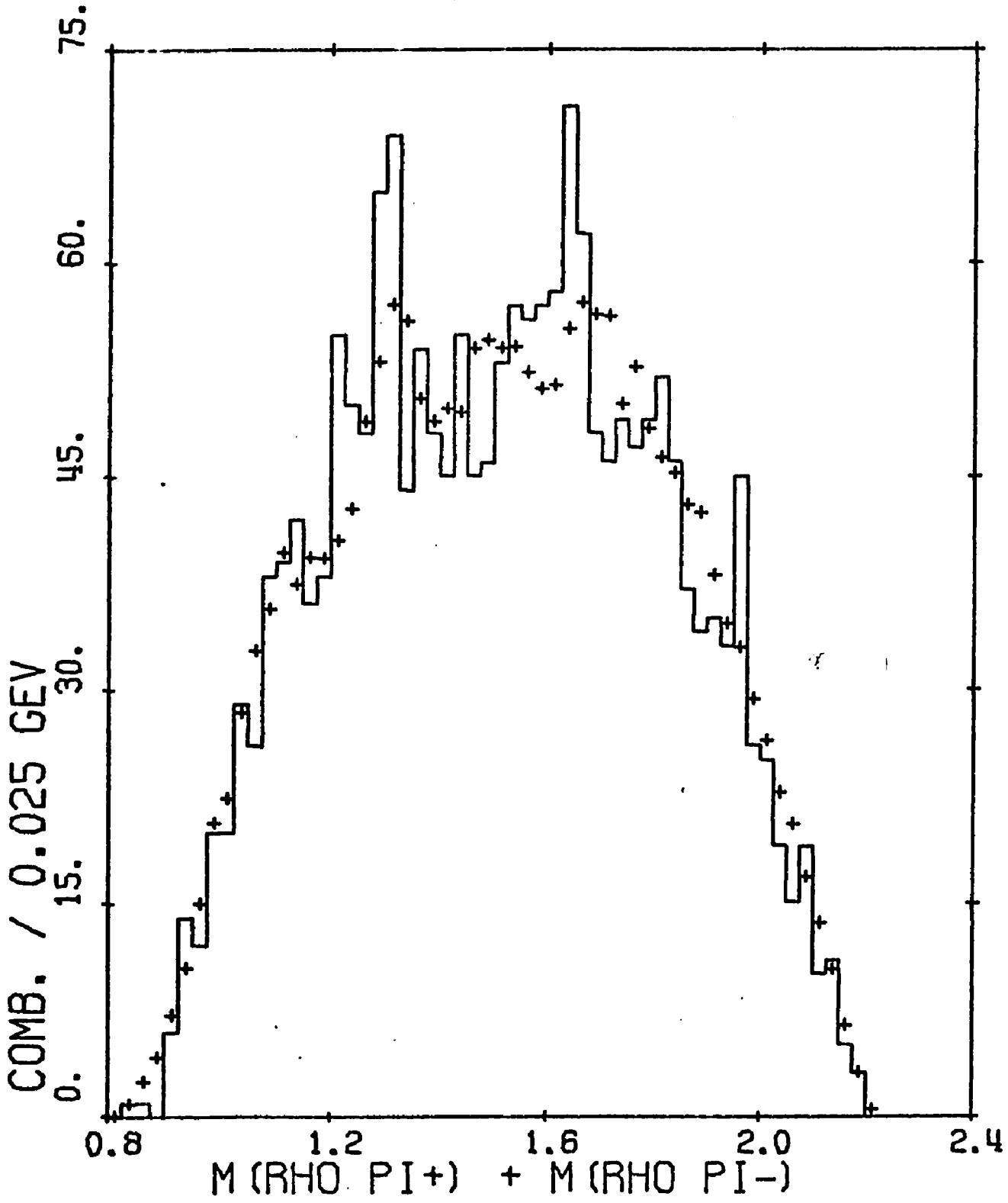


Figure 2.3-22. Mass spectrum of $\rho^{\circ}\pi^{\pm}$ combinations for momenta sets 1.63 and 1.77 GeV/c.

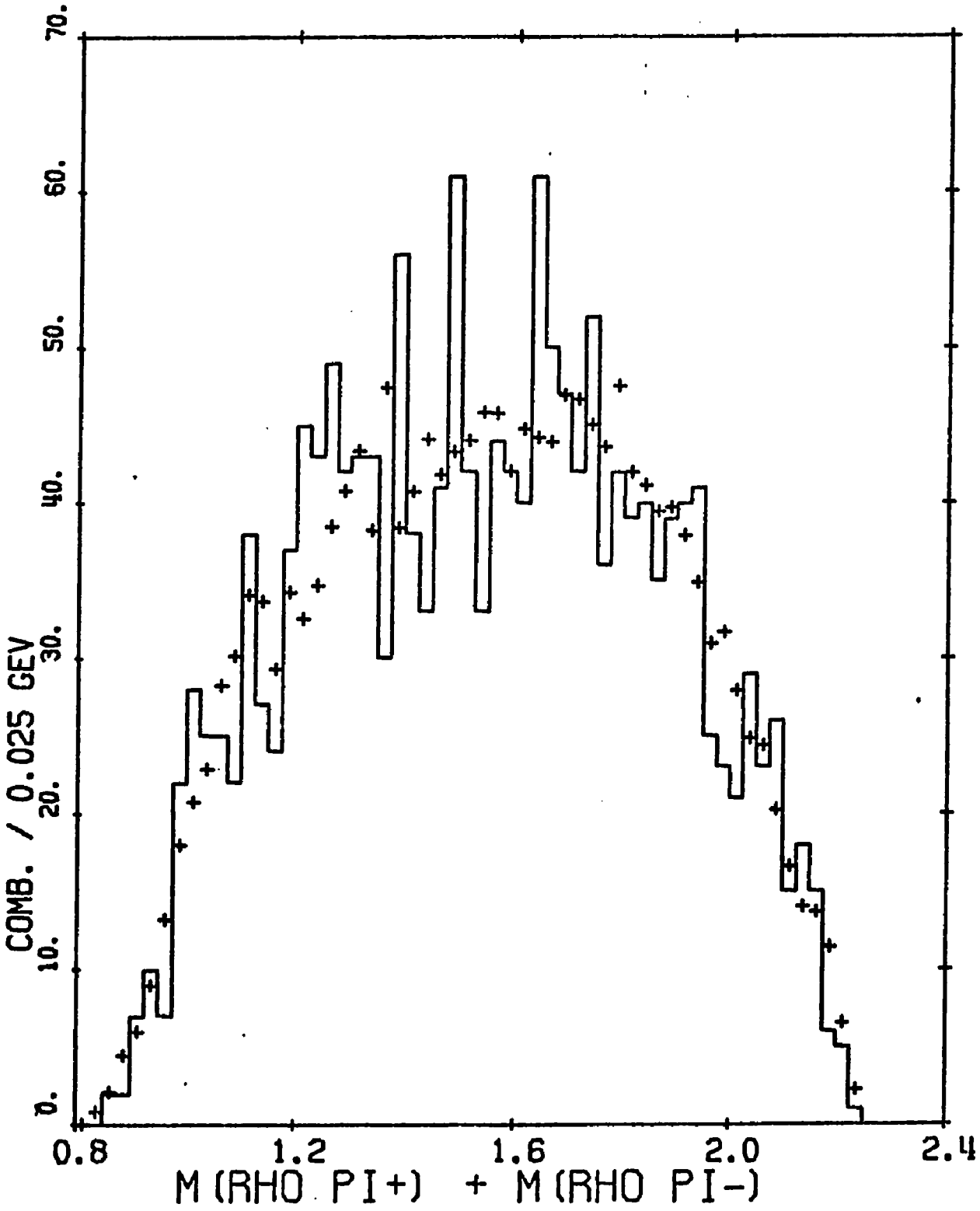


Figure 2.3-23. Mass spectrum of $\rho^{\circ}\pi^{\pm}$ combinations for momenta sets 1.83 and 1.88 GeV/c.

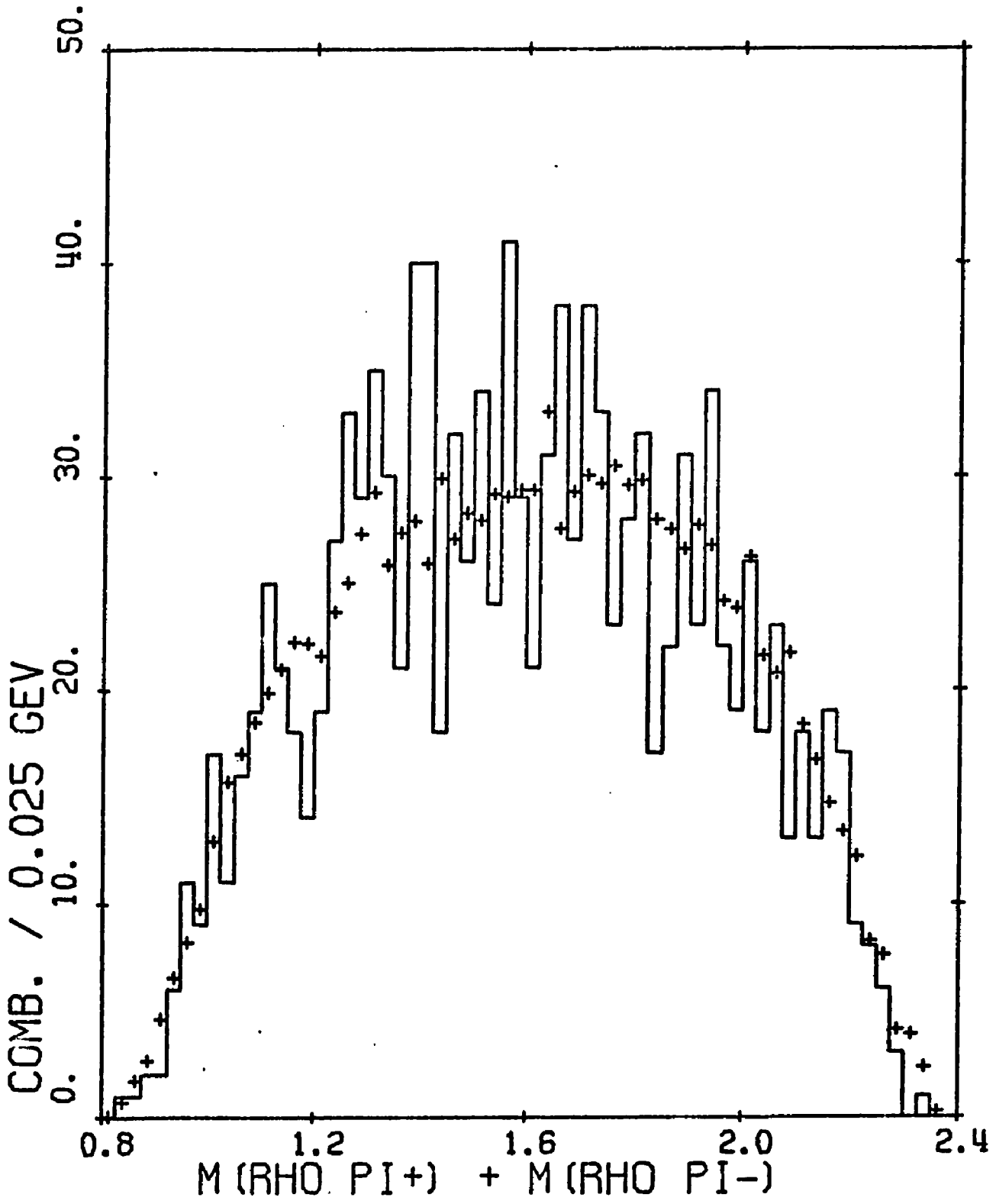


Figure 2.3-24. Mass spectrum of $\rho^{\circ}\pi^{\pm}$ combinations for momenta sets 1.95 and 2.20 GeV/c.

2.4 Resonance Production

The method of maximum likelihood was used to determine the percentages of resonance production. These values were found with the program SHERLOCK (R. Green, 1972), which is similar to the program MURTLEBERT (J. Friedman, 1964; 1966). R. Green has discussed SHERLOCK in great detail; we will give a brief description following a similar notation.

Using the transition rate formula and assuming interference between the resonance channels can be neglected, the probability of a given event is

$$P_\zeta(a_1, a_2, \ldots, a_n) = \sum_{i=1}^{n} a_i |M_i|^2 \rho_\zeta N_i^{-1}$$

where,

a_i = fraction proceeding by channel i($\Sigma a_i = 1$),

M_i = matrix element for the channel i,

ρ_ζ = phase space for ζ th event,

$N_i = \int |M_i|^2 \rho \, dx_i$

ρ = phase space for the transition,

x_i = variables associated with M_i and ρ,

n = number of channels.

The likelihood function, being defined as the probability of the entire experiment, is equal to the product of the probabilities for the individual events

$$L(a_1, a_2, \ldots a_n) = \prod_{\zeta=1}^{NEV} \left(\sum_{i=1}^{n} a_i |M_i|^2 \rho_\zeta N_i^{-1} \right)$$

where,

NEV = the number of events.

The function L is the quantity to be maximized. It is advantageous to maximize log(L) rather than L; this allows us to convert a product into a sum. These are equivalent since log(L) is a monotonically increasing function of L. Dropping the $\Sigma\log(\rho_\zeta)$ term which is a constant for a given set of events, the function to be maximized is

$$g(a_1,a_2,\ldots a_n) = \sum_{\zeta=1}^{NEV} \log\left(\sum_{i=1}^{n} a_i P_{i\zeta}\right)$$

where,

$$P_{i\zeta} = N_i^{-1}|M_i|^2.$$

Instead of maximizing $g(a_1,a_2,\ldots a_n)$, we actually minimized -g the negative of the log likelihood function. This was accomplished with the program MINUIT (F. James, 1969). Both TAUROS and MIGRAD were used to find the minimum; the errors were determined by MINOS.

In the matrix elements, BA(i,j,k,..) represents the Breit-Wigner amplitude and B(i,j,k,..) the Breit-Wigner intensity. The following forms were used:

$$BA(i,j,k,..) = m\Gamma/[m^2_{i,j,k,..} - m^2 - \sqrt{-1}\, m\Gamma],$$

$$B(i,j,k,\ldots) = m^2\Gamma^2/[(m^2_{i,j,k,..} - m^2)^2 + m^2\Gamma^2]$$

where,

$m_{i,j,k,..}$ = effective mass of the i,j,k,.. pion combination,

Γ = width(FWHM),

m = mass of the resonance.

Each $|M_i|^2$ element was appropriately symmetrized with the sums being added incoherently.

The channels included in this analysis were:

(1) $\rho\pi\pi$,

(2) ρf,

(3) $f\pi\pi$,

(4) ff,

(5) $\rho\rho$,

(6) $S^*\pi\pi$,

(7) $A_3\pi$,#

(8) $A_2\pi$,

(9) $A_1\pi$,

(10) $\pi\pi\pi\pi$

Letting 1,2(3,4) represent the negative (positive) pions, the following forms for $|M|^2$ were used.

For phase space: $|M|^2 = 1$;

For $\rho\pi\pi$, $f\pi\pi$, and $S^*\pi\pi$: $|M|^2 = B(1,3)+B(1,4)+B(2,3)+B(2,4)$;

For $\rho\rho$ and ff: $|M|^2 = B(1,3)B(2,4) + B(1,4)B(2,3)$;

For ρf: $|M|^2 = B_\rho(1,3)B_f(2,4) + B_\rho(1,4)B_f(2,3) + B_\rho(2,3)B_f(1,4) + B_\rho(2,4)B_f(1,3)$;

The symbol A_3 is used simply as a convenient notation for the enhancement at 1640 MeV.

For $A_1\pi$ and $A_3\pi$: $|M|^2 = B(1,2,3) + B(1,2,4) + B(1,3,4) + B(2,3,4)$;

For the $A_2\pi$ ($A_2 \to \rho\pi$, $\rho \to \pi\pi$) with Zemach factors (C. Zemach, 1964; 1965 a,b):

$$|M|^2 = \sum_{i=1}^{3}\sum_{j=1}^{3} \{B(1,2,3)|BA(1,3)Z13_{ij} - BA(2,3)Z23_{ij}|^2 + B(1,2,4)|BA(1,4)Z14_{ij} - BA(2,4)Z24_{ij}|^2 + B(1,3,4)|BA(1,3)Z31_{ij} - BA(1,4)Z41_{ij}|^2 + B(2,3,4)|BA(2,3)Z32_{ij} - BA(2,4)Z42_{ij}|^2\}$$

where,

$$Zk\ell_{ij} = (1/2)[(p_{\ell i})(q_j) + (p_{\ell j})(q_i)]/NORM$$

for k = 1,2: $\vec{q} = \vec{p}_1 \times \vec{p}_2$ (evaluated in rest frame of 1,2,ℓ particle comb.)

$$NORM = (m^2_{12\ell} - (3m_\pi)^2)^{3/2},$$

for k = 3,4: $\vec{q} = \vec{p}_3 \times \vec{p}_4$ (evaluated in rest frame of 3,4,ℓ)

$$NORM = (m^2_{34\ell} - (3m_\pi)^2)^{3/2}$$

A general increase in $Zk\ell$ with an increase in the $\pi\pi\pi$ effective mass has been removed by dividing by NORM.

Monte Carlo generated events with weights w_j were used to compare each fit to the data. The weight was calculated from:

$$w = \sum_{i=1}^{n} a_i |M|^2/N_i.$$

The a_i values were determined by the MINUIT fits. Interesting mass distributions were plotted and a χ^2 value for each histogram was calculated giving a measure of the goodness of the fit:

$$\chi^2 = [NEV/(NEV + \sum_k w_k^2)] \sum_{i=1}^{Nb} (\nu_{i_{MC}} - \nu_{i_{EXP}})^2/\nu_{i_{MC}}$$

where,

$\nu_{i_{MC}}$ = number of Monte Carlo events in bin i,

$\nu_{i_{EXP}}$ = number of experimental events in bin i,

w_k = weight of Monte Carlo event k (Σw_k = NEV),

NEV = number of experimental events,

Nb = number of bins.

The factor NEV/(NEV + Σw^2) removes from the χ^2, the part due to the fluctuations in the Monte Carlo (R. Green, 1972).

Phase space plus the following resonance hypotheses were used to fit the 3135 4π events:

(1) $\rho\pi\pi$,

(2) $\rho\pi\pi + \rho f$,

(3) $\rho\pi\pi + \rho f + f\pi\pi$,

(4) $\rho\pi\pi + \rho f + ff$,

(5) $\rho\pi\pi + f\pi\pi + ff$,

(6) $\rho\pi\pi + \rho f + f\pi\pi + ff$,

(7) $\rho\pi\pi + \rho f + f\pi\pi + ff + \rho\rho$,

(8) $\rho\pi\pi + \rho f + f\pi\pi + ff + \rho\rho + S^*\pi\pi + A_3\pi + A_2\pi$,

(9) $\rho\pi\pi + \rho f + f\pi\pi + ff + \rho\rho + S^*\pi\pi + A_3\pi + A_2\pi + A_1\pi$.

Fits were made with a ρ mass from 720-780 MeV and a width from 110-170 MeV; the mass for the f meson ranged from 1240-1280 MeV with a width from 115-160 MeV. The values which produced the best χ^2 were a mass and width of 740, 125 MeV for the ρ and 1260, 150 MeV for the f.* These values differ by about 2 standard deviations from the initial fit in section 2.3. The values used for the other resonances were:

Resonance	Mass (MeV)	Width (MeV)
S^*	1052	76
A_3	1640	30
A_2	1297	91
A_1	1073	97

The results of fits (1) thru (9) are given in Table 2.4-1. We note the dominant channels appear to be $\rho\pi\pi$, ρf, and ff. Looking at fits (3) thru (6), it is observed the f$\pi\pi$ channel goes to 0 +5% in preference to ρf and ff. With such a large error it is difficult to conclude f$\pi\pi$ is not present; however the fit clearly prefers the ff channel. This is surprising since our CM energy ranges from 2300 to 2500 MeV. Because of the relative crudeness of our parameterization, it may well be the ff percentage of 15 ±2 is not an accurate reflection of nature. What appears to be stable are the overall ρ and f percentages. We see that $\rho\rho$, $S^*\pi\pi$ and $A_3\pi$ production are all small and consistent with zero. Slightly more significant percentages of $A_1\pi$ and $A_2\pi$ are indicated, but even these are

*This was for fit (7).

Table 2.4-1. Results of maximum likelihood fits to all the 3135 $\pi^-\pi^-\pi^+\pi^+$ events in percent of the 4π cross section using hypotheses (1) thru (9)--see text.

Channel	Fit								
	(1)	(2)	(3)	(4)	(5)	(6)	(7)	(8)	(9)
$\rho\pi\pi$	51±4	33±4	50±5	43±4	58±4	43±4	39±6	32±7	30±6
ρf	-	24±3	12±4	19±3	-	19±3	20±3	20±3	21±3
$f\pi\pi$	-	-	26±5	-	22±5	0+5**	0+4	0+4	0+5
ff	-	-	-	15±2	10±3	15±2	14±2	14±2	15^{+3}_{-2}
$\rho\rho$	-	-	-	-	-	-	2±2	2±2	2±2
$S^*\pi\pi$	-	-	-	-	-	-	-	0+1	0+1
$A_3\pi$	-	-	-	-	-	-	-	1±2	2±2
$A_2\pi$	-	-	-	-	-	-	-	4±2	5±2
$A_1\pi$	-	-	-	-	-	-	-	-	4±6
Phase Space	49	43	12	23	10	23	25	27	21
All ρ	51	57	62	62	58	62	63	60	60
All f	-	24	37	49	42	49	48	48	51

**When negative error is not given the percentage is consistent with zero.

only ~2 standard deviations away from zero.

The results of the Monte Carlo simulations for fits (1) thru (9) are given in Table 2.4-2; χ^2 values for 100 % phase space are included for completeness. Comparing fits (3) and (4), we see a markedly better χ^2 when the ff channel is included instead of $f\pi\pi$. Even our best fit to the data is not very good, giving a total χ^2 of 747 for 368 bins; the mass distributions generated by this simulation are shown as plus marks in Figures 2.3-1 thru 6.

Fits were done to various data sets to examine variations with $\bar{p}$ momentum. Table 2.4-3 presents the results. Even with the large errors we see the following trends: (1) the percentage ρf decreases with $\bar{p}$ momentum; (2) a decrease in $\rho\pi\pi$ with increasing $\bar{p}$ momentum is suggested; (3) $\rho\rho$ may be present at our lowest momentum; (4) $f\pi\pi$ begins to be favored over ff at our highest momentum 2.20 GeV/c.

Examining the doubly charged mass spectrum (Figure 2.3-1) the Monte Carlo simulation is observed to systematically predict too many events with high invariant mass. A possible explanation has been known for over a decade (G. Goldhaber, 1960). The effect of Bose-Einstein statistics(BES) for identical particles is incorporated by Goldhaber into Fermi phase space. BES lead to a tendency for identical particles to leave the interaction volume in the same direction. This shifts the $\pi^{\pm}\pi^{\pm}$ spectrum towards lower mass.

The Goldhaber effect has been incorporated into our maximum likelihood fits. This changes the $|M|^2$ element for

Table 2.4-2. χ^2 values from Monte Carlo generated distributions for fits (1) thru (9)--(see text). Histograms (1) thru (6) correspond to Figures 2.3-1 thru 2.3-6, respectively.

Fit	χ^2 for Histograms						
	(1)	(2)	(3)	(4)	(5)	(6)	Total
Phase Space	171	801	200	197	138	330	1837
(1)	245	363	188	103	159	315	1374
(2)	202	164	129	168	112	230	1005
(3)	207	179	111	113	112	192	914
(4)	184	182	118	58	107	178	827
(5)	204	198	124	77	131	184	918
(6)	184	182	118	58	107	178	827
(7)	176	211	108	64	110	183	852
(8)	165	211	102	67	96	167	808
(9)	177	168	102	57	91	152	747
Bins	70	69	59	39	59	72	368

Table 2.4-3. Results of maximum likelihood fits in percent of $\pi^-\pi^-\pi^+\pi^+$ cross section for various momentum sets.

Channel	Beam momentum and number of events in each set.					
	1.63 (569)	1.77,1.83 1.88,1.95 (2244)	2.20 (322)	1.63 1.77 (1172)	1.83 1.88 (1147)	1.95 2.20 GeV/c (816)
$\rho\pi\pi$	10±17	32^{+7}_{-8}	48±20	30±11	26^{+10}_{-11}	44±14
ρf	27±9	21±4	11±11	28±6	20±5	6+8**
$f\pi\pi$	0+13	0+5	6+18	0+8	0+4	14±13
ff	14^{+7}_{-8}	16±3	1+6	14^{+5}_{-4}	15±4	11^{+6}_{-5}
$\rho\rho$	9±5	0+2	1+6	2±3	1+3	2+4
$S^*\pi\pi$	0+3	0+1	1+7	0+2	0+2	0+2
$A_3\pi$	4+4	1+2	4+6	2+3	1+3	3+3
$A_2\pi$	7^{+5}_{-4}	4±2	7±6	7±3	4±3	5^{+4}_{-3}
$A_1\pi$	0+4	5±3	3+6	4±3	5±3	4^{+4}_{-3}
Phase Space	29	21	18	13	28	11

**When negative error is not given, the percentage is consistent with zero.

phase space from unity to:

$$|M|^2 = G(\pi_1^-, \pi_2^-) \cdot G(\pi_3^+, \pi_4^+)$$

where,

$G(\pi_i, \pi_j) = 1 + e^{-\alpha x_{ij}}$,

$\alpha = (1/2.15)^2 (\gamma \Lambda_\pi)^2$,

$\Lambda_\pi = h/m_\pi c$ = pion Compton wavelength,

γ = dimensionless parameter measuring size of interaction volume,

$x_{ij} = |\vec{p}_i - \vec{p}_j|^2$,

$\vec{p}_i$ = three-momentum of particle i in the CM.

Fits were made with γ ranging from 0.0 to 1.6. Table 2.4-4 gives the results. The best χ^2 value is obtained with $\gamma = 0$, i.e., no Goldhaber effect. Nevertheless, the values do not change very markedly; χ^2 is quite insensitive to γ. In contrast, however, the $f\pi\pi$ and phase space percentages are especially sensitive with $f\pi\pi$ varying from 0 to 14 and phase space from 21 to 1 percent. We see there is significant uncertainties which depend on the parameterization in addition to the statistical errors. This fact must be kept in mind when the results are compared to other experiments.

In Table 2.4-5 the results of our maximum likelihood analysis are compared to fits that have been done at $\bar{p}$ momentum 0.94, 1.20, 2.50 GeV/c. The experiments agree reasonably well; several trends are clear from 0.94 to 2.50 GeV/c. The $\rho\pi\pi$ channel increases to ~50 percent at 2.5 GeV/c from ~10 percent . Over the momentum range ρf decreases from ~30 percent to ~0 at 2.5 GeV/c; $S^*\pi\pi$ increases from ~0 to ~10

Table 2.4-4. Results of maximum likelihood fits in percent of $\pi^-\pi^-\pi^+\pi^+$ cross section and χ^2 values for entire set of 3135 events with Goldhaber parameter ranging from 0.0 to 1.6 pion Compton wavelengths--(see text). Histograms (1) thru (6) correspond to Figures 2.3-1 thru 2.3-6, respectively.

Channel	γ Values									
	0.00	0.04	0.10	0.20	0.40	0.50	0.60	0.80	1.20	1.60
$\rho\pi\pi$	30	32	42	45	45	45	43	38	32	31
ρf	21	20	16	14	14	14	15	18	20	20
$f\pi\pi$	0	0	10	13	14	13	10	5	0	1
ff	15	16	14	13	13	13	14	15	16	15
$\rho\rho$	2	2	0	0	0	0	0	1	2	1
$S^*\pi\pi$	0	0	0	0	0	0	0	0	0	0
$A_3\pi$	2	2	2	2	2	2	2	2	2	2
$A_2\pi$	5	5	5	5	5	5	5	5	5	5
$A_1\pi$	4	4	6	6	6	6	6	5	4	4
Phase Space	21	19	5	2	1	2	5	11	19	21
Histogram	χ^2 Values									
(1)	177	177	183	188	188	188	188	189	184	181
(2)	168	168	177	183	183	183	179	175	171	170
(3)	102	102	103	101	101	101	102	102	102	103
(4)	57	57	57	58	58	58	57	56	57	57
(5)	91	91	91	93	93	93	92	93	93	92
(6)	152	152	153	154	154	154	154	154	154	155
Total	747	747	764	777	777	777	772	769	761	758

Table 2.4-5. Comparison of $\pi^-\pi^-\pi^+\pi^+$ maximum likelihood fits from this experiment with those at 0.94 GeV/c (R. Burns, et al., 1970), 1.2 GeV/c (R. Donald, et al., 1968), and 2.5 GeV/c (J. Clayton, et al., 1970) in percent of 4π cross section.*

Channel	$\bar{p}$ Momentum (GeV/c)					
	0.94	1.20	1.63	1.77 1.88 1.83 1.95	2.20	2.50
$\rho\pi\pi$	19±8	0±11	10±17	32^{+7}_{-8}	48±20	51±3
ρf	30±3	21±4	27±9	21±4	11±11	$<10^{-2}$
$f\pi\pi$	8±4	9±4	0+13	0+5	6±18	39±3
ff	-	-	14^{+7}_{-8}	16±3	1+6	$<10^{-3}$
$\rho\rho$	8±3	11±4	9±5	0+2	1+6	$<10^{-3}$
$S^*\pi\pi$	-	-	0+3	0+1	1+7	9±2
$A_3\pi$	-	-	4+4	1+2	4+6	-
$A_2\pi$	10±3	21±4	7^{+5}_{-4}	4±2	7±6	no evidence
$A_1\pi$	no evid.	11±4	0+4	5±3	3+6	-
$\pi\pi\pi\pi$	25	27	29	21	18	1

*The parameterizations used in the earlier experiments are similar but not identical to our formulation. The errors quoted in the 2.50 GeV/c experiment appear to be too small.

at 2.5 GeV/c; $A_{2\pi}$ decreases from ~15 to ~0 percent. Because of the problems already discussed in the $f\pi\pi$ and ff channels, it is hard to say what is happening in detail; it appears that $f\pi\pi$ may be increasing from ~10 percent at 0.94 GeV/c to ~40 percent at 2.5 GeV/c.

2.5 Angular Distributions

The CM $\cos(\theta)$ distribution for the pions is presented in Figure 2.5-1.* The angular distributions for the plus and minus pions were combined, since within statistics the distributions were identical. An effect which we have called "charge inertia" is present. There is a large peak in the forward direction and a much smaller backward peak. Other experiments reveal this effect becomes more pronounced as the CM energy is increased (R. Burns, et al., 1971; R. Donald, et al.,1970; A. Accensi, et al., 1966). No striking differences were observed when the distributions were examined for each momentum set.

The Forward-Backward ratio is shown in Figure 2.5-2 as a function of the pion momentum in the CM. F(B) is defined as the number of pions having $\cos(\theta)$ greater than zero (less than zero). As expected the positive and negative pions have similar distributions and have been combined. The ratio is basically increasing with pion momentum. The same behavior was seen at 1.2 GeV/c (R. Donald, et al., 1968).

*Throughout this section the angle of a pion is measured relative to its nucleon of like charge.

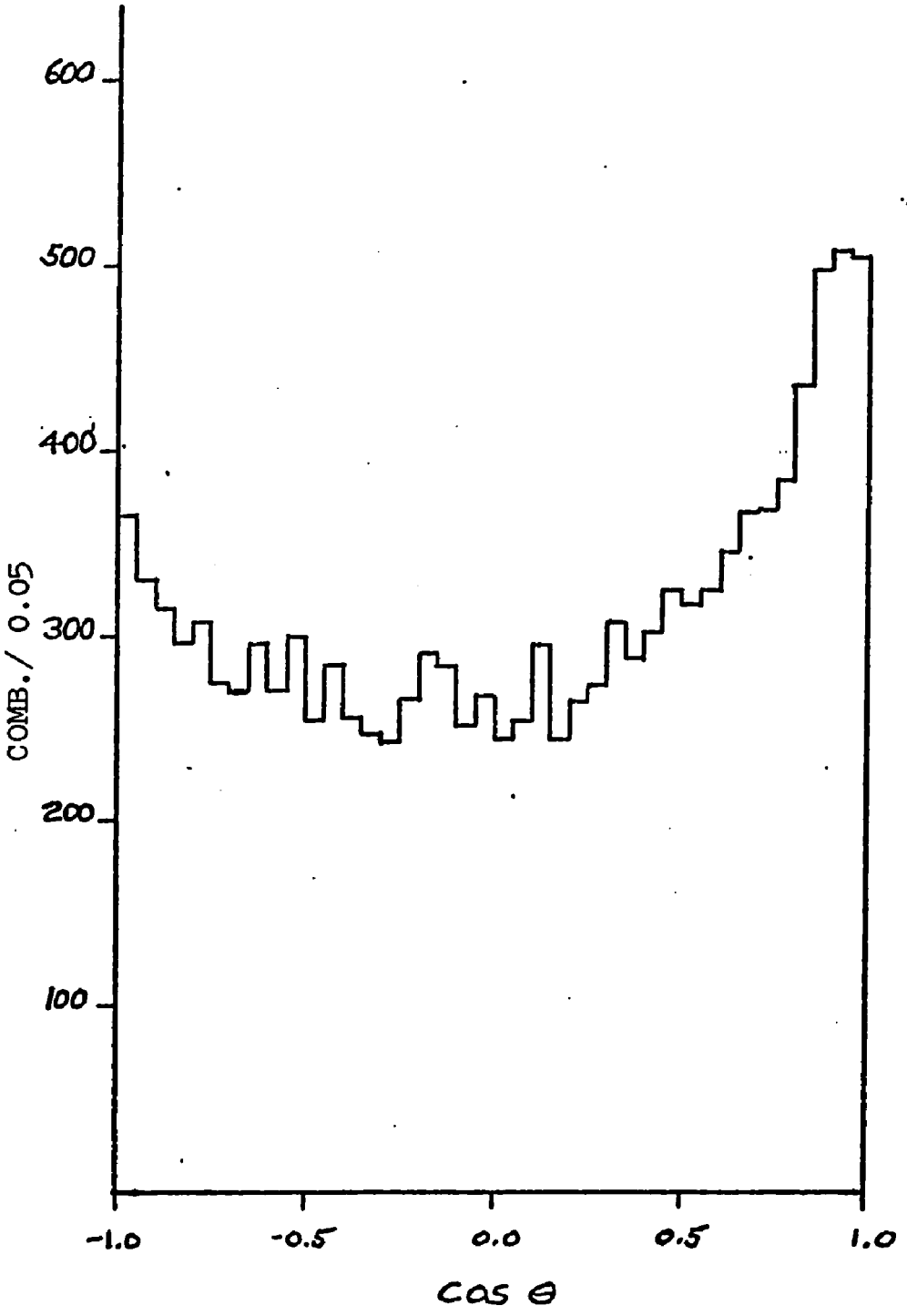


Figure 2.5-1. Angular distribution of pions in center of momentum frame.

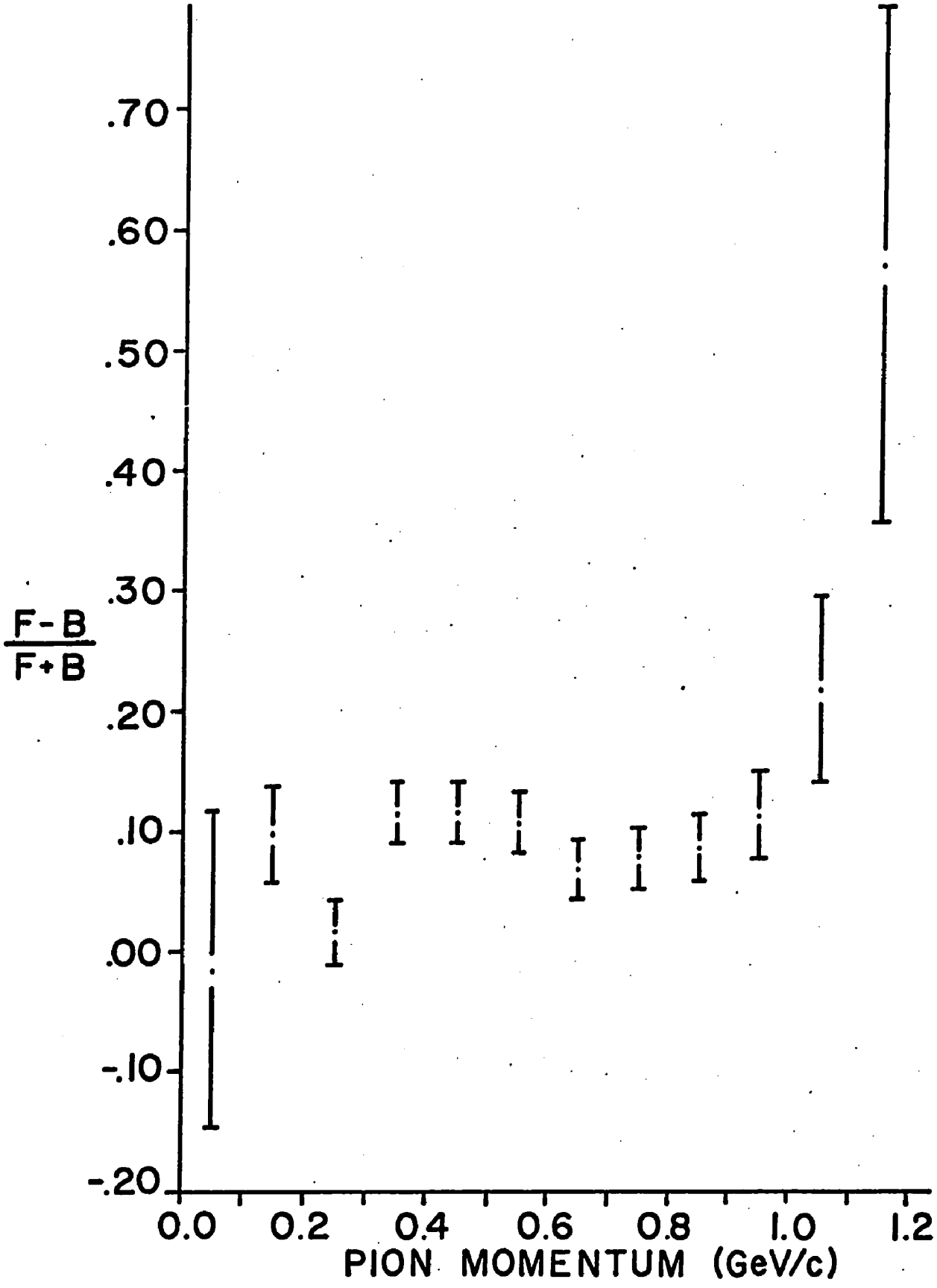


Figure 2.5-2. Forward-Backward ratio as a function of pion momentum in the CM system.

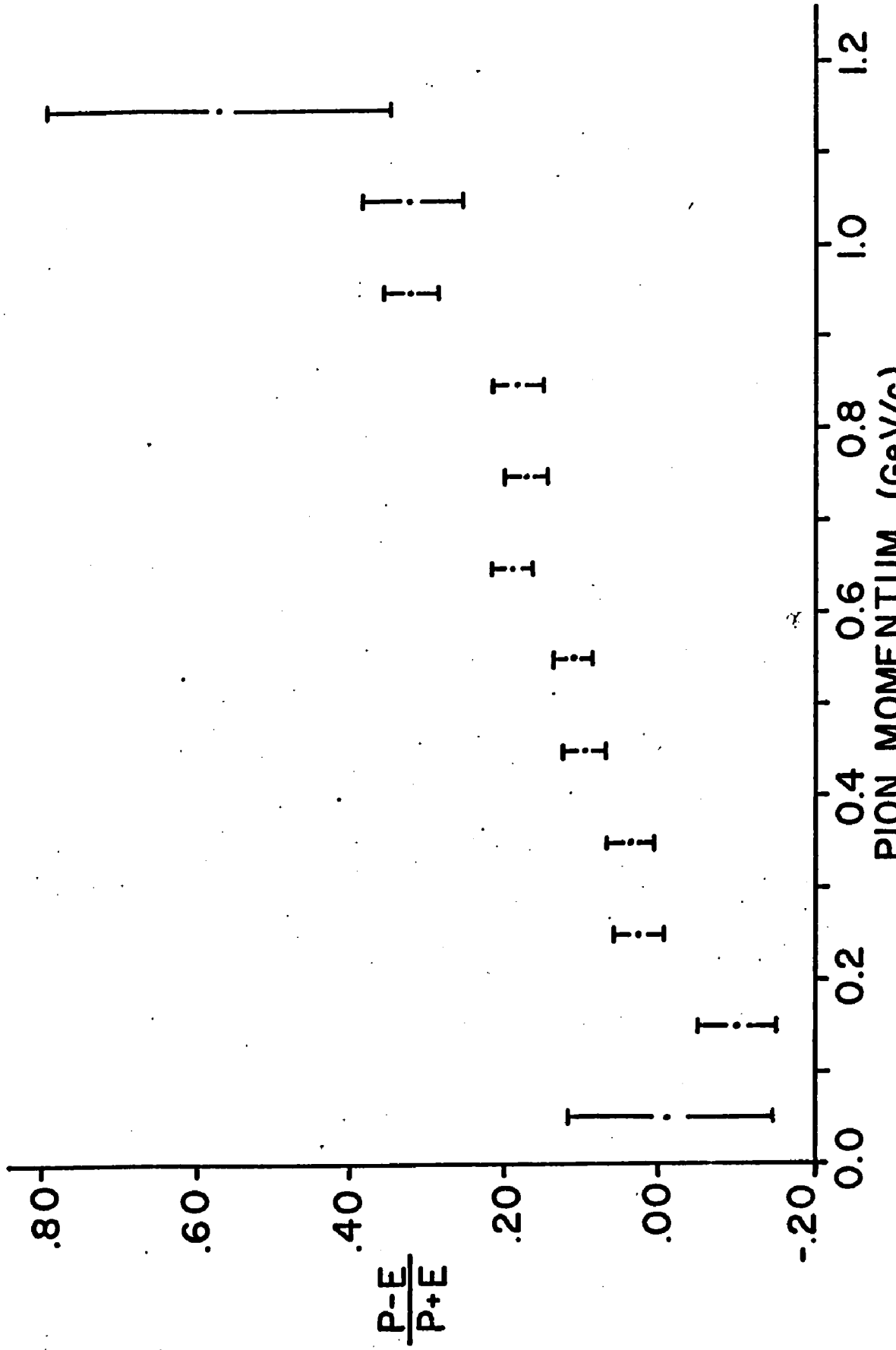


Figure 2.5-3. Polar-Equatorial ratio as a function of pion momentum in the CM.

Figure 2.5-3 shows the Polar-Equatorial ratio (P-E)/(P+E) depends on the pion momentum in the CM; P (E) is the number of pions inside (outside) a double cone with an opening angle of 60° centered about the $\bar{p}p$ axis. This ratio also generally increases with pion momentum. Donald, et al., see a similar dependence.

2.6 Spin Density Matrix Elements

When a resonance with spin J decays into two pions (spin 0), the spin angular momentum is transformed into orbital angular momentum. The angular part of this final state can be described by the wave function

$$\Psi_J = \sum_{m=-J}^{J} a_{Jm} Y_J^m(\theta,\varphi),$$

where Y_J^m is a spherical harmonic. The decay distribution is then given by

$$\langle \Psi_J | \Psi_J \rangle = \sum_{m=-J}^{J} \sum_{\ell=-J}^{J} a_{Jm}\, a_{J\ell}^*\, Y_J^m(\theta,\varphi)\; Y_J^\ell(\theta,\varphi)^*$$

The density matrix elements for a pure state such as this are defined as $\rho_{nm} = a_{Jn} a_{Jm}^*$. For a state which is a mixture of various angular momenta, the general definition is

$$\rho_{nm} = \sum_i p_i\, a_{J_i n}\, a_{J_i m}^* \,/ \left(\sum_i p_i\right)$$

where,

p_i = weight of the pure state J_i.

The properties of the neutral dipion decay distributions have been examined in both the Gottfried-Jackson (GJ) and the Helicity reference frames. These are defined in the dipion CM by the unit vectors:

GJ Frame	Helicity Frame
$\hat{z} = \vec{P}_b / \lvert\vec{P}_b\rvert$	$\hat{z} = -\vec{P}_r / \lvert\vec{P}_r\rvert$
$\hat{y} = \vec{P}'_b \times \vec{P}_d / \lvert\vec{P}'_b\rVert\vec{P}_d\rvert$	$\hat{y} = \vec{P}'_b \times \vec{P}_d / \lvert\vec{P}'_b\rVert\vec{P}_d\rvert$
$\hat{x} = \hat{y} \times \hat{z}$	$\hat{x} = \hat{y} \times \hat{z}$

where,

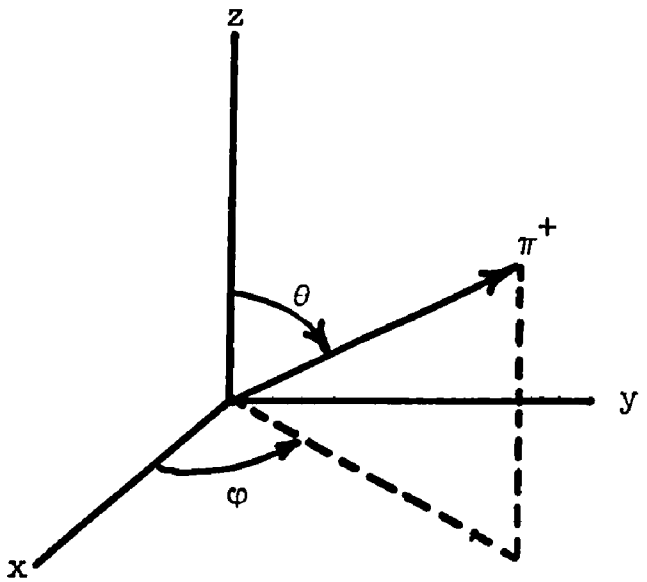
$\vec{P}_b$= beam momentum in dipion CM,

$\vec{P}'_b$= beam momentum in lab frame,

$\vec{P}_d$= dipion momentum in lab frame,

$\vec{P}_r$= recoil $\pi^+\pi^-$ momentum in dipion CM.

The decay angles θ and φ in the dipion CM are defined below.



Figures 2.6-1 thru 2.6-20 show the $\cos(\theta)$ and φ distributions as a function of the dipion mass. The curves indicated with plus marks are the results of fitting the data assuming only S and P waves are present. The normalized S and P wave decay distribution has the following form (L. Lovell, 1968):

$$W(\theta,\varphi) = (1/4\pi)\{[1 + 3(\rho_{00}-\rho_{11})(\cos^2(\theta) - (1/3)] - 3\sqrt{2}\,\mathrm{Re}(\rho_{10})\sin(2\theta)\cos(\varphi) + -3\rho_{1-1}\sin^2(\theta)\cos(2\varphi) + 2\sqrt{3}\mathrm{Re}(\rho_{00}^{int})\cos(\theta) + -2\sqrt{6}\,\mathrm{Re}(\rho_{10}^{int})\sin(\theta)\cos(\varphi)\}.$$

A moment analysis was used to determine the best fit. Table 2.6-1 gives the parameters and their errors for the 0-668, 668-810, 810-1154, 1154-1332, and above 1332 MeV mass bands. In order to examine in greater detail the behavior of the spin density parameters, the fits were repeated using smaller mass bands. The results are presented in Figures 2.6-21 thru 2.6-25. All of the parameters vary rather smoothly with the dipion mass; no striking changes occur in the ρ region. The χ^2 values for these fits are given in Table 2.6-2.

The neutral dipion combinations in the ρ region were also studied as a function of t, the four-momentum transfer squared.

$$t = (P_{beam} - P_{dipion})^2$$

$$= (E_{beam} - E_{dipion})^2 - (\vec{P}_{beam} - \vec{P}_{dipion})^2$$

Table 2.6-1. Results of (S,P) wave fit to the neutral dipion distributions in the Gottfried-Jackson and the Helicity Frames for various mass cuts--(see text).

Mass Range (MeV)	$(\rho_{00}-\rho_{11})$	$Re(\rho_{10})$	ρ_{1-1}	$Re(\rho_{00}^{int})$	$Re(\rho_{10}^{int})$	$\chi^2(\theta)$ (50)	$\chi^2(\varphi)$ (50 bins)
GJ Frame:							
0-668	-.05±.02	-.02±.01	.01±.01	-.02±.01	.02±.01	52	58
668-810	-.09±.02	-.03±.01	.01±.01	-.04±.01	.04±.01	40	73
810-1154	.03±.02	-.07±.01	-.03±.01	-.06±.01	.02±.01	56	42
1154-1332	.14±.03	-.11±.01	-.01±.01	-.06±.01	.02±.01	51	54
>1332	.31±.03	-.09±.01	.01±.01	-.10±.01	.03±.01	74	41
Helicity Frame:							
0-668	-.05±.02	.00±.01	.01±.01	.00±.01	-.02±.01	64	43
668-810	-.09±.02	.01±.01	.01±.01	.00±.01	-.04±.01	45	72
810-1154	-.05±.02	.01±.01	-.05±.01	-.01±.01	-.05±.01	65	50
1154-1332	-.09±.03	.01±.01	-.09±.02	.02±.01	-.02±.01	38	60
>1332	-.05±.03	.03±.01	-.11±.02	.01±.01	-.01±.01	48	84

Table 2.6-2. The χ^2 values for (S,P) wave fits in the Gottfried-Jackson and the Helicity Frames. Each distribution was divided into 50 bins.

Mass Range (MeV)	GJ Frame $\chi^2(\theta)$	GJ Frame $\chi^2(\varphi)$	Helicity Frame $\chi^2(\theta)$	Helicity Frame $\chi^2(\varphi)$
275-400	56	35	55	56
400-475	40	80	47	62
475-525	86	56	92	50
525-575	47	82	42	69
575-625	74	43	69	33
625-675	35	96	34	52
675-725	49	55	46	59
725-775	52	50	59	56
775-825	32	58	54	67
825-875	56	42	85	50
875-925	55	68	64	73
925-975	81	54	51	47
975-1025	65	96	53	50
1025-1075	111	69	62	57
1075-1125	91	99	56	93

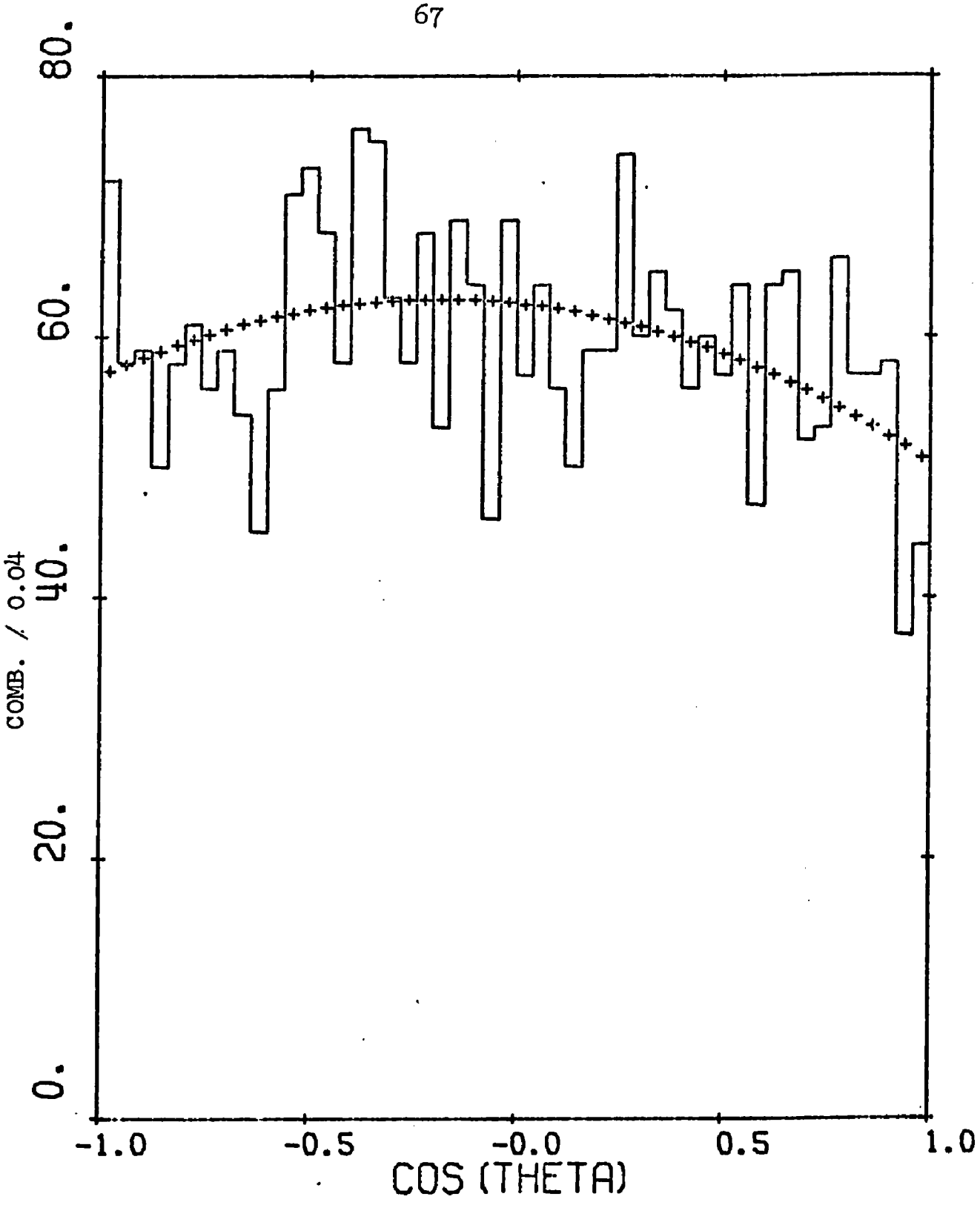


Figure 2.6-1. Cos(θ) decay distribution in GJ frame of the neutral dipion combinations with invariant mass $\leq$ 668 MeV.

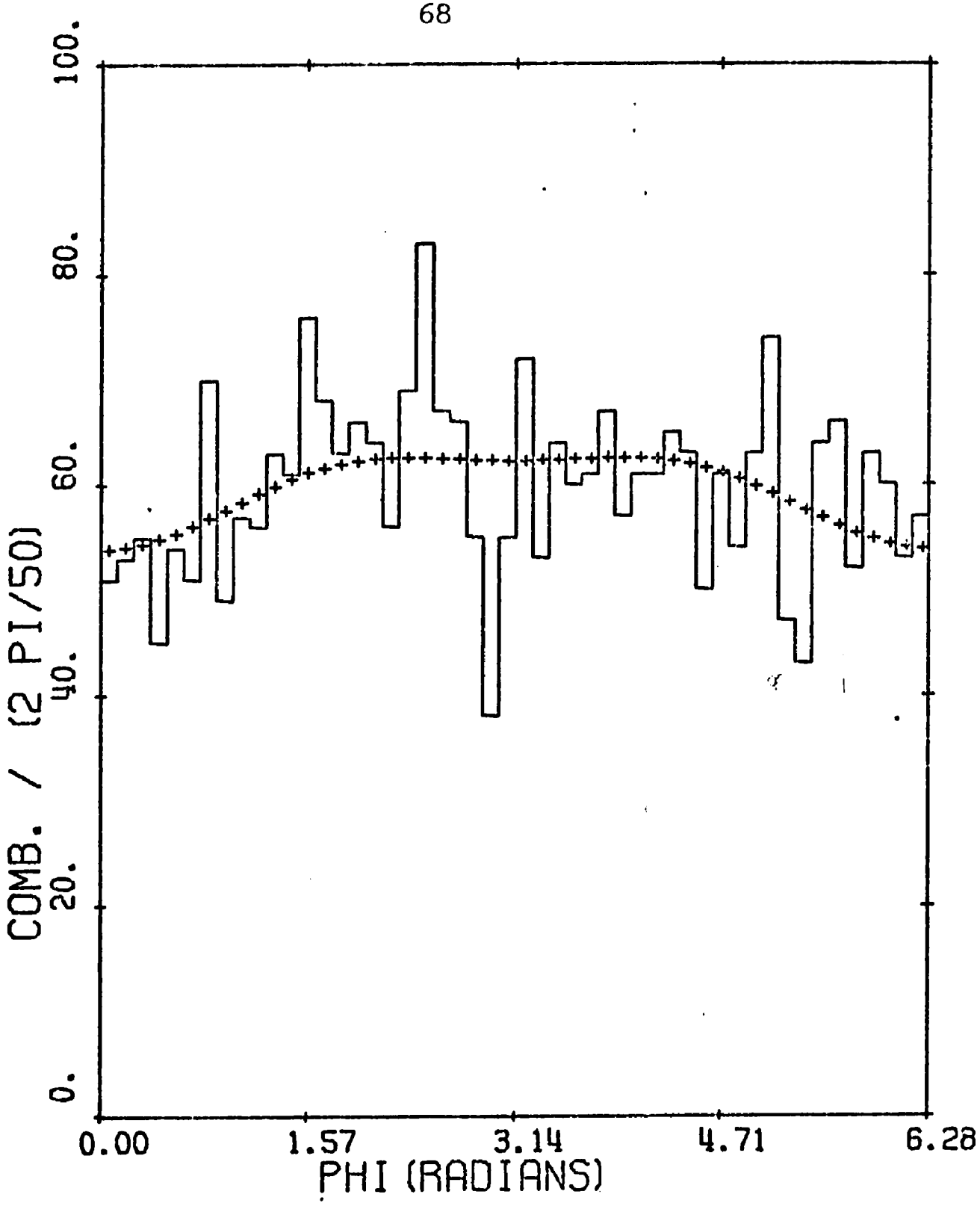


Figure 2.6-2. The φ decay distribution in GJ frame of neutral dipion combinations with invariant mass $\leq$ 668 MeV.

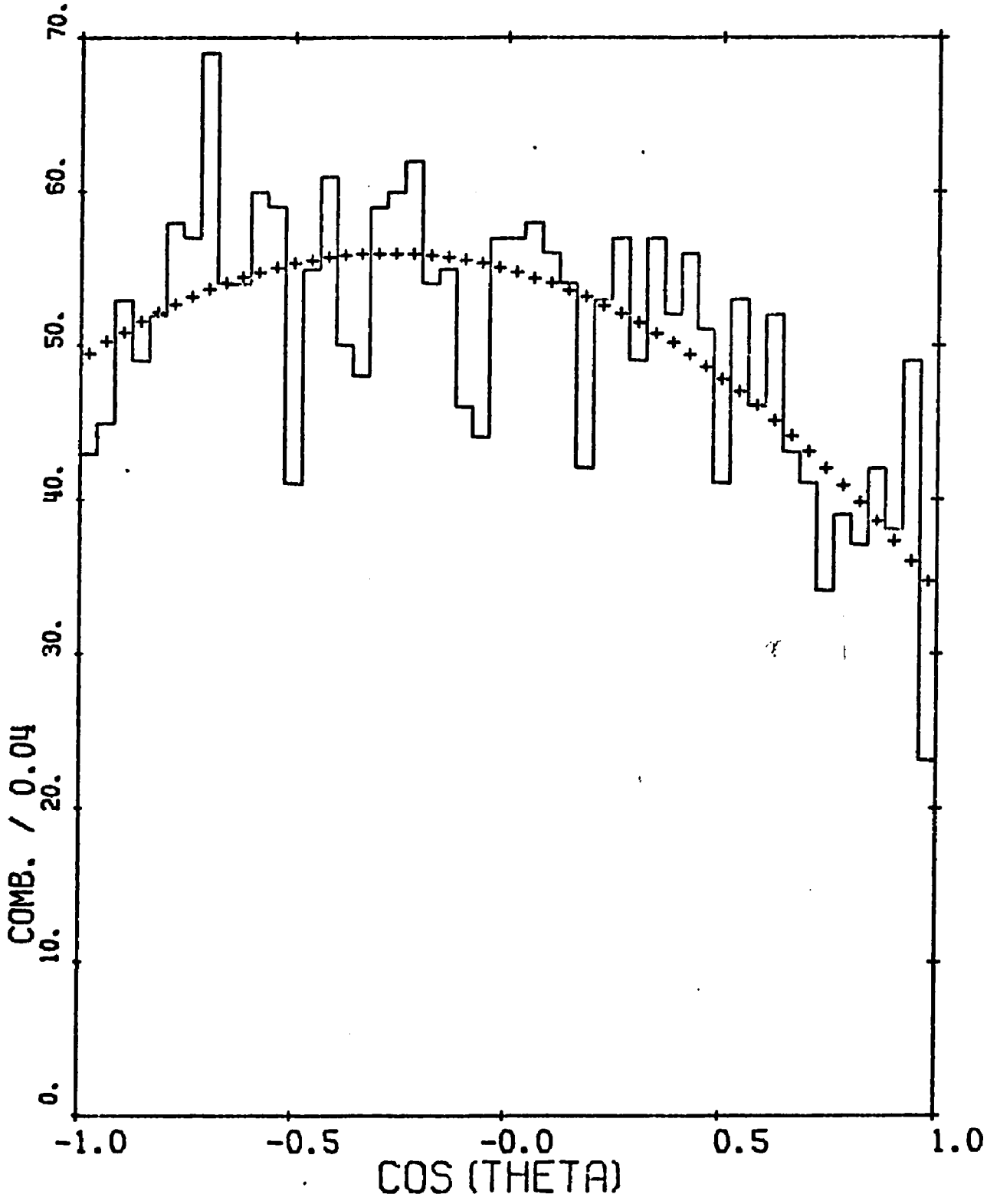


Figure 2.6-3. Cos(θ) decay distribution in GJ frame of neutral dipion combinations with invariant mass in the ρ region(668-810 MeV).

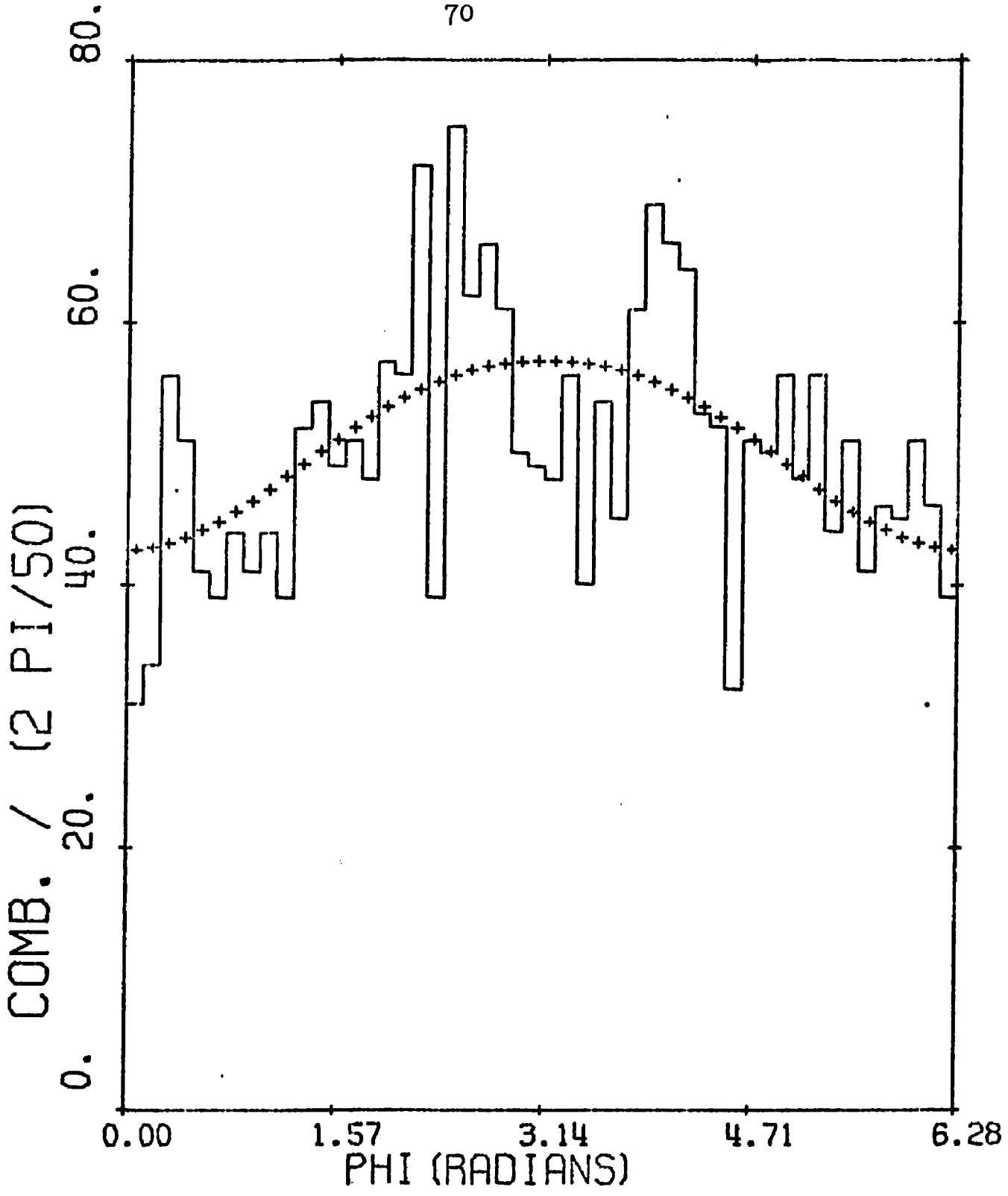


Figure 2.6-4. The φ decay distribution in GJ frame for neutral dipion combinations with invariant mass in ρ region.

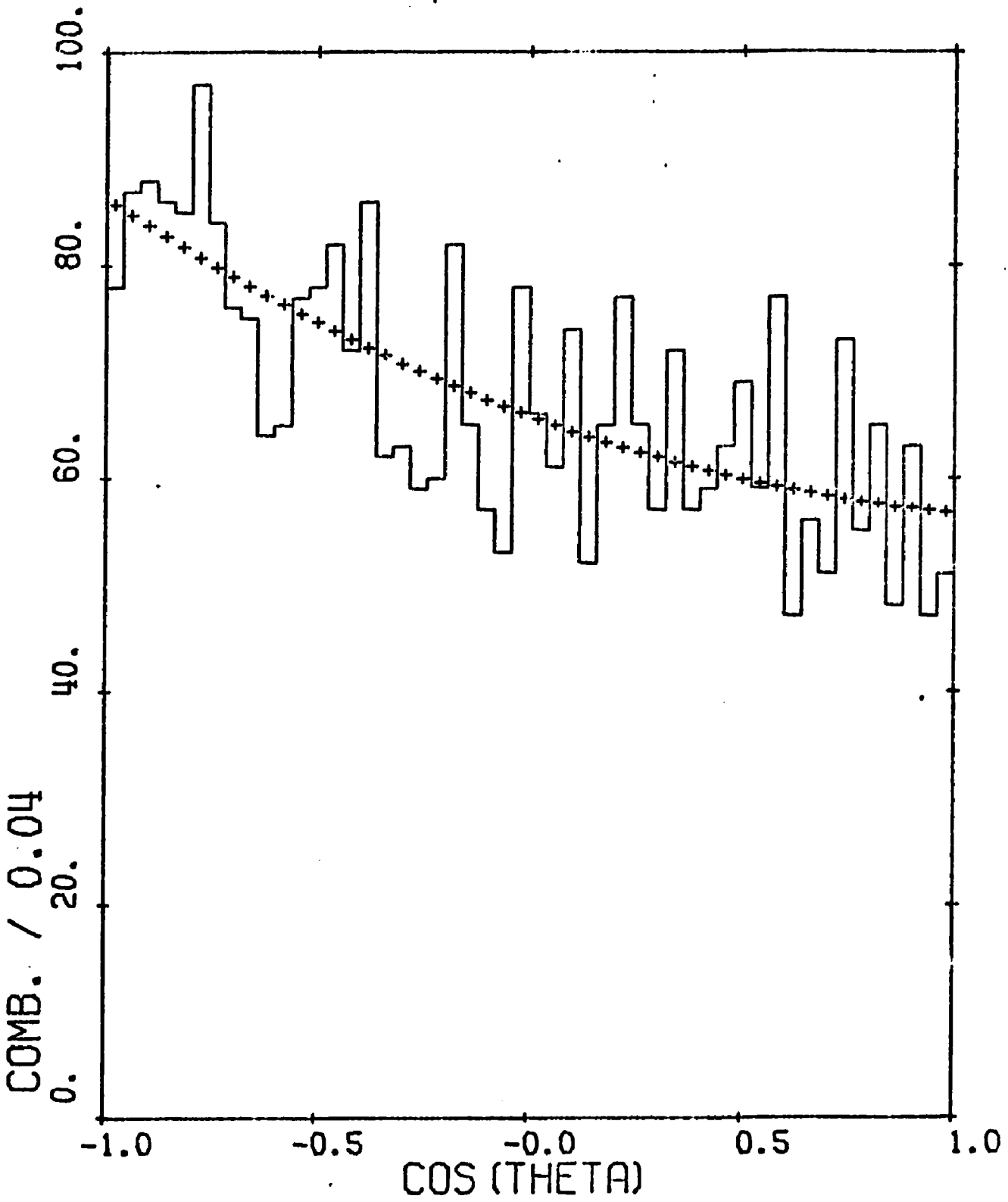


Figure 2.6-5. Cos(θ) decay distribution in GJ frame of neutral dipion combinations with invariant mass between 810 and 1154 MeV.

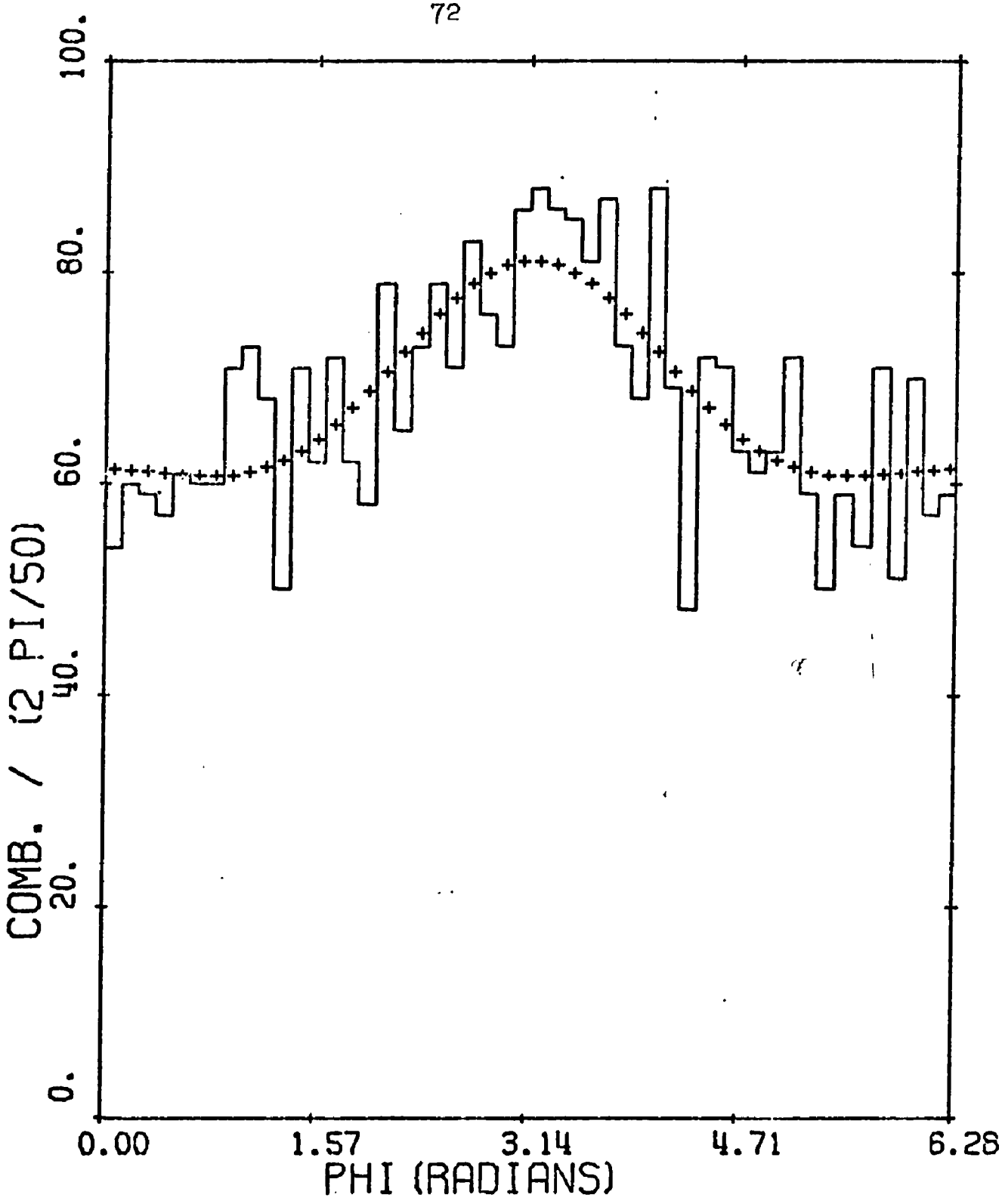


Figure 2.6-6. The φ decay distribution in GJ frame for neutral dipion combinations with invariant mass between 810 and 1154 MeV.

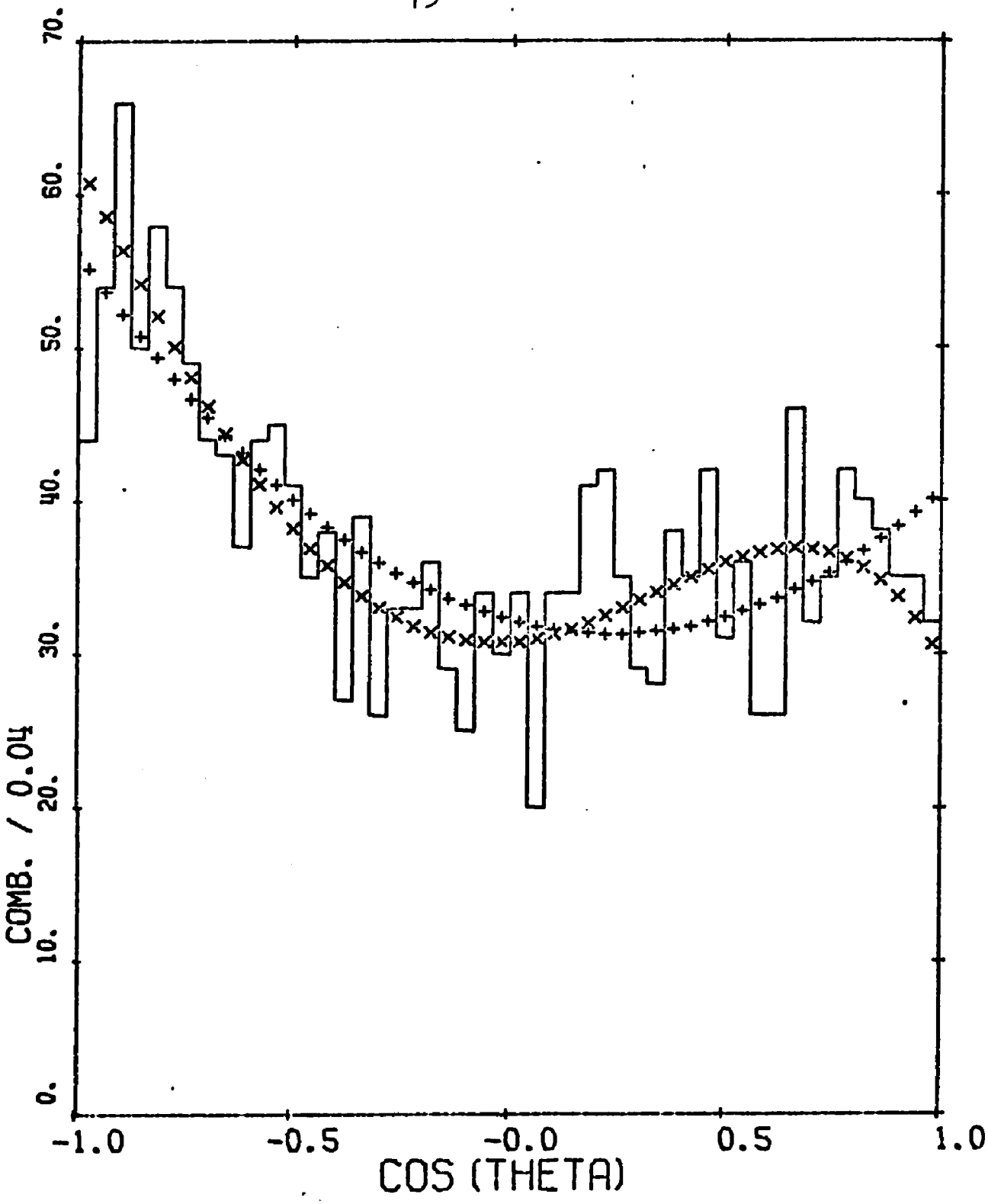


Figure 2.6-7. Cos(θ) decay distribution in GJ frame of neutral dipion combination with invariant mass in f region (1154-1332 MeV).

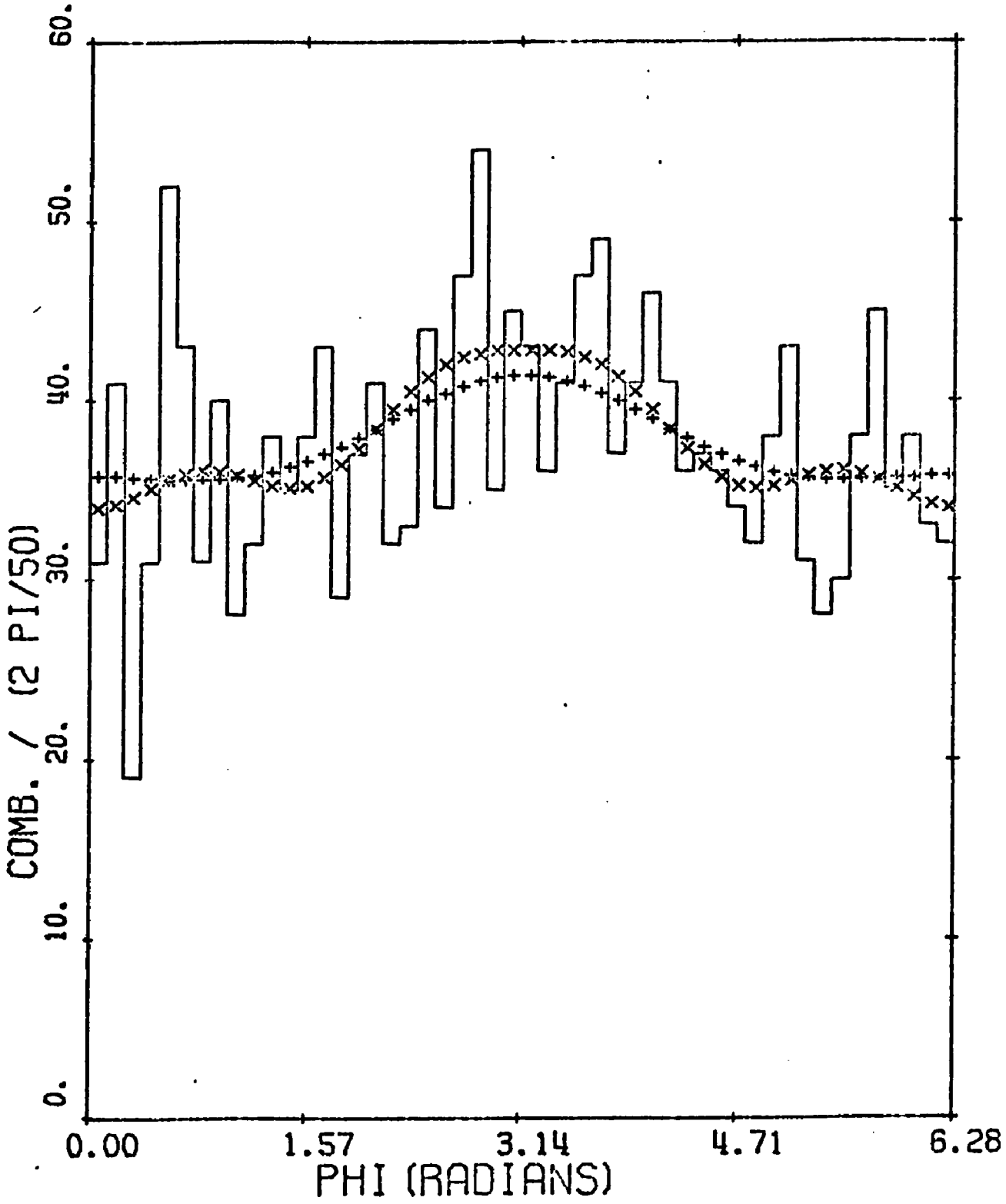


Figure 2.6-8. The φ decay distribution in GJ frame for the neutral dipion combinations with invariant mass in the f region.

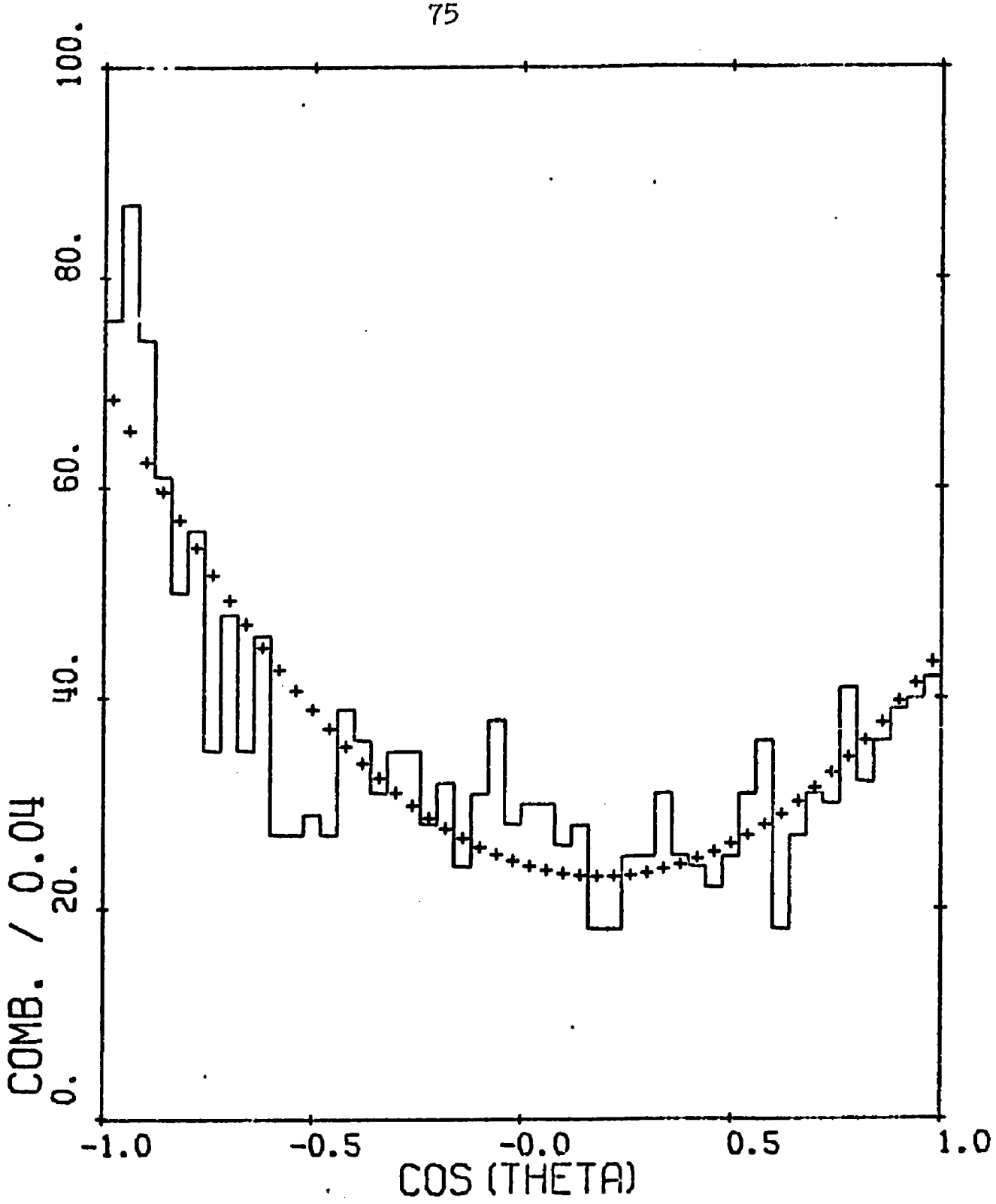


Figure 2.6-9. Cos(θ) decay distribution in GJ frame of neutral dipion combinations with invariant mass greater than 1332 MeV.

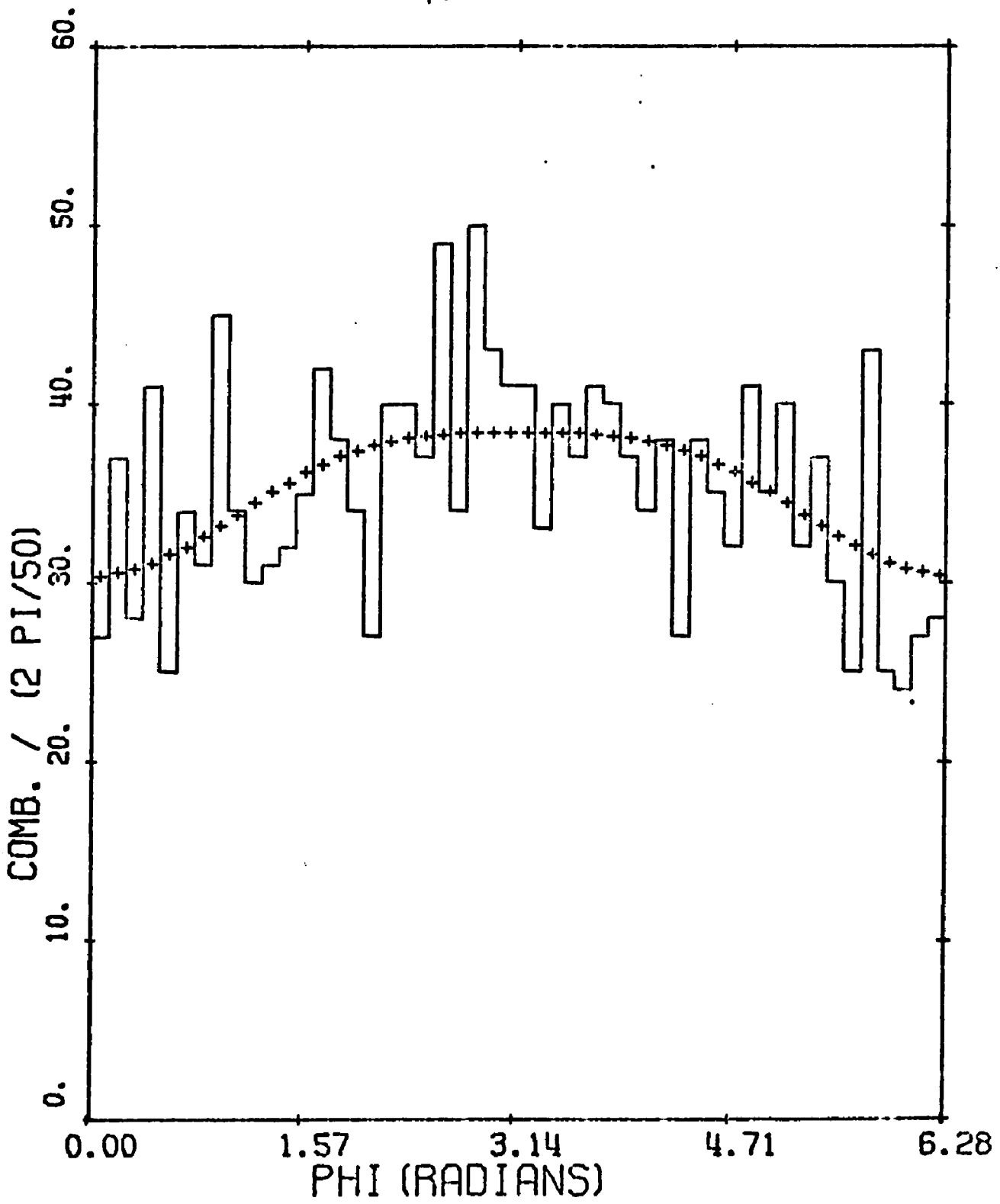


Figure 2.6-10. The φ decay distribution in the GJ frame of the neutral dipion combinations with invariant mass greater than 1332 MeV.

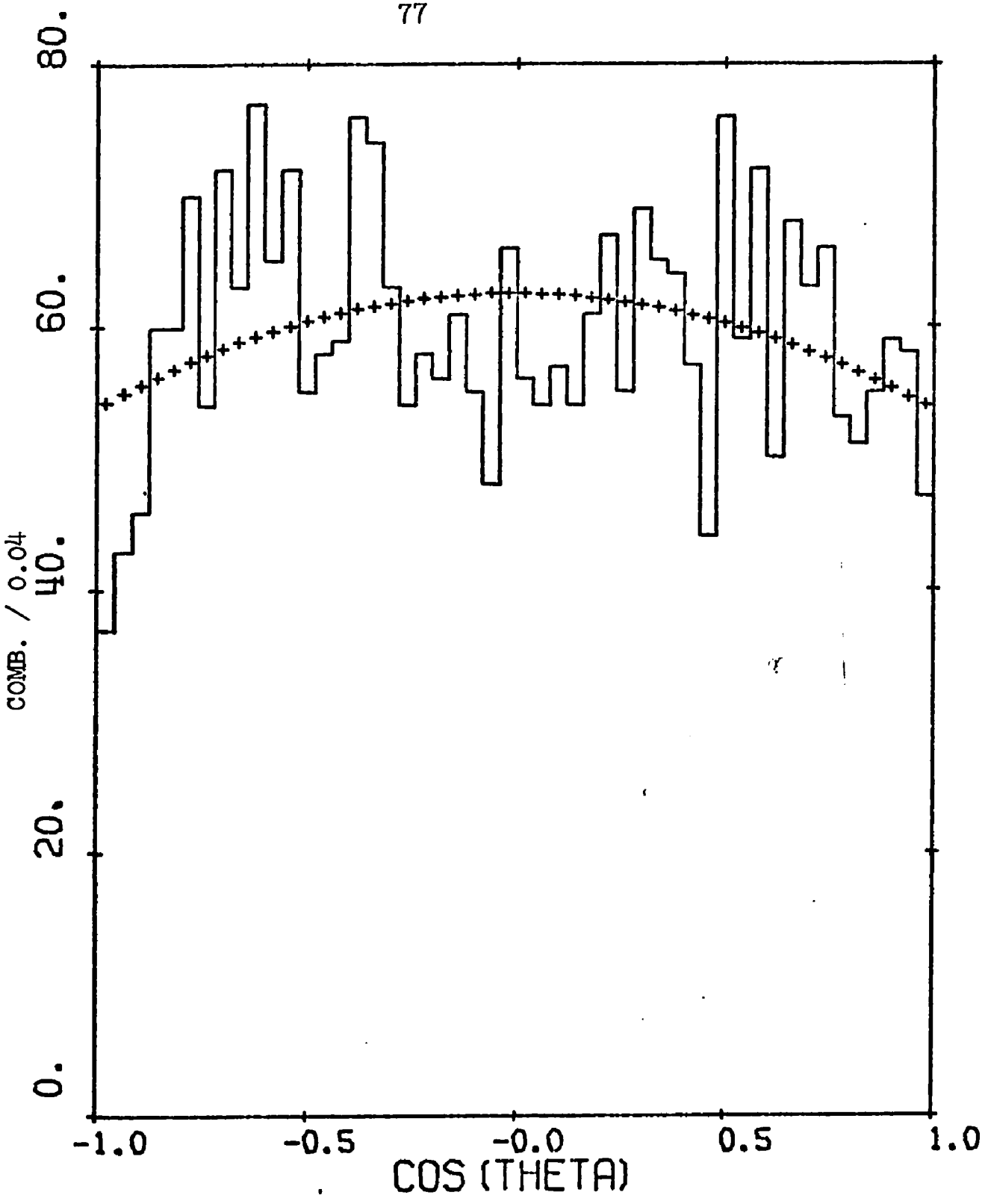


Figure 2.6-11. The cos(θ) decay distribution in the Helicity frame of the neutral dipion combination with the mass ≤ 668 MeV.

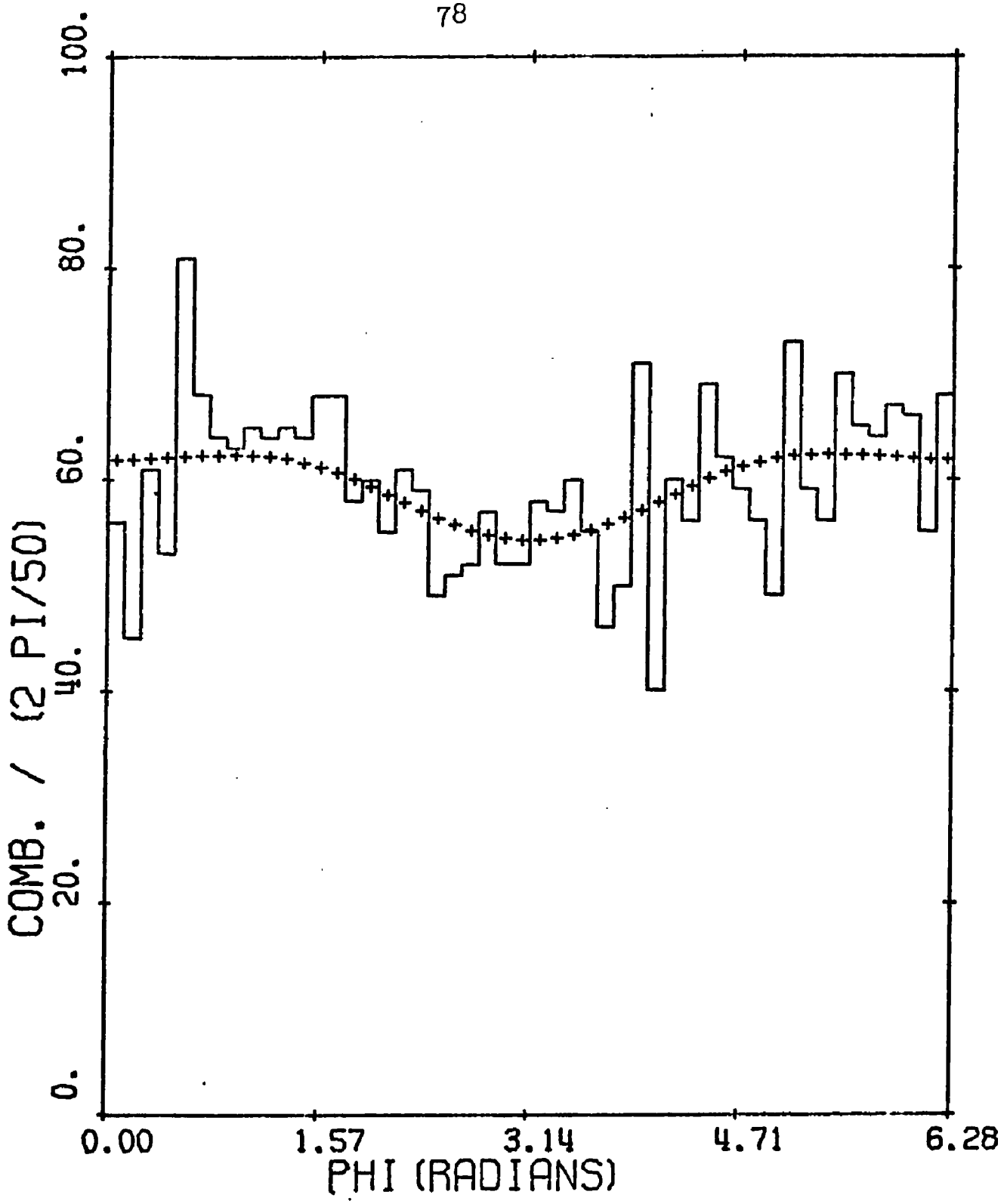


Figure 2.6-12. The φ decay distribution in the Helicity frame of the neutral dipion combinations with invariant mass ≤ 668 MeV.

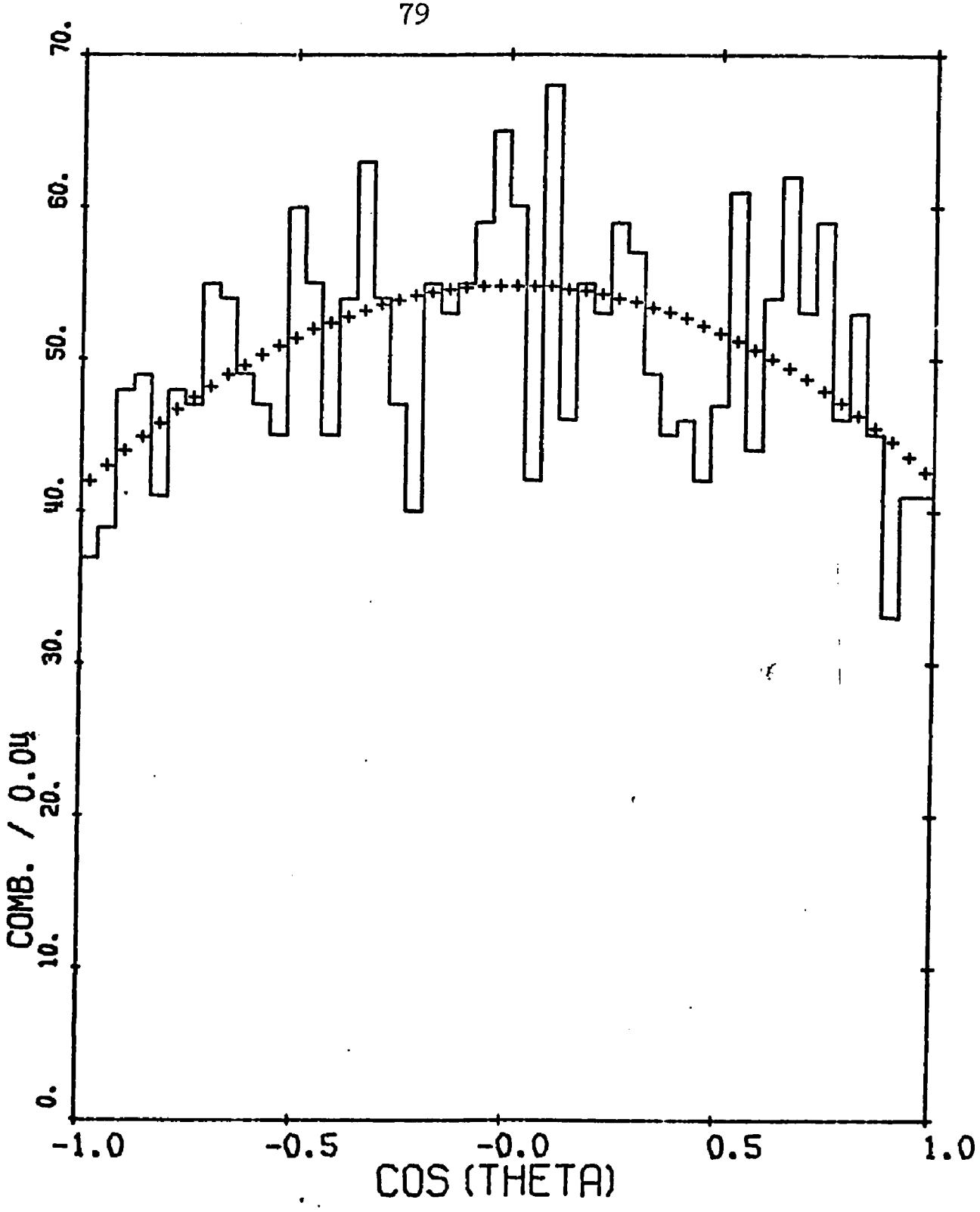


Figure 2.6-13. The cos(θ) decay distribution in the Helicity frame of the neutral dipion combinations with invariant mass in the ρ region (668-810 MeV).

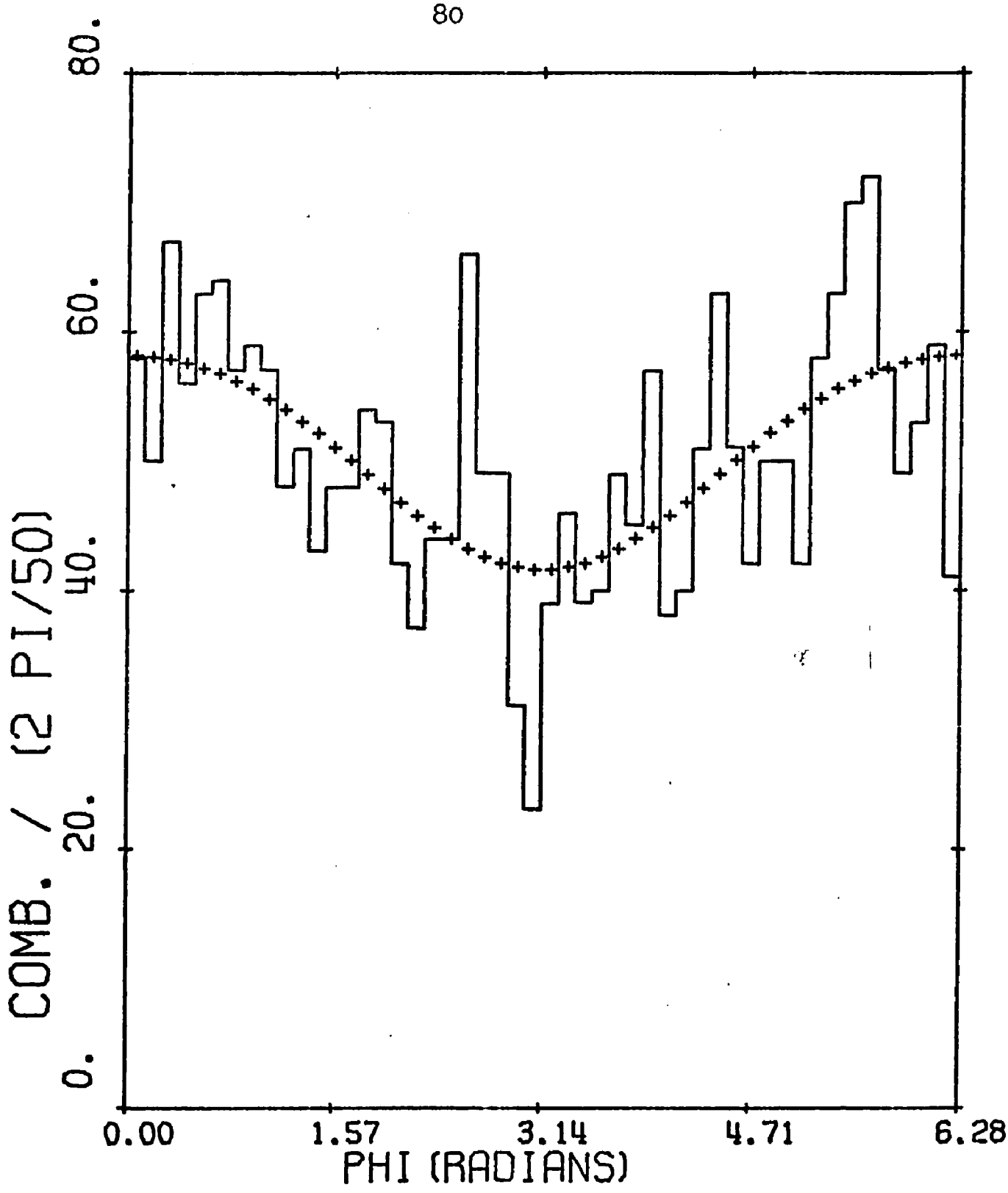


Figure 2.6-14. The φ decay distribution in the Helicity frame of the neutral dipion combinations with invariant mass in the ρ region.

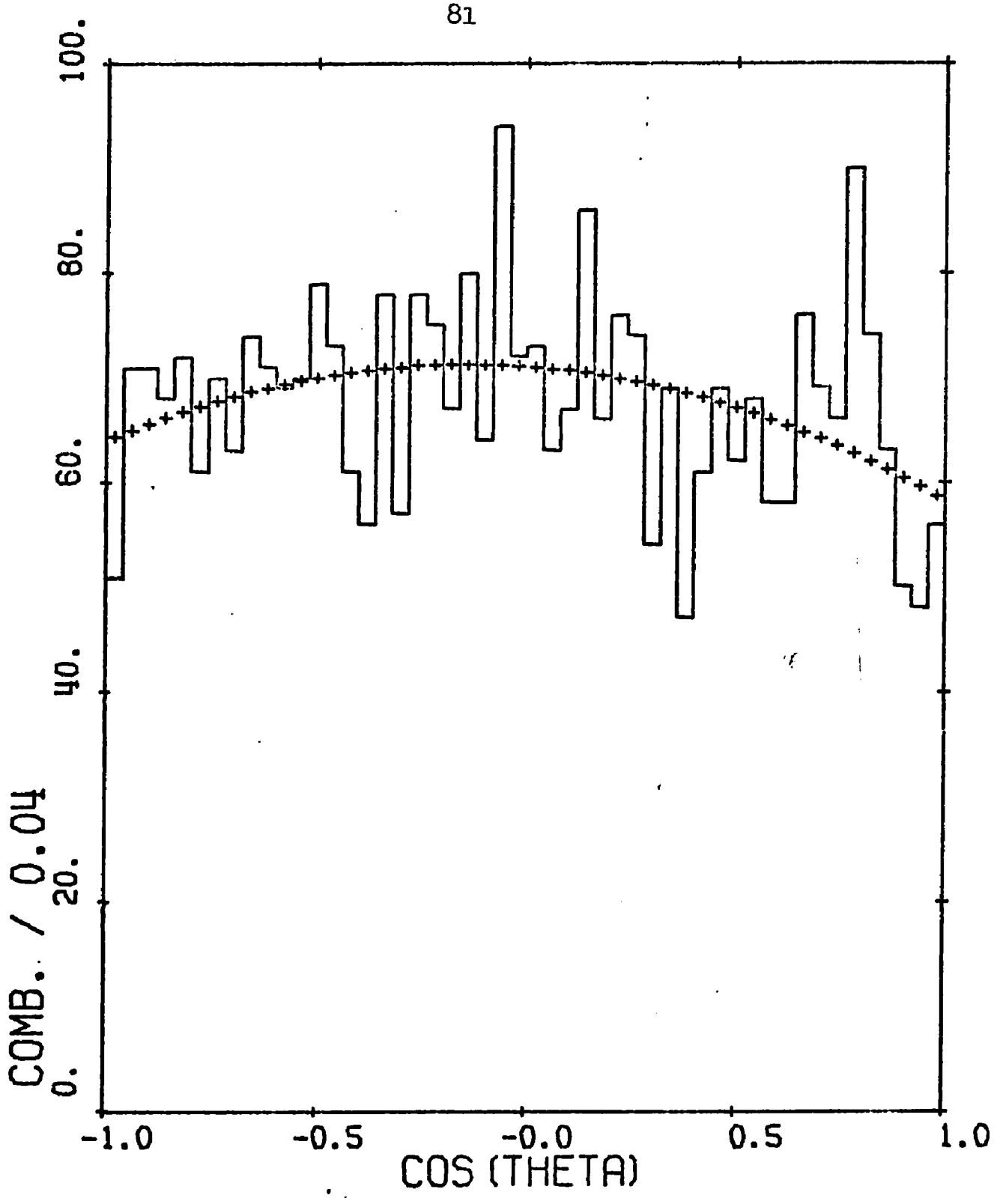


Figure 2.6-15. The cos(θ) decay distribution in the Helicity frame for the neutral dipion combinations with invariant mass between 810 and 1154 MeV.

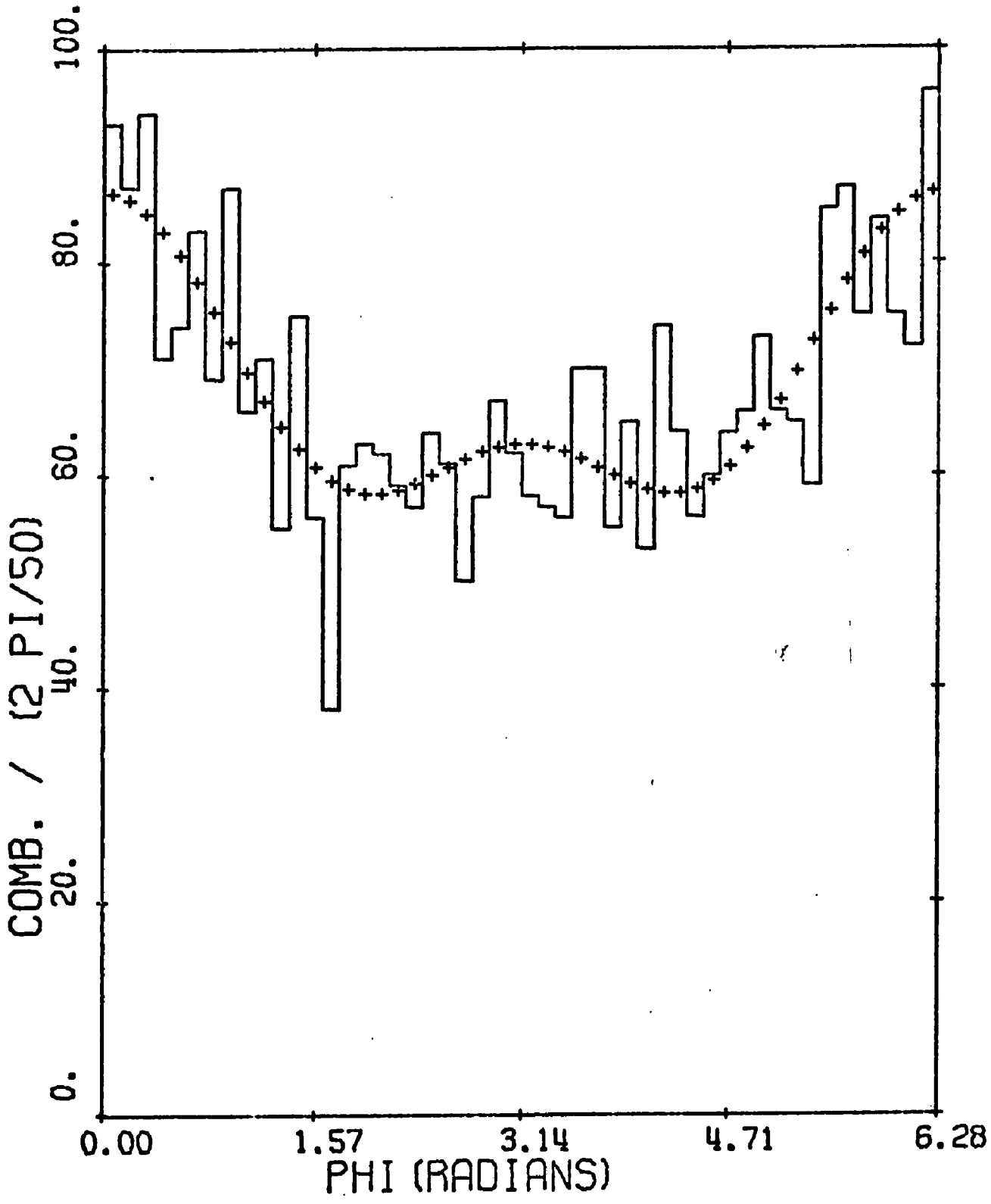


Figure 2.6-16. The φ decay distribution in the Helicity frame of the neutral dipion combinations with invariant mass between 810 and 1154 MeV.

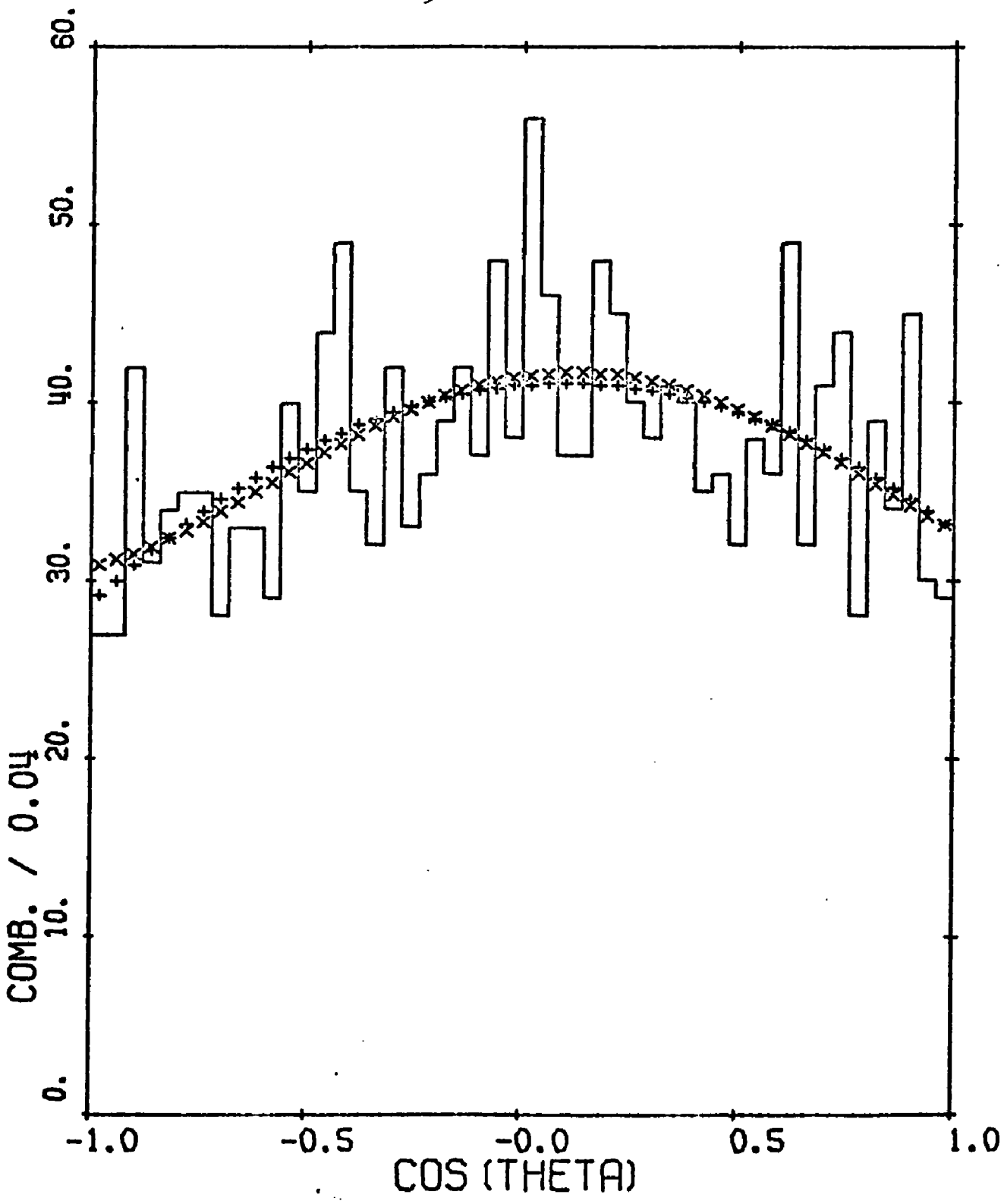


Figure 2.6-17. The cos(θ) decay distribution in the Helicity frame of the neutral dipion combinations with the invariant mass in the f region (1154-1332 MeV).

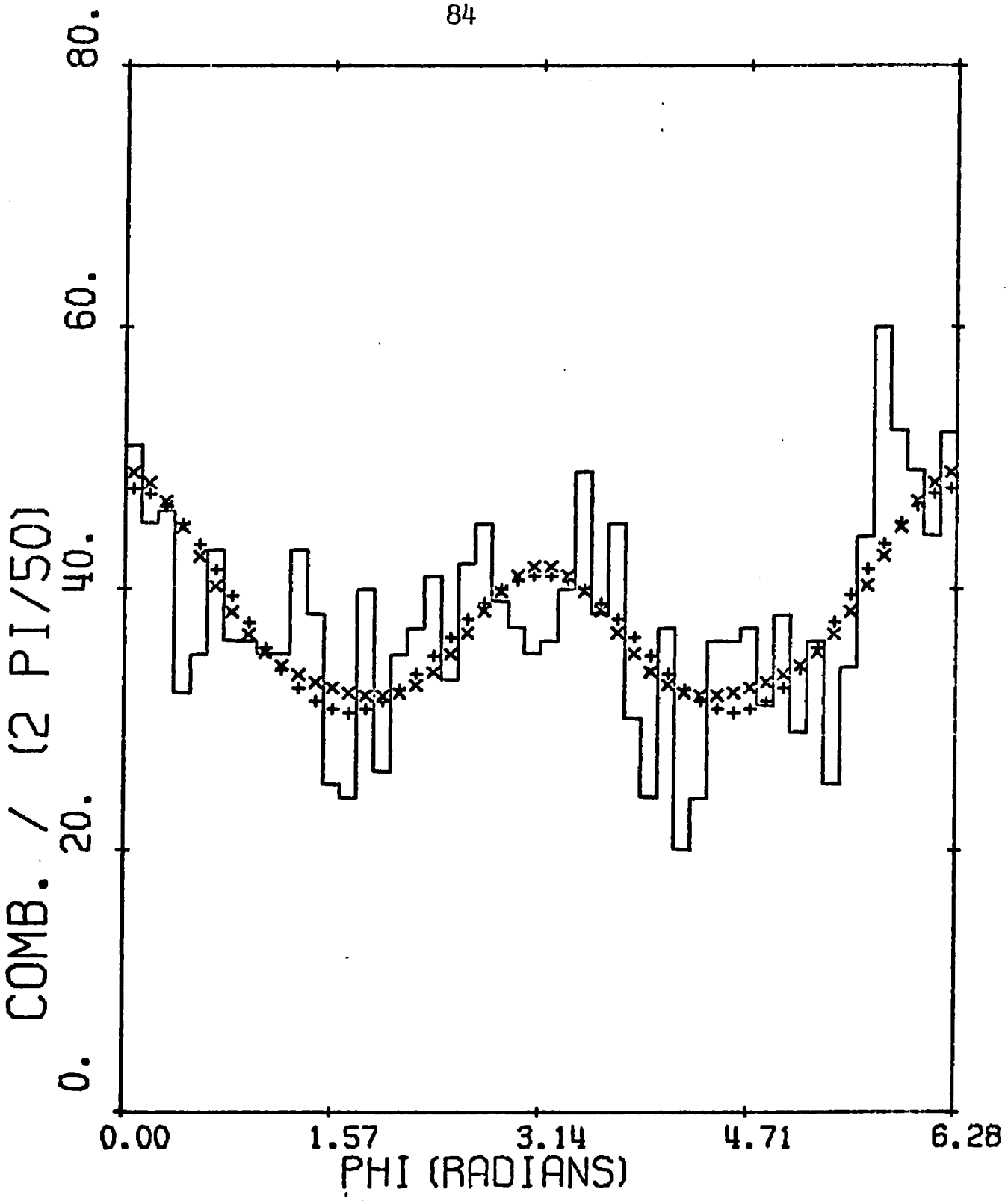


Figure 2.6-18. The φ decay distribution in the Helicity frame of the neutral dipion combinations with invariant in the f region.

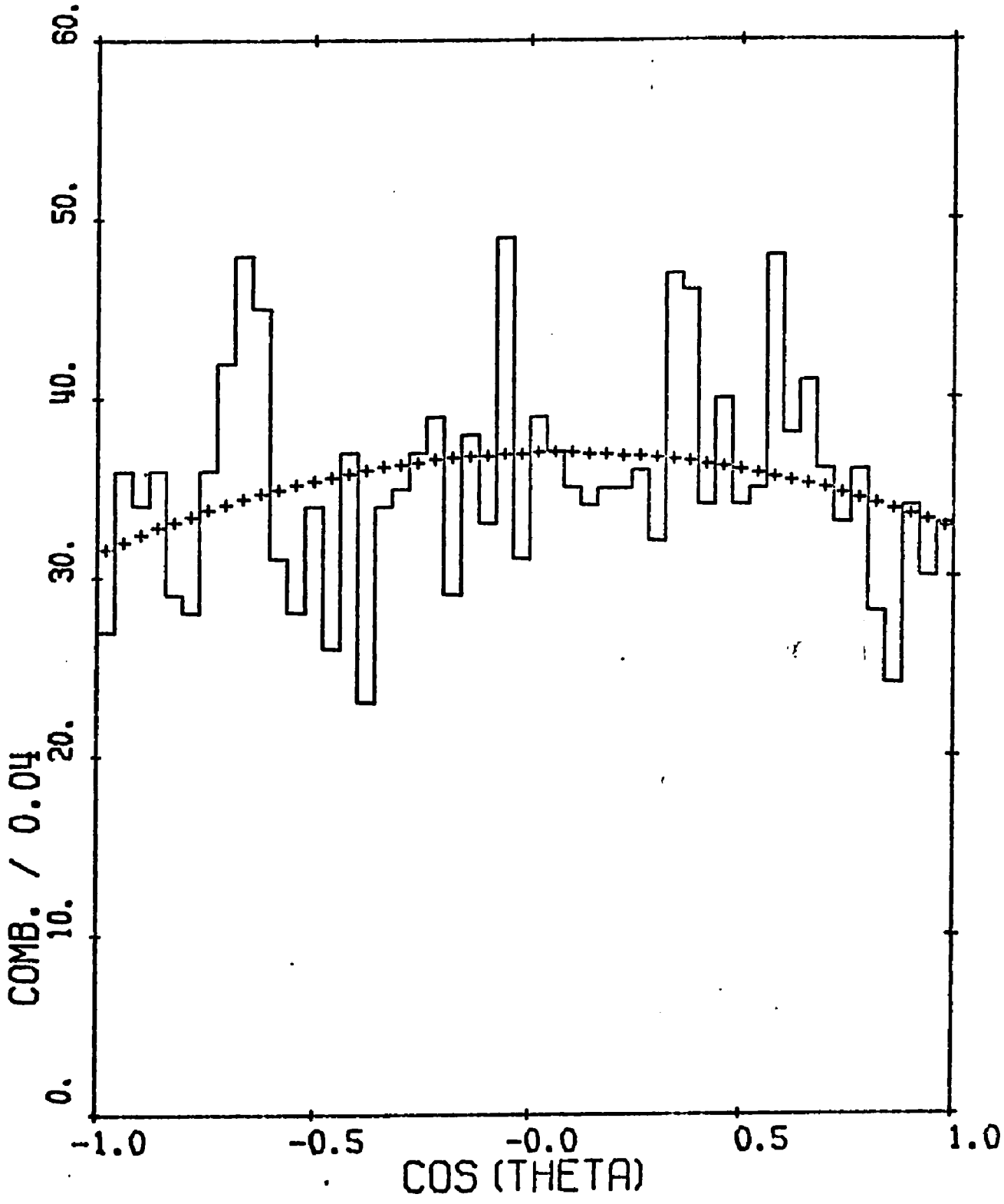


Figure 2.6-19. The cos(θ) decay distribution in the Helicity frame of the neutral dipion combinations with invariant mass greater than 1332 MeV.

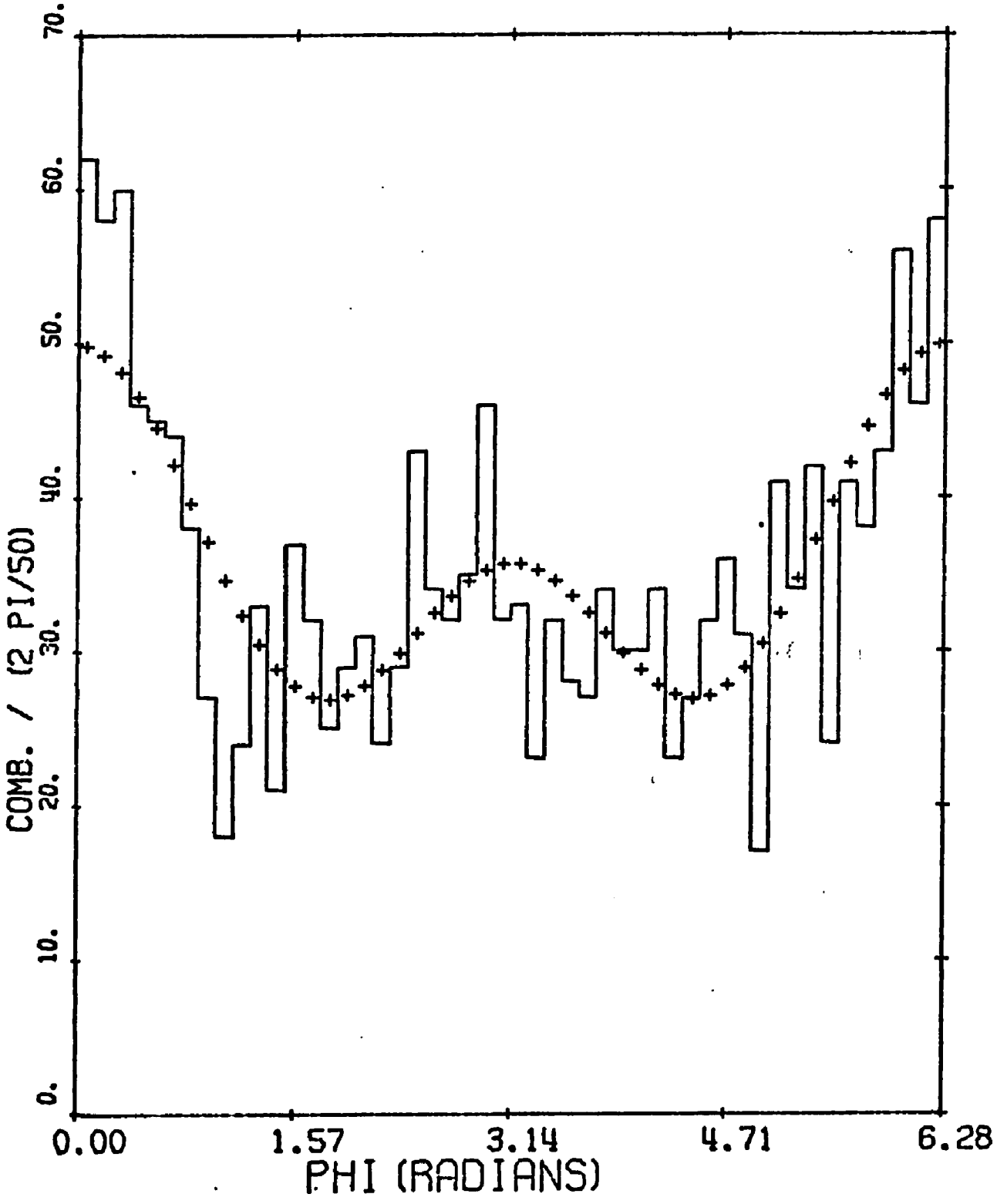


Figure 2.6-20. The φ decay distribution in the Helicity frame of the neutral dipion combinations with invariant mass greater than 1332 MeV.

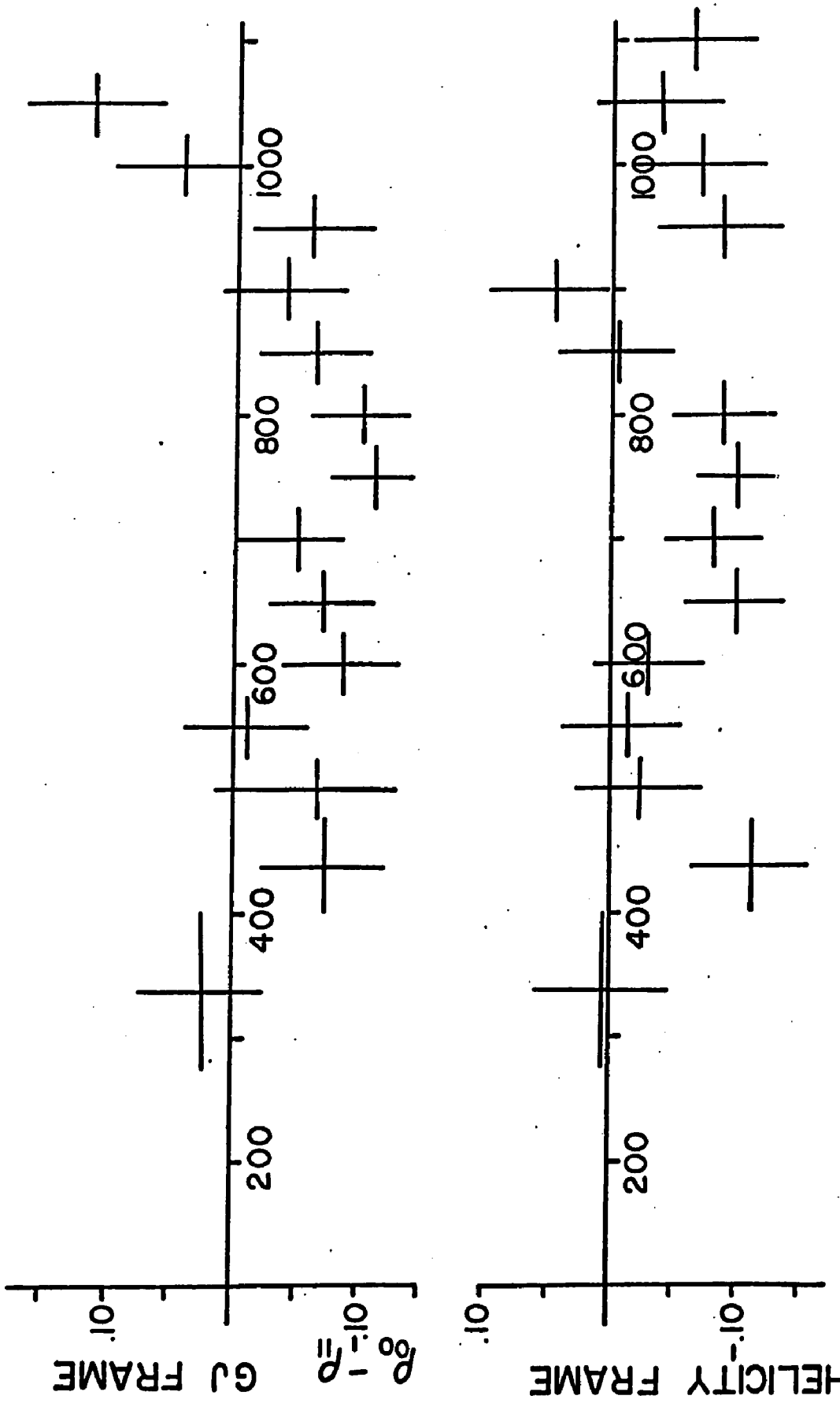


Figure 2.6-21. The $(\rho_{00}-\rho_{11})$ as a function of $\pi^+\pi^-$ mass in the GJ and Helicity frames.

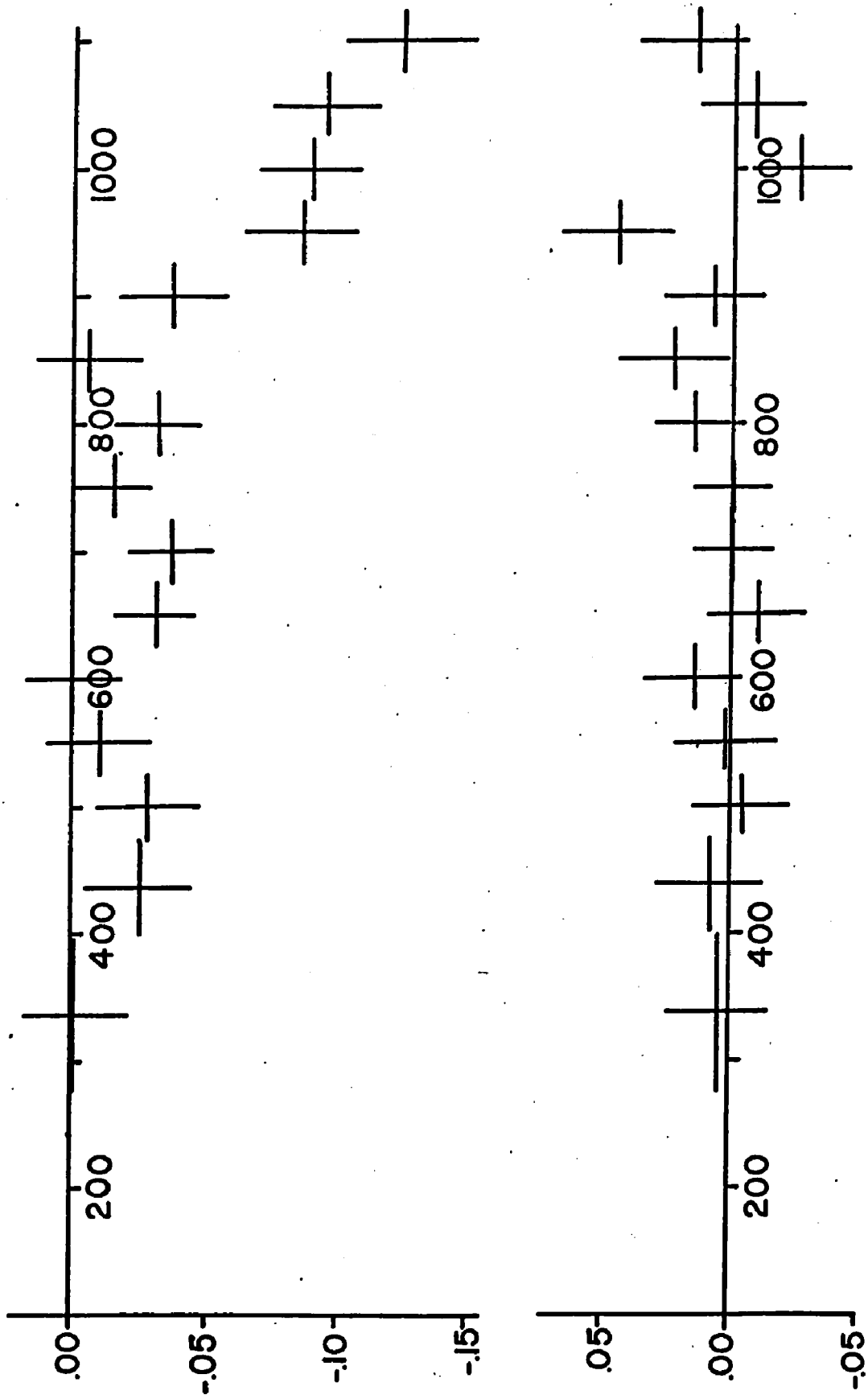


Figure 2.6-22. Re(ρ_{10}) as a function of $\pi^+\pi^-$ mass.

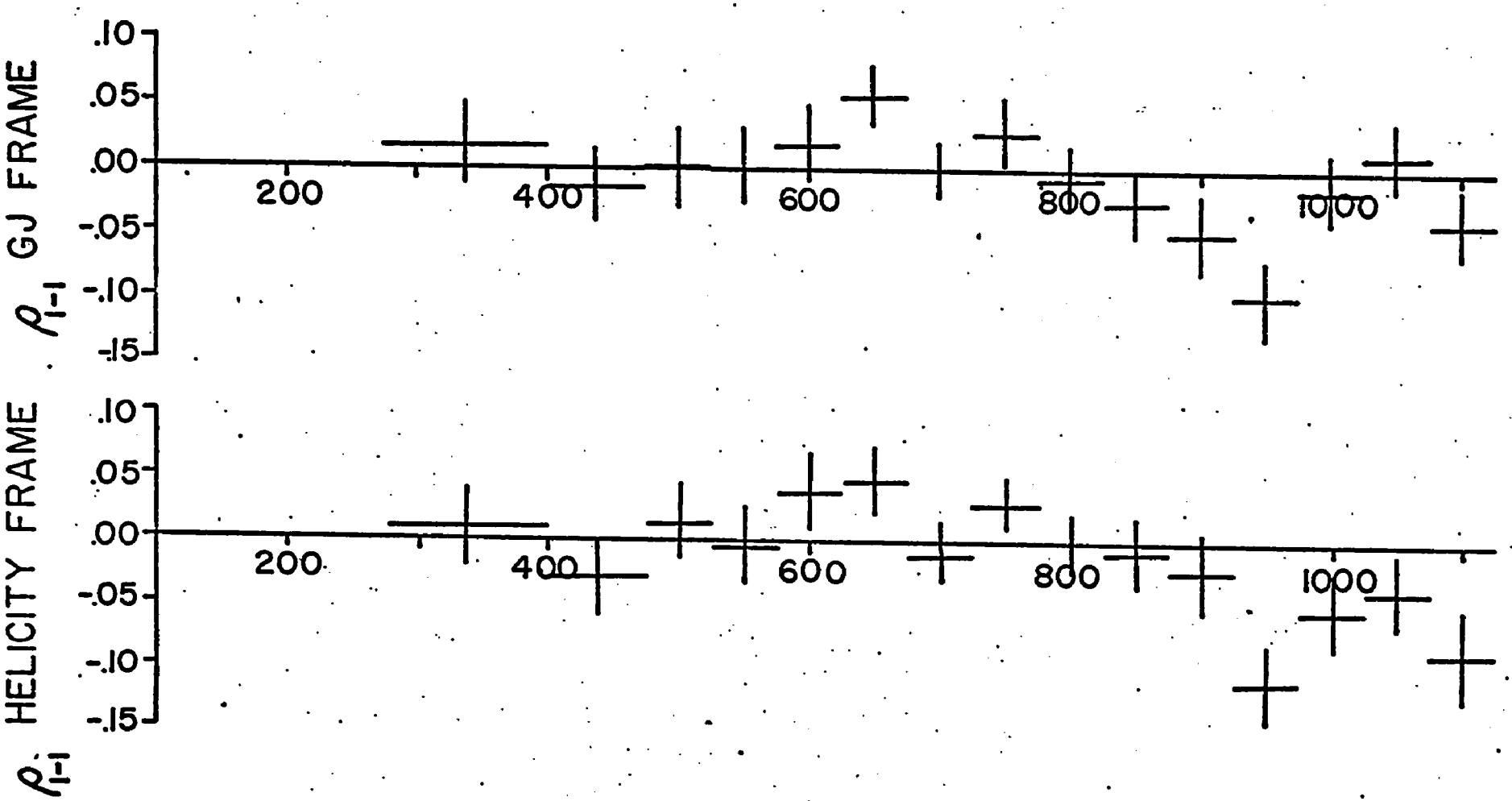


Figure 2.6-23. The ρ_{1-1} parameter as a function of $\pi^+\pi^-$ mass.

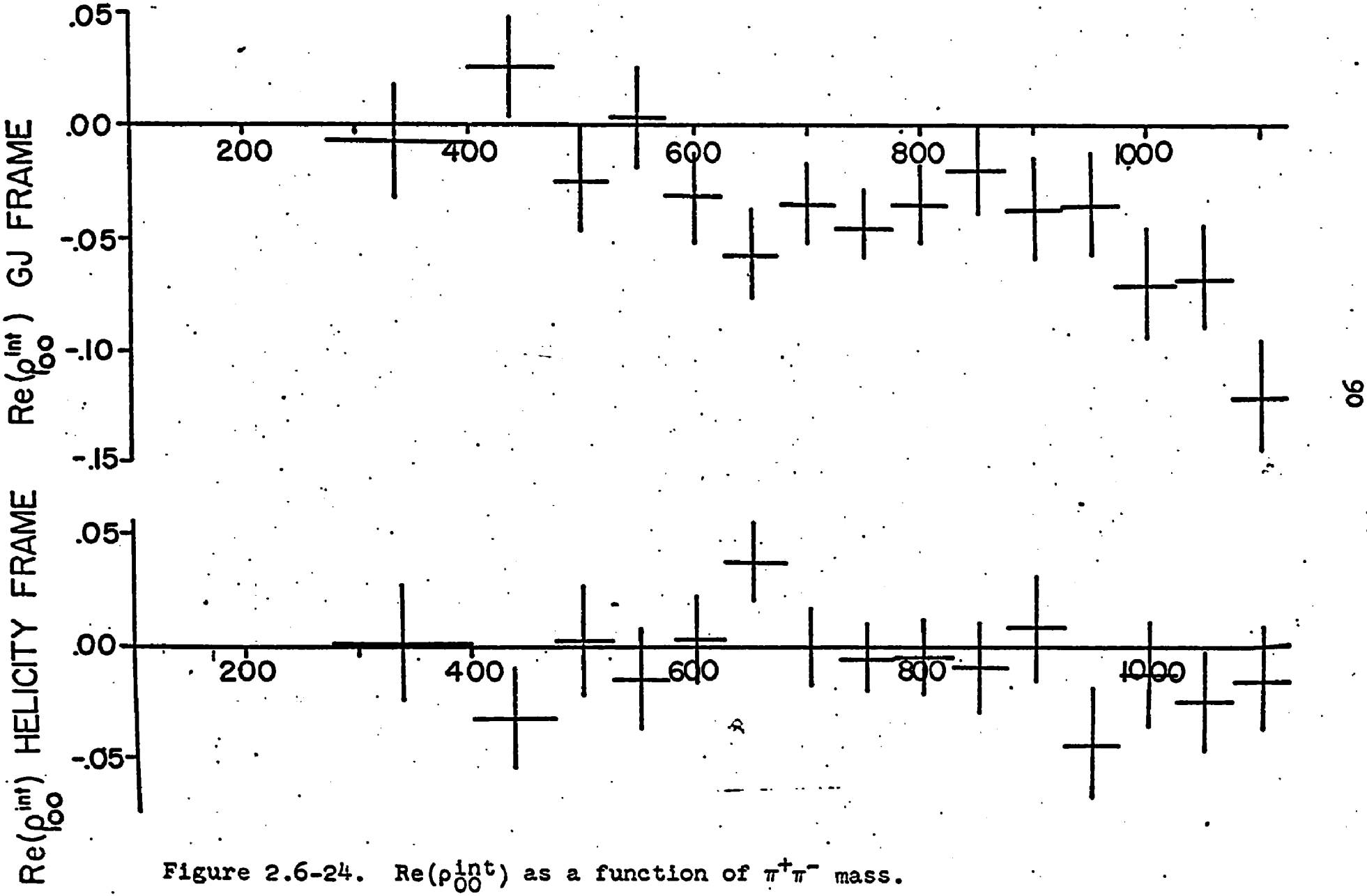


Figure 2.6-24. $Re(\rho_{00}^{int})$ as a function of $\pi^+\pi^-$ mass.

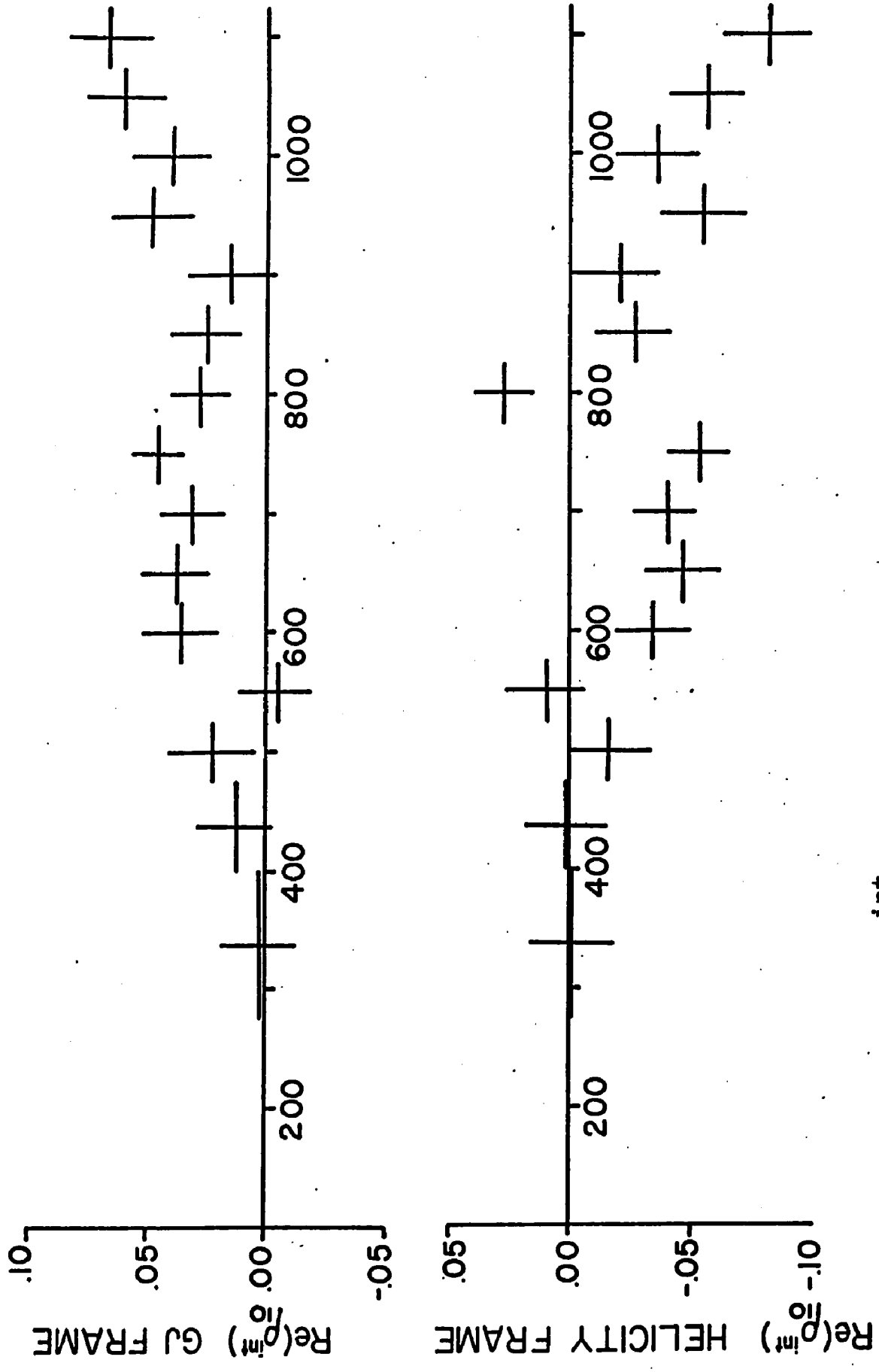


Figure 2.6-25. Re(ρ_{10}^{int}) as a function of $\pi^+\pi^-$ mass.

Figures 2.6-26 thru 2.6-30 give the values of the parameters found by a moment analysis. Again, there is a rather smooth and undramatic dependence on the variable. In both frames $(\rho_{00}-\rho_{11})$ decreases as -t ranges from ~0.0 to 3.5 $(GeV/c)^2$.

The angular histograms for the f region (1154-1332 MeV) are in Figures 2.6-7, 8, 17, 18. Because the f is a spin two object, an additional fit assuming a pure D wave was considered. This, however, is clearly not satisfactory since the spectrum is not symmetric about $\cos(\theta)$ equal to zero (as predicted by a D wave distribution). This implies that interference terms are significant. Consequently, S, P, and D waves were used in a final fit to the f region.

$$W(\theta,\varphi) = \left| \sum_{\ell=0}^{2} \sum_{m=-\ell}^{\ell} A_{\ell m}\, Y_\ell^m(\theta,\varphi) \right|^2$$

$$w(\theta) = \int_0^{2\pi} W(\theta,\varphi)\, d\varphi$$

$$= \beta_1\cos(\theta) + \beta_2(3\cos^2(\theta) - 1) + \beta_3\cos^2(\theta)\sin^2(\theta) + \beta_4\cos(\theta)\sin^2(\theta) + [(15/16) - (3/2)\beta_2 - (1/4)\beta_3]\sin^4(\theta)$$

where,

$$\beta_1 = \sqrt{3}\,\mathrm{Re}(\rho_{00}^{sp}) + \sqrt{15}\,\mathrm{Re}(\rho_{00}^{pd}),$$

$$\beta_2 = (5/8)\rho_{00}^{d} + (1/8)(\rho_{00}^{s} + 3\rho_{00}^{p} + 2\sqrt{5}\,\mathrm{Re}(\rho_{00}^{sd})),$$

$$\beta_3 = (15/2)\rho_{11}^{d} + (3/2)\rho_{00}^{s} + 3\rho_{00}^{p} + (3/2)\rho_{11}^{p} + (3/2)\sqrt{5}\,\mathrm{Re}(\rho_{00}^{sp}),$$

$$\beta_4 = 3\sqrt{5}\,\mathrm{Re}(\rho_{11}^{pd}) - (3/2)\sqrt{15}\,\mathrm{Re}(\rho_{00}^{pd}),$$

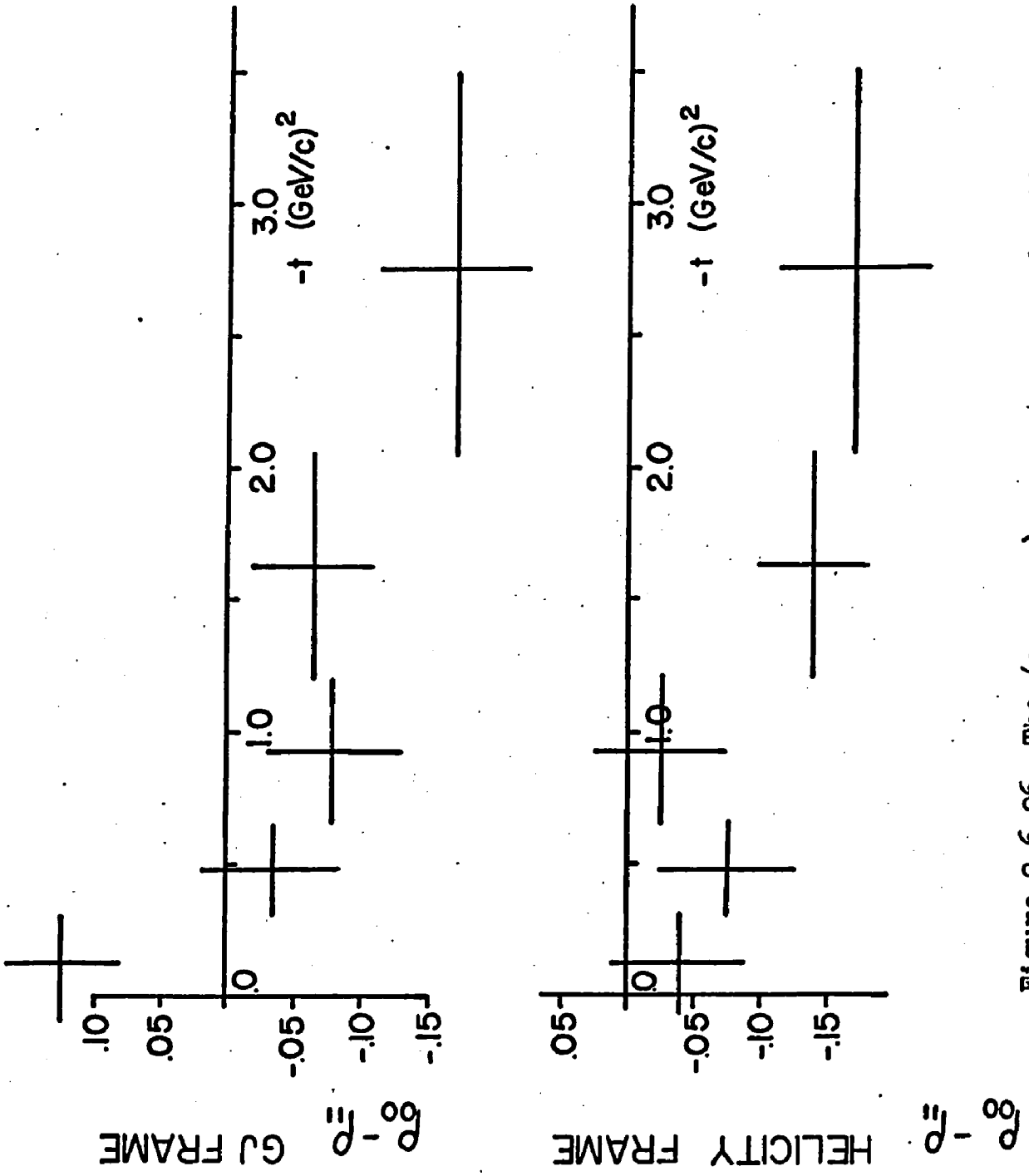


Figure 2.6-26. The $(\rho_{00}-\rho_{11})$ parameter as a function of t in the ρ mass region.

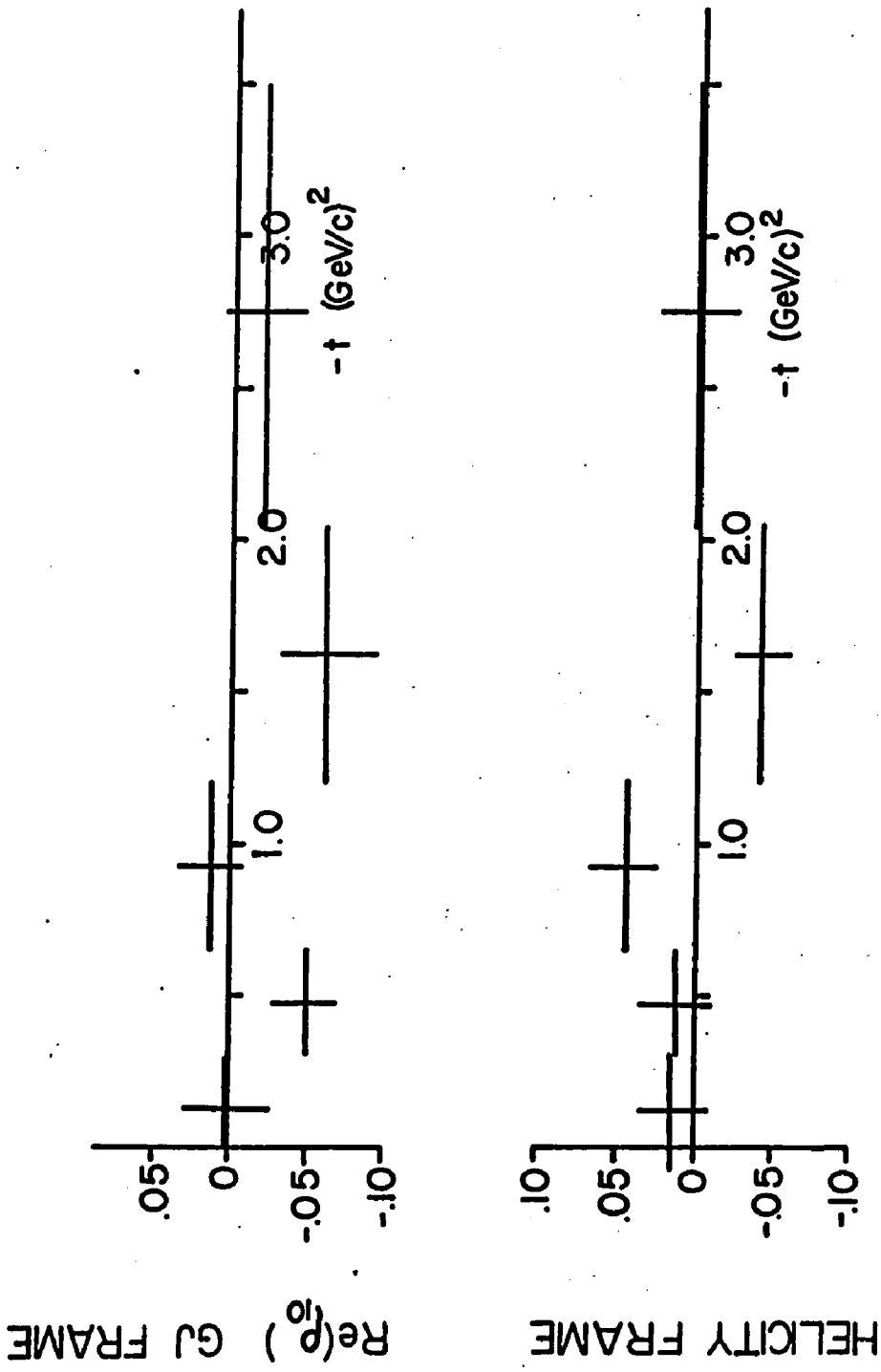


Figure 2.6-27. The $Re(\rho_{10})$ parameter as a function of t in the ρ mass region.

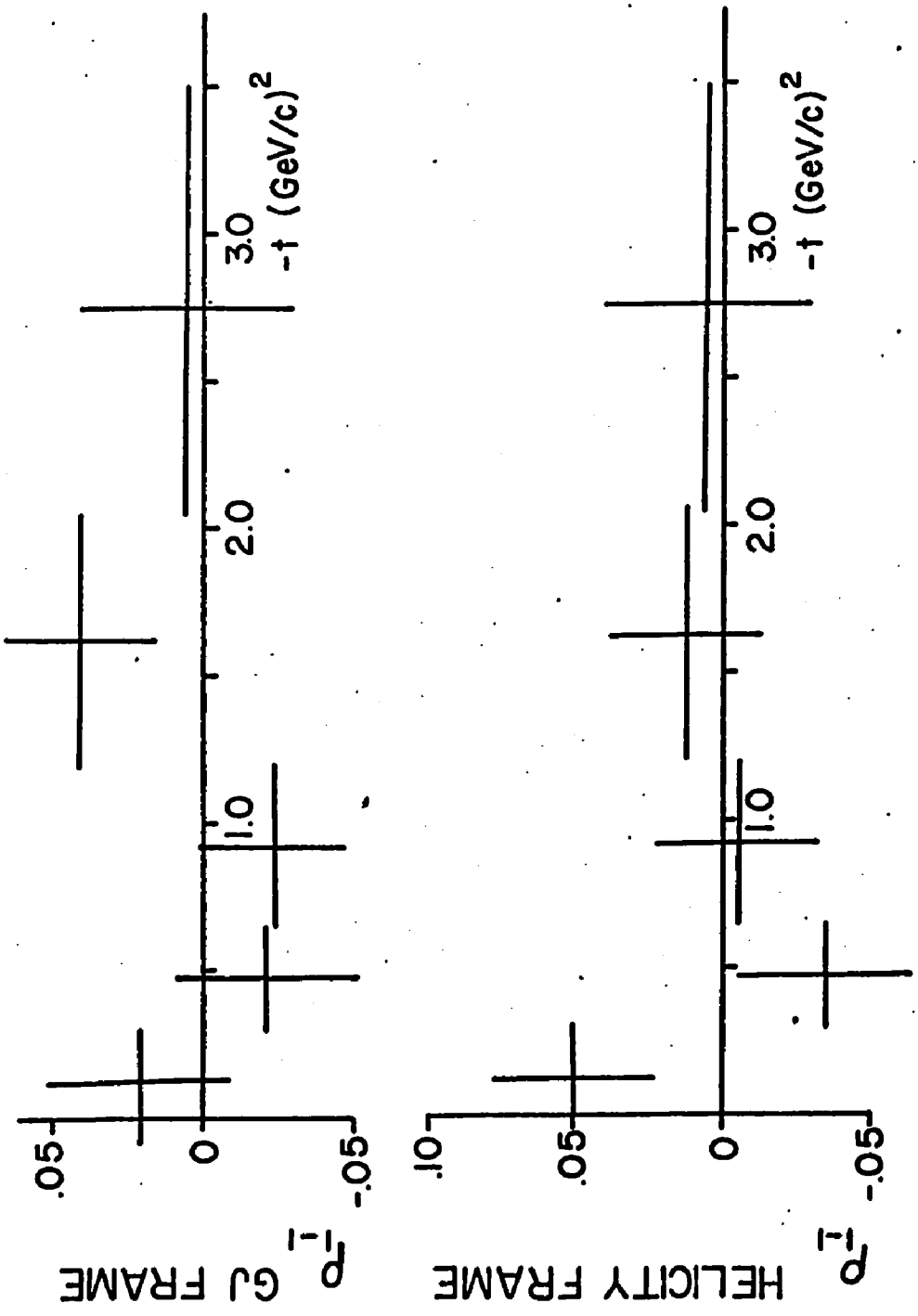


Figure 2.6-28. The ρ_{1-1} parameter as a function of t in the ρ mass range.

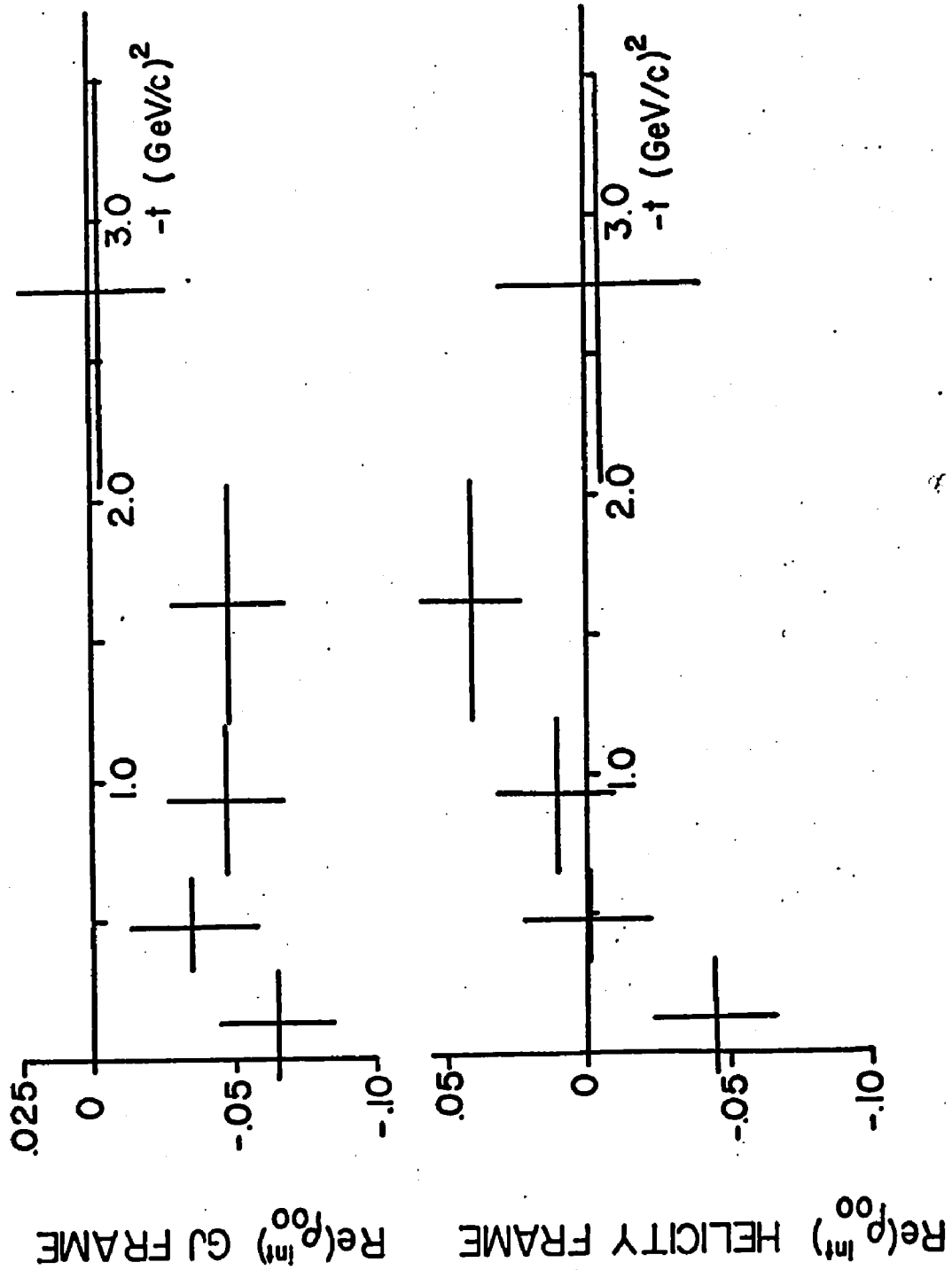


Figure 2.6-29. Re(ρ_{00}^{int}) as a function of $\bar{t}$ in the ρ mass region.

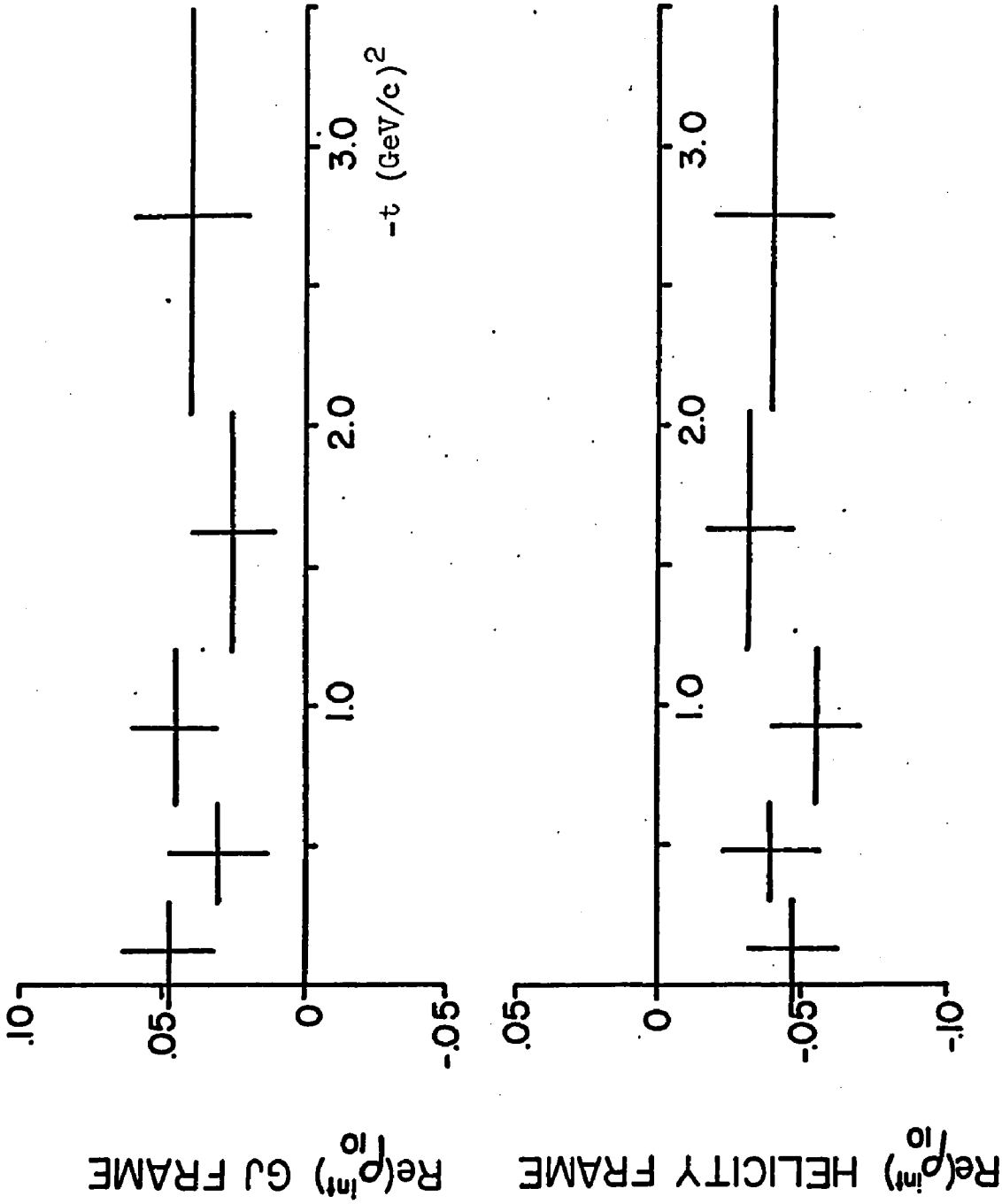


Figure 2.6-28. Re(ρ_{10}^{int}) as a function of t in the ρ mass region.

$$w(\varphi) = \int_0^{\pi} W(\theta,\varphi)\,\sin\theta\,d\theta$$

$$= (1/2\pi) + \gamma_1\cos(\varphi) + \gamma_2\cos(2\varphi) + \gamma_3\cos(3\varphi) + \gamma_4\cos(4\varphi)$$

where,

$$\gamma_1 = -\sqrt{(3/8)}\,\mathrm{Re}(\rho^{sp}_{01}) - (9/32)\sqrt{5}\,\mathrm{Re}(\rho^{pd}_{12}) + (1/16)\sqrt{(15/2)}\,\mathrm{Re}(\rho^{pd}_{10}),$$

$$\gamma_2 = (1/\pi)\{\sqrt{(10/3)}\,\mathrm{Re}(\rho^{sd}_{02}) - \rho^{p}_{1-1} - \sqrt{2/3}\,\mathrm{Re}(\rho^{d}_{20}) - 5\rho^{d}_{1-1}\},$$

$$\gamma_3 = -(9/32)\sqrt{5}\,\mathrm{Re}(\rho^{pd}_{1-2}),$$

$$\gamma_4 = (1/\pi)\rho^{d}_{2-2},$$

by definition (for example):

$$\rho^{d}_{2-2} = A_{22}A^{*}_{2-2}$$

$$\rho^{pd}_{00} = A_{10}A^{*}_{20}$$

$$\mathrm{Re}(\rho^{pd}_{11}) = (1/2)\mathrm{Re}(A_{11}A^{*}_{21} + A_{1-1}A^{*}_{2-1})$$

$$\mathrm{Re}(\rho^{sd}_{02}) = (1/2)\mathrm{Re}(A_{00}A^{*}_{22} + A_{00}A^{*}_{2-2})$$

Table 2.6-3 gives the results of a maximum likelihood fit to the separate $\cos(\theta)$ and φ distributions. The joint distribution was not fitted because of its complexity (23 parameters) and our limited statistics. The χ^2 values are good; the curves predicted by these fits are indicated by the x-marks in the f region histograms.

Table 2.6-3. The β_i and γ_i parameters and χ^2 values (50 bins) for the (S,P,D) wave fits to the $w(\theta)$ and $w(\varphi)$ distributions in the f mass region--(see text).

Parameter	GJ Frame	Helicity Frame
β_1	-0.27	0.01
β_2	0.15	0.11
β_3	1.81	1.33
β_4	0.25	0.04
γ_1	0.016	0.015
γ_2	0.007	0.028
γ_3	-0.002	0.001
γ_4	-0.003	0.002
$\chi^2(\theta)$	48	38
$\chi^2(\varphi)$	52	59

2.7 Rho-Omega Interference*

In the early sixties a suggestion was made that ρ and ω could perhaps mix through an electromagnetic interaction (S. Glashow, 1961). Predictions of the branching ratio for the direct decay of $\omega \to 2\pi$ to $\omega \to 3\pi$ ranged from 0.07 % (R. Gatto, 1963) up to the order of several percent(J. Bernstein and G. Feinberg 1962). This led to an intensive search for the effect. Several experiments found an anomaly in their $\pi^+\pi^-$ mass spectrum near the mass of the ω meson which was attributed to ρ-ω interference. This effect has been seen in the following reactions: $\bar{p}p$ (W. Allison, 1970), πp (G. Goldhaber, et al., 1969; M. Abramovitch, et al., 1970), K^-p (S. Flatté, 1970), e^+e^- (J. Augustin, et al., 1969), and γC (P. Biggs, et al., 1970; H Alvensleben, et al.,1970).**

The $\pi^+\pi^-$ mass spectrum for the ρ region in 10 MeV bins is shown in Figure 2.7-1. One notes a rather large drop in the bin from 790 to 800 MeV. In order to investigate this, the data was fit with two theoretical expressions for ρ-ω interference. In all our fits a Gaussian resolution function was folded in with a σ of 5 MeV. The resolution was determined from a study of the ω peak in the $\pi^+\pi^-\pi^\circ$ mass plot for events which fit the $\pi^+\pi^+\pi^-\pi^-\pi^\circ$ final state. In our fits an ω mass of 783.86 MeV and a width of 10.4 MeV were used.

---

*The results of an analysis of this data has been published (J. Chapman, et al., 1970). This inital work was done by J. Lys; it was reanalyzed by the author.

**This is only a partial list. For a survey of the experi-

The first formulation (J. Harte and R. Sachs, 1965; M. Gourdin, et al., 1969) has the following form:

$$\frac{dN}{dm} = [A_{PS} + A_\rho^2 \left|BW_\rho\right|^2 + A_\omega \left|BW_\omega\right|^2 + 2\alpha A_\omega A_\rho \cdot \mathrm{Re}(e^{i\varphi} BW_\omega BW_\rho^*)](PS) \qquad \text{[Eq. (1)]}$$

where,

$BW_\rho = \Gamma^{1/2}/((m_\rho^2 - m^2) - im_\rho\Gamma)$

$\Gamma = \Gamma_\rho \cdot (m_\rho/m)\,(q/q_\rho)^3$

$BW_\omega = \Gamma_\omega^{1/2}/((m_\omega^2 - m^2) - im_\omega\Gamma_\omega)$

PS = phase space distribution for 2 out of 4 pions,

α = coherence factor ($0 \leq \alpha \leq 1$),

φ = relative phase of A_ρ and A_ω,

q = magnitude of the momentum of either pion in the dipion CM.

The free parameters were taken to be m_ρ, Γ_ρ, A_ω, φ, α, and A_ρ with A_{PS} determined by normalization. Setting A_ω equal to zero, we find $\chi^2 = 66$ for 34 degrees of freedom with $m_\rho = 747$ MeV and $\Gamma_\rho = 124$ MeV. If A_ω is allowed to vary, it is found that $\chi^2 = 50$, $M_\rho = 750$, $\Gamma_\rho = 200$, $\varphi = 119^\circ$, $\alpha = 0.6$, and R = 4.7%. R is the ratio of $\omega \to \pi^+\pi^-$ decays to $\omega \to \pi^+\pi^-\pi^\circ$. The number of $\omega \to 3\pi$ decays is estimated to be 2147 and the number of 2π decays is calculated from

$$N(\omega \to \pi^+\pi^-) = \int A_\omega^2 \left|BW_\omega\right|^2 PS\, dm.$$

mental work on ρ-ω interference see G. Goldhaber, Experimental Meson Spectroscopy, edited by C. Baltay and A. Rosenfeld, Columbia University Press, 59(1970).

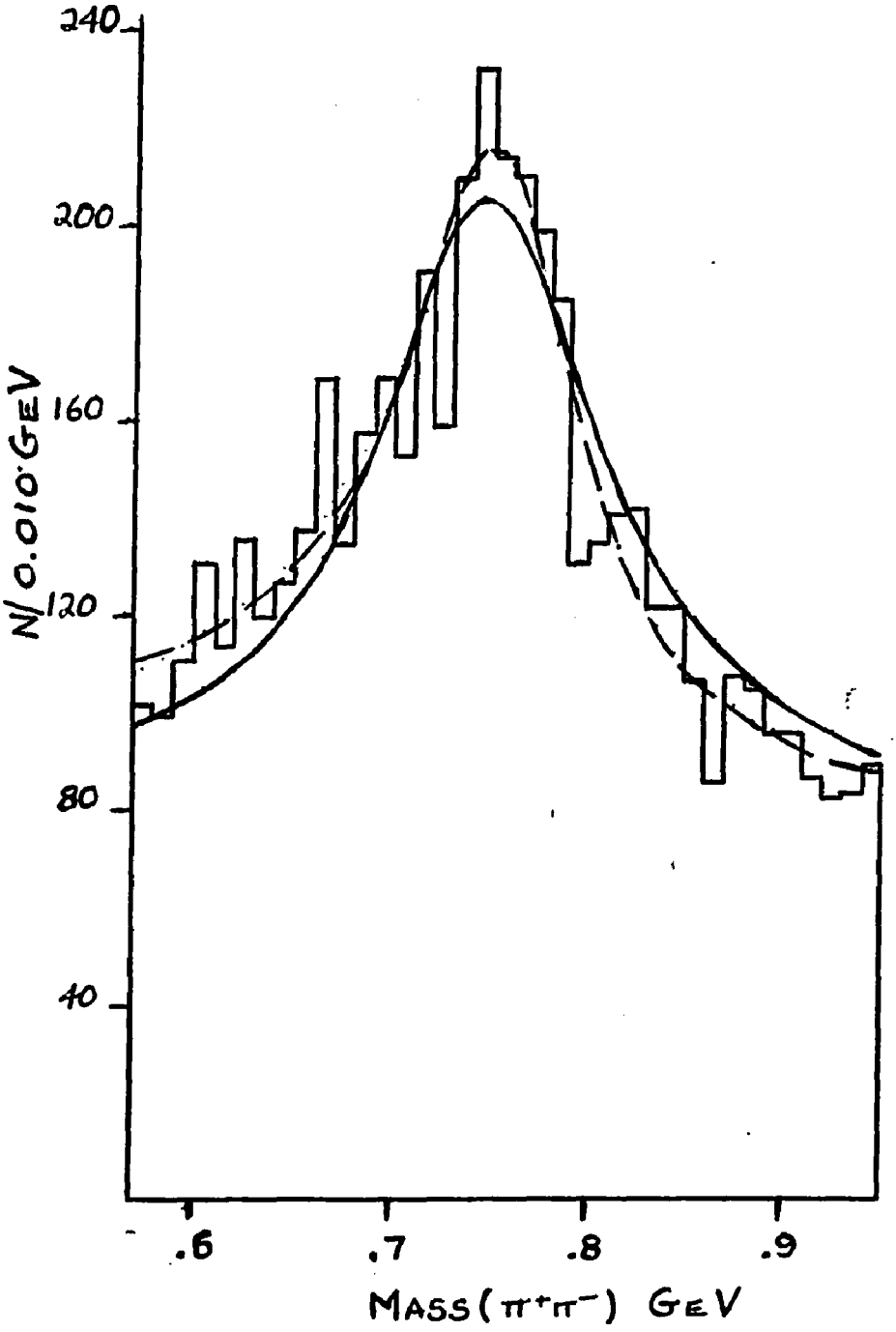


Figure 2.7-1. The $\pi^+\pi^-$ mass spectrum used in the fit to all the data. The solid curve is fit (a) to eq. (2) and the dashed curve is fit (b) (see text).

If Γ_ρ is constrained to be $\leq$ 145 MeV, then χ^2 equals 52, M_ρ = 745 MeV, Γ_ρ = 145 MeV, $\varphi = 105^\circ$, α = 0.9, and R = 1.8%. These results are similar to those reported for 4π channel at incident $\bar{p}$ momentum 1.26-1.65 GeV/c (W. Allison, et al., 1970). In this earlier experiment α was found to be greater than 0.4 and R greater than 1.4%. An important criticism of this formulation is that it does not allow for interference between the ρ and the non-resonant background.

A second theoretical expression (S. Flatté, 1970) used to parameterize the effect has the form:

$$\frac{dN}{dm} = [\alpha_1 + \alpha_2|BW_\rho|^2 + \alpha_3|BW_\omega|^2 + \alpha_4 Re(BW_\rho) + \alpha_5 Re(BW_\omega)]PS \qquad \text{[Eq. (2)]}$$

where,

$$BW_\rho = (m_\rho \Gamma_\rho q/q_\rho)/((m_\rho^2 - m^2) - im_\rho \Gamma)$$

$$BW_\omega = (m_\omega \Gamma_\omega q/q_\omega)/((m_\omega^2 - m^2) - im_\omega \Gamma_\omega)$$

Γ, q, and PS have the same definitions as in the first formulation.

This expression is an attempt to be as general as possible in the description of any anomaly in the ω mass region. It allows the ρ to interfere with the phase space background via the term containing $Re(BW_\rho)$.

Table 2.7-1 gives the results of fitting this expression to several subsets of our data. We have made cuts on the

Table 2.7-1. The χ^2 values for least square fits using the formulation by S. Flatté for various data selections. P=incident $\bar{p}$ momentum(GeV/c); t = 4-momentum transfer squared$(GeV/c)^2$; M=recoil mass(GeV); N= number of $\pi^+\pi^-$ mass combinations--(see text for definitions of fits (a) thru (d))*.

Data Selection	Fit(a)	Fit(b)	Fit(c)	Fit(d)	N
All Data	69	43	46	36	5200
P=2.20, 1.95	44	41	41	38	1328
P=1.88, 1.83	34	24	28	23	1869
P=1.77, 1.63	45	28	29	23	2003
-t=0.0-0.3	75	56	50	45	2030
-t=0.3-0.6	44	43	39	39	1409
-t=0.6-0.9	33	33	32	32	898
-t=0.9-1.2	35	35	35	35	469
-t=0.0-0.1	45	42	42	38	651
-t=0.1-0.2	57	45	50	44	745
-t=0.2-0.3	62	54	28	28	634
P=2.20, 1.95 -t=0.0-0.3	51	45	48	44	458
P=1.88, 1.83 -t=0.0-0.3	63	52	48	43	703
P=1.77, 1.63 -t=0.0-0.3	43	36	32	31	869
M=668-810	68	66	67	66	765
M=1154-1332	38	36	23	22	1246
M=810-1154 or M<668 or M>1332	69	30	53	28	3189
P=1.63-1.88 -t=0.0-0.3	69	54	43	40	1572
M=1154-1332 -t=0.0-0.3	44	43	33	28	523

* χ^2 values are for 38 bins.

incident $\bar{p}$ momentum, the recoil mass, and t (the square of the four-momentum transfer between the $\pi^+\pi^-$ system and either the p or $\bar{p}$, taking the t which is algebraically larger. Four fits were made to each data set: (a) α_3, α_4, α_5 set equal to zero--incoherent ρ plus background; (b) α_3, α_5 set to zero--ρ plus background with interference between them; (c) α_4 set to zero--incoherent background as in the first formulation; (d) all parameters allowed to vary. In each case α_1 is determined by normalization. The mass and width of the ρ have been constrained to lie within the probable limits: m_ρ = 755-775 MeV, Γ_ρ = 105-145 MeV (Review of Particle Properties, 1971)

From the fits listed in Table 2.7-1, the following conclusions are reached. First, the fit to all of the data does not give convincing evidence for ρ-ω interference--χ^2 changes by 7 with the addition of two parameters between fits (b) and (d). In fact for this data set, the need for interference between the ρ and the nonresonant background is much stronger--with the addition of one parameter χ^2 changes by 26 between fits (a) and (b), and by 10 between fits (c) and (d). Fits (a) and (b) are shown in Figure 2.7-1. Secondly, there is little indication of either ρ-ω interference or ρ-background interference in the two highest momentum sets--χ^2 changes by 6 between fits (a) and (d) with the addition of three parameters. Thirdly, when t cuts are made on the data, we see a significant signal only in the -t = 0.2 to 0.3 range. This is our strongest evidence for ρ-ω

interference--χ^2 changes by 26 between fits (b) and (d). Figure 2.7-2 presents the data for this cut, as well as the curves generated by fits (a) and (d). Finally, when cuts are made on the recoil mass, a signal is seen for ρ-ω interference only in the f region. Thus, indications for ρ-ω interference are seen for $\bar{p}$ momentum between 1.63-1.88 GeV/c consistent with being all in the ρf channel having a maximum strength for $-t = 0.2$ to 0.3 $(\text{GeV/c})^2$.

A lower limit for the branching ratio can be found by assuming complete coherence of the ρ, ω, and background (M. Abramovitch, et al., 1970)

$$N(\omega \to \pi^+\pi^-) = A\int \left|BW_\omega\right|^2 PS \; dm$$

where,

$$A = b - (b^2 - \alpha_3^2 - \alpha_5^2)^{1/2}$$

$$b = 2\alpha_1 + 2\alpha_2 \left|BW_\rho\right|^2 + \alpha_3 + 2\alpha_4 [\mathrm{Re}(BW_\rho)]_{m=m_\omega}$$

The results are $R = 0.4\%$ for all the data and $R = 5.1\%$ for $-t = 0.2$ to 0.3. By fixing A, a plot of χ^2 versus A can be made, and a lower limit on the value of R can be found. This was done at a 95% confidence level ($\Delta\chi^2 = 4.0$). The results are 0.03% and 1.9%, respectively for all the data and $-t = 0.2$ to 0.3 $(\text{GeV/c})^2$.

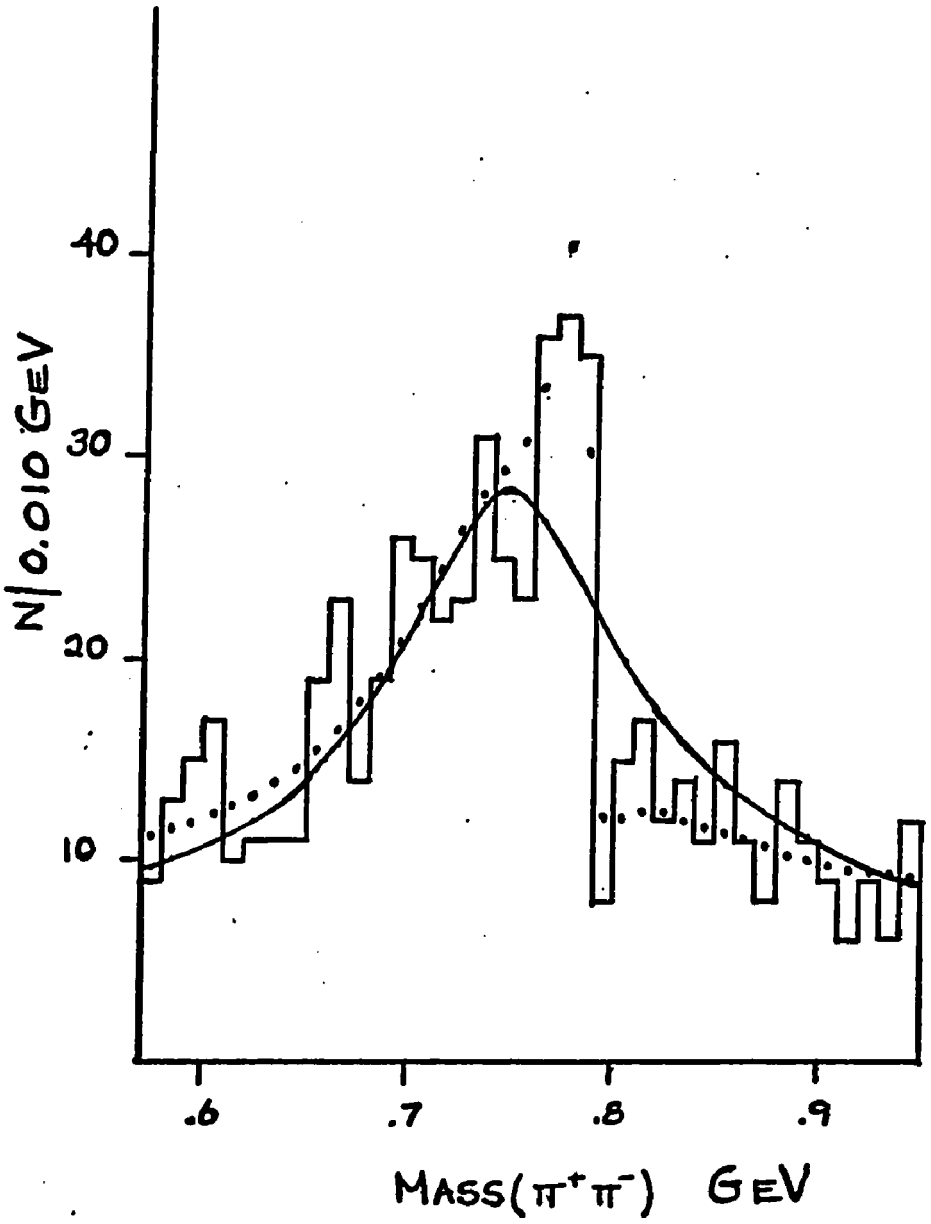


Figure 2.7-2. The subset of the $\pi^+\pi^-$ mass spectrum with squared momentum transfer in the range -0.2 to -0.3 $(GeV/c)^2$. The solid curve and circles are fits (a) and (d) respectively, to eq. (2).

CHAPTER III

THE REACTION $\bar{p}p \rightarrow \pi^-\pi^+K^-K^+$

3.1 Introduction

In contrast to the $\pi^-\pi^-\pi^+\pi^+$ channel, the $\bar{p}p$ annihilation into $\pi^-\pi^+K^-K^+$ has been the topic of only one paper with 93 events at 1.2 GeV/c beam momentum (A. Frodesen, et al., 1969). We have 785 events which fit the $2\pi 2K$ hypothesis with a confidence level $\geq 10^{-6}$ and two or more constraints. The events were required to be in a fiducial volume fixed to be 2 half-right cylinders centered on the z axis, such that for $x > 0$ (downstream) radius $r \equiv (x^2 + y^2)^{1/2} \leq 24$ cm; we required $r \leq 28$ cm for $x < 0$. This was done to aid the bubble density analysis. Events close to the edge of the visible region were eliminated.

Approximately 90 percent of these events had more than one fit. In order to resolve as many ambiguities as possible and to verify the correctness of the unique fits, all the events were examined on a scan table. The observed density of each track was compared to the densities predicted for the π, K and p particles. These were determined from the well-known fact that the ionization is roughly proportional to $1/\beta^2$ ($\beta=v/c$). The projected densities were determined for each view.# The beam track

---

#The program to calculate the projected density was written by J. Lys.

was used for normalization.

This scan reduced the number of $2\pi 2K$ candidates from 785 to 662. Sixty-one percent were identified to be a unique $2\pi 2K$ final state. The following ambiguities remained:

13 %	multiple $2\pi 2K$,
12 %	$2\pi 2K$, $\pi^-\pi^-\pi^+\pi^+\pi^\circ$
5 %	$2\pi 2K$, $\pi^-\pi^+\pi^\circ K^-K^+$
2 %	$2\pi 2K$, $\pi^-\pi^-\pi^+\pi^+$
7 %	ambiguous among several states.

Events that were still ambiguous after bubble density were treated in the following manner. The confidence level (CL) of the $2\pi 2K$ fit was compared to the CL of all the other successful SQUAW fits which were consistent with bubble density. The $2\pi 2K$ hypothesis was rejected if either there was a 4-constraint (4C) fit with a CL > CL($2\pi 2K$), or a 1-constraint (1C) fit with a CL > 4·CL($2\pi 2K$). The factor of 4 is somewhat arbitrary; a 1C fit is easier to fake than a 4C. Our final sample is very insensitive to this value. If we change it from 4 to 2, our number of events changes from 573 to 571. The factor of 4 was arrived at by looking at a scatterplot of CL(4C) versus CL(1C) ambiguous events. After making the above cuts, the confidence level distribution for our final sample of 573 events is shown on Figure 3.1-1. We see that it it flat except for the lowest bin from 0.00 to 0.02.

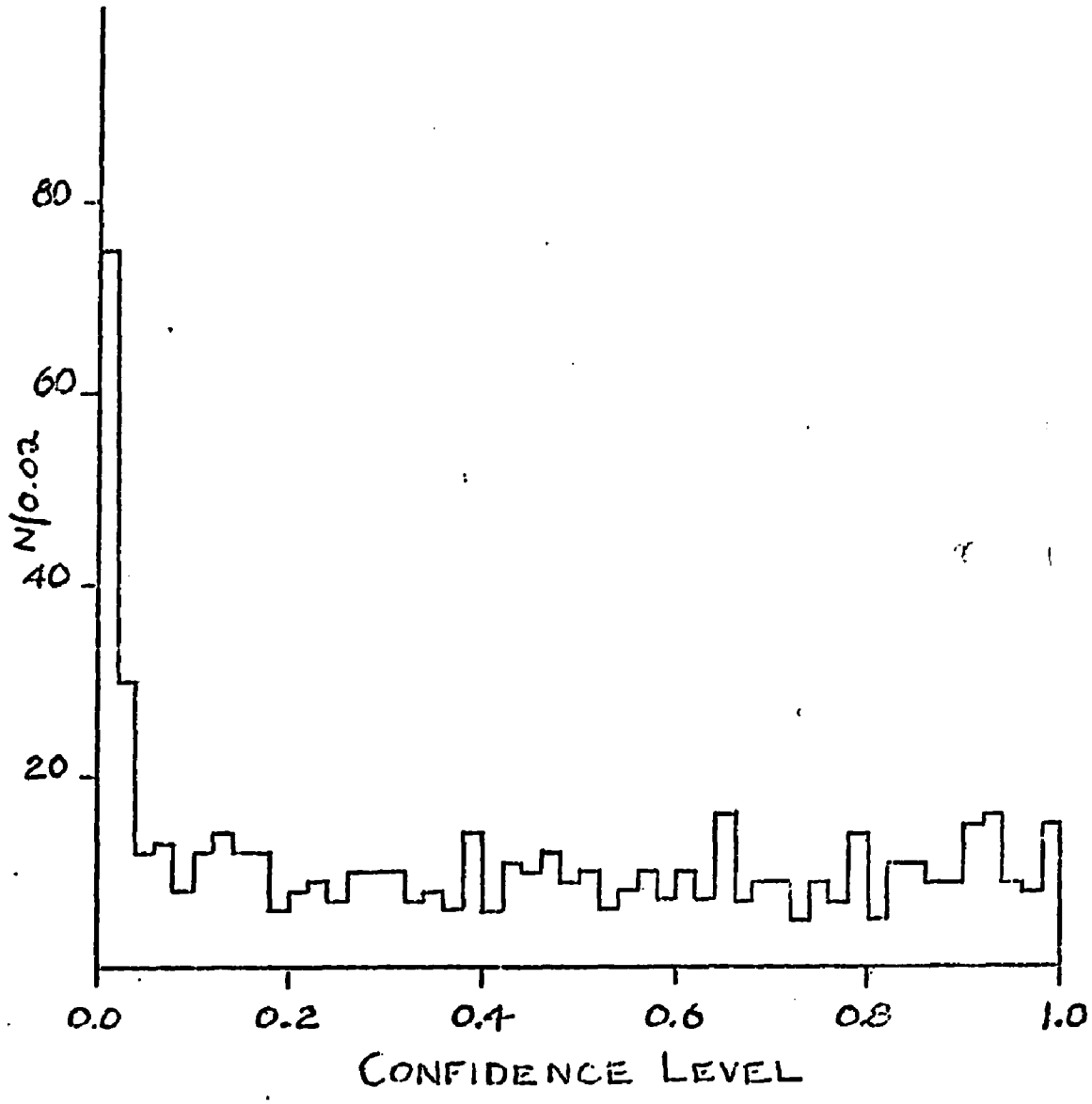


Figure 3.1-1. Confidence level distribution for the 575 $\pi^-\pi^+K^-K^+$ events.

3.2 Cross Section for $\pi^-\pi^+K^-K^+$

The cross section is calculated from the ratio of $2\pi2K$ events to the total number of events in the fiducial volume:

$$\sigma(2\pi2K) = \sigma(4 \text{ prong}) \cdot N/N_4$$

where,

N = number of $2\pi2K$ events,

N_4= number of 4-prongs.

Table 3.2-1 gives the results. Figure 3.2-1 presents the points that have been measured thus far as a function of $\bar{p}$ momentum. The data is suggestive of a ~100μb rise in the cross section centered at ~1.75 GeV/c.

3.3 Mass Distributions

As was the case in the earlier experiment at 1.2 GeV/c, the $2\pi2K$ channel in our energy range is dominated by $K^*(890)$ production; the φ and ρ mesons are also observed. Figures 3.3-1 thru 3.3-7 give the invariant mass distributions for the 573 $2\pi2K$ events. The following mass projections are presented:

(3.3-1) $M(\pi^{\pm}K^{\pm})$,

(3.3-2) $M(\pi^-\pi^+)$,

(3.3-3) $M(\pi^{\pm}K^{\mp})$,

(3.3-4) $M(K^-K^+)$,

(3.3-5) $M(\pi^-\pi^+K^{\pm})$,

Table 3.2-1. The $\pi^-\pi^+K^-K^+$ cross section $\sigma(2\pi 2K)$ as a function of $\bar{p}$ momentum. N = number of $2\pi 2K$ events; N_4 = number of 4-prongs.

Momentum GeV/c	N	N_4	σ(4-prong) mb	$\sigma(2\pi 2K)$ μb
1.63	87	6345	29.8 ±0.8	410 ±45
1.77	120	7491	27.1 ±0.7	434 ±42
1.83	104	7031	27.4 ±0.8	405 ±42
1.88	95	7506	25.8 ±0.7	327 ±35
1.95	91	7401	25.5 ±0.7	314 ±34
2.20	76	6115	23.1 ±0.6	287 ±34

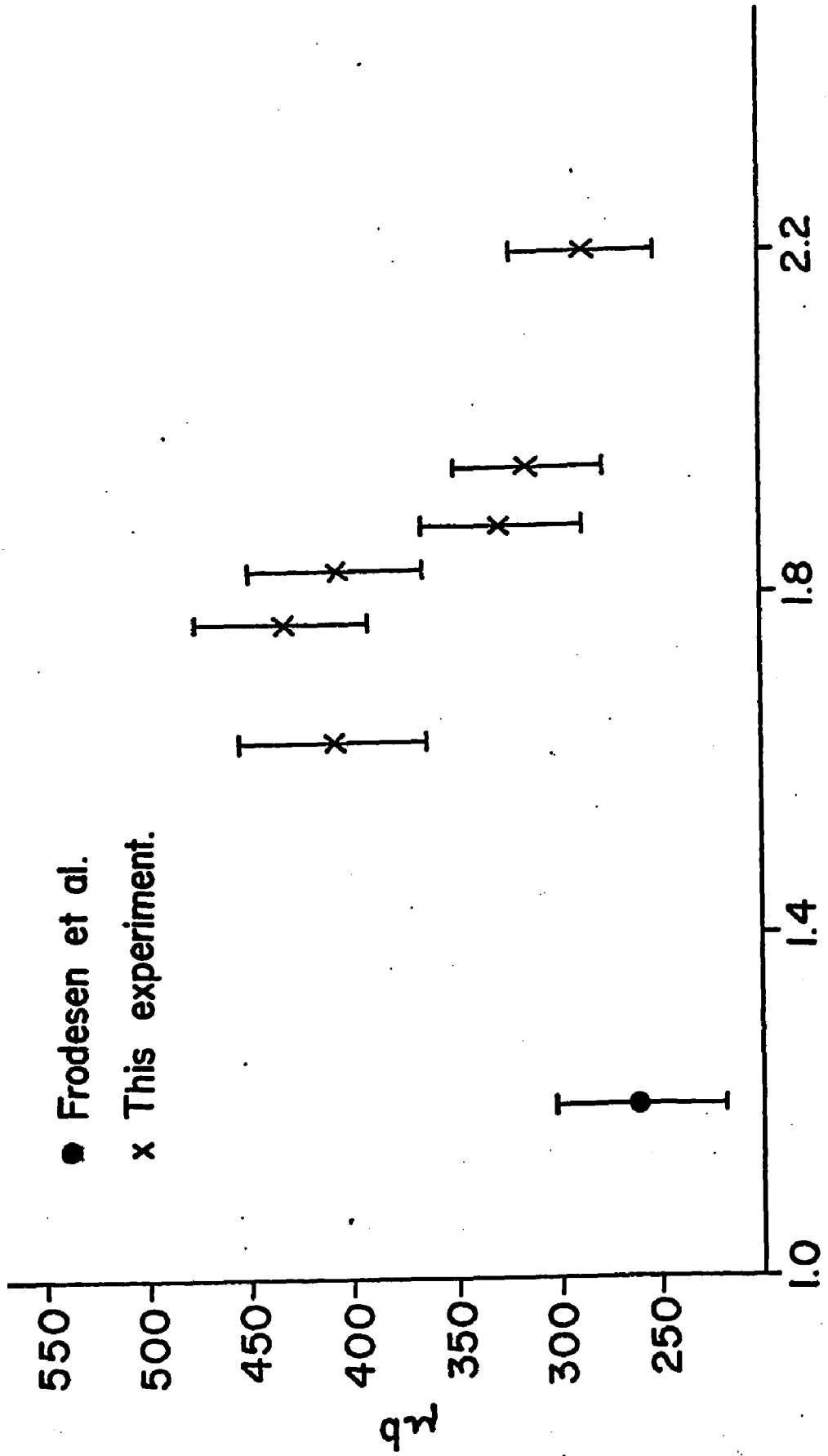


Figure 3.2-1. The $\pi^-\pi^+K^-K^+$ cross section as a function of $\bar{p}$ momentum.

(3.3-6) $M(\pi^{\pm}K^{-}K^{+})$,

(3.3-7) $M(\pi^{\pm}K^{\mp})$, with recoil mass in K^{*} region, 850 to 930 MeV.

The points in the figures are from a Monte Carlo simulation to be discussed in section 3.4.

Comparing the doubly charged and neutral mass distributions, we see strong production of $K^{*}(890)$. The KK mass spectrum has a clear φ signal at ~1015 MeV. There is also possible production of the A_2 meson at 1300 MeV (see section 3.4). Additionally, we observe in the KK histogram a ~4σ(standard deviation) bump at 1420 MeV, which however contains only 15 events. A narrow peak has been seen at 1425 MeV in the $K^{-}K^{\circ}$ mass spectrum at 20.3 GeV/c in $\pi^{-}p \rightarrow K^{-}K^{\circ}_{S}p$ (K. Foley, et al., 1971). In the $\pi\pi$ mass histogram we see an indication of ρ production. Possible evidence for $K^{*}K^{*}$ production is indicated in Figure 3.3-7.

The $\pi\pi K$ spectrum has a 3.7σ peak at 1278 ±5 MeV with a FWHM of 25 ±10 MeV. These parameters were determined from a fit assuming a simple Breit-Wigner and phase space. The results of the fit are shown in Figure 3.3-8. The peak does not appear to have a simple Breit-Wigner shape. This effect has also been observed in other experiments (A. Firestone, 1970). A fit with two Breit-Wigners was not tried because of the meager statistics.

The $\pi\pi K$ mass interval 1240-1400 MeV is known as the Q region.# A peak in the spectrum has been seen, but its

#For a survey of the Q region see A. Firestone, Experimental Meson Spectroscopy, edited by C. Baltay and A. Rosenfeld, Columbia University Press, 229(1970).

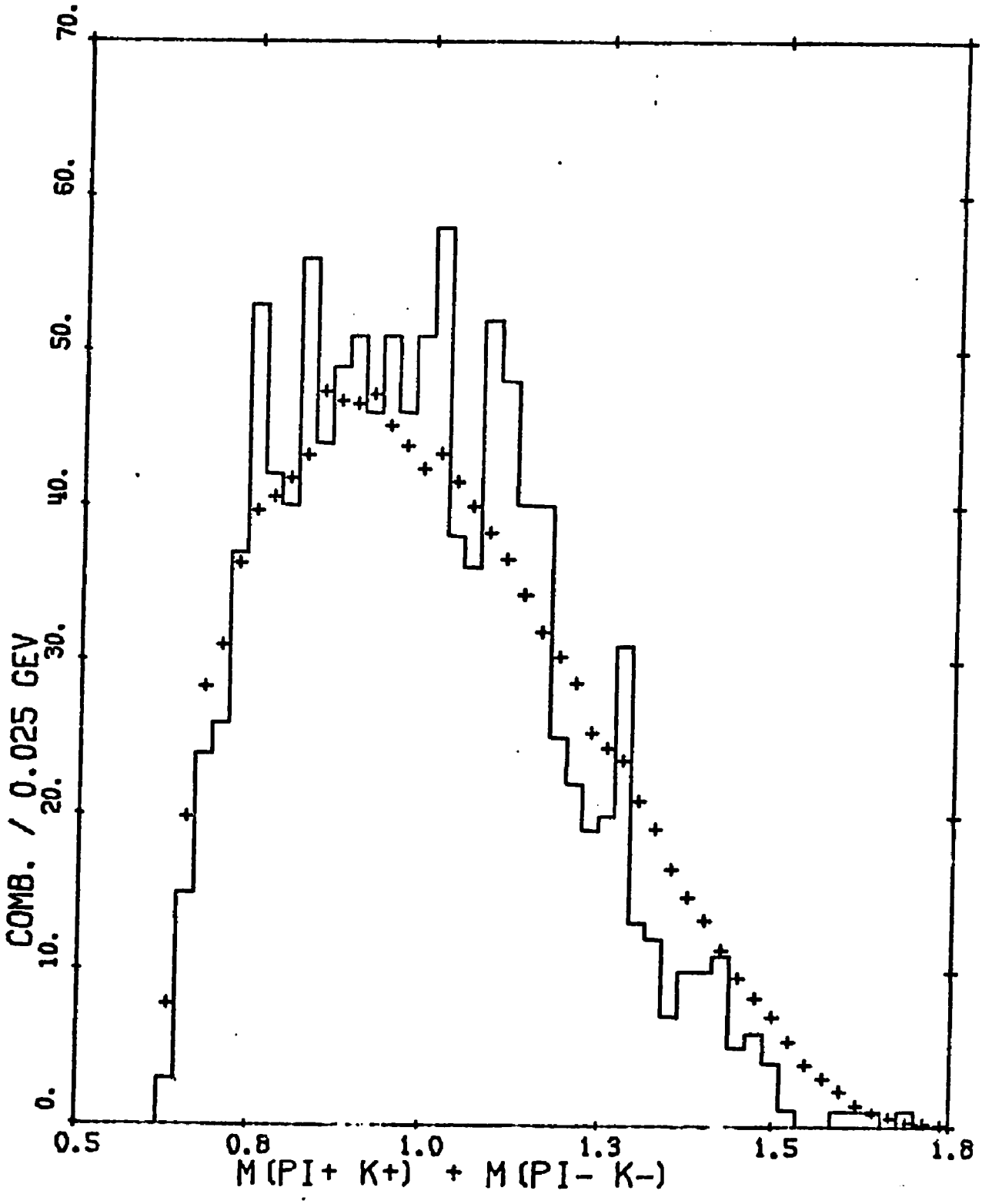


Figure 3.3-1. The $\pi^{\pm}K^{\pm}$ mass spectrum.
(2 combinations/event)

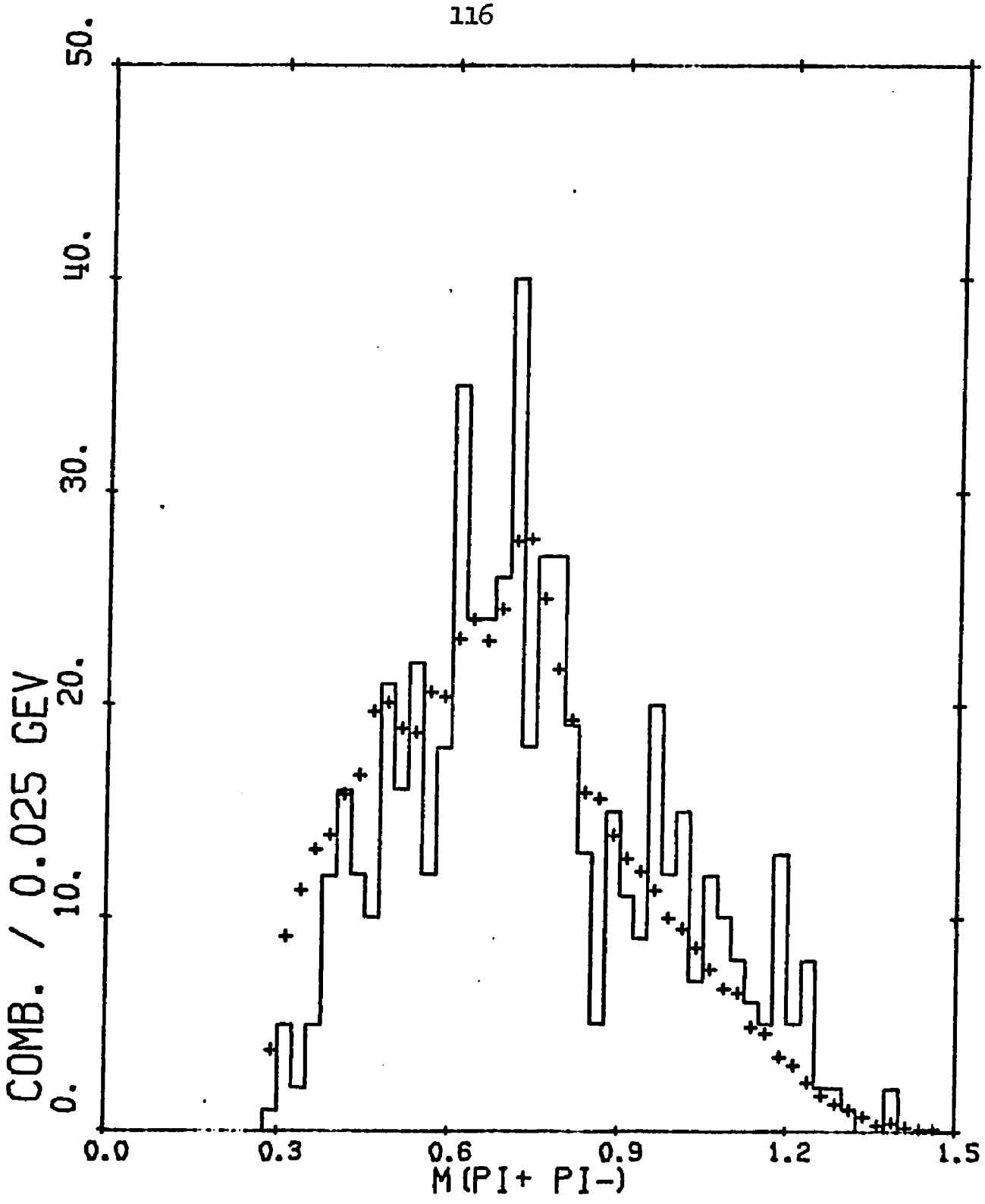


Figure 3.3-2. The $\pi^-\pi^+$ mass spectrum for the $2\pi 2K$ final state. (1 combination/event)

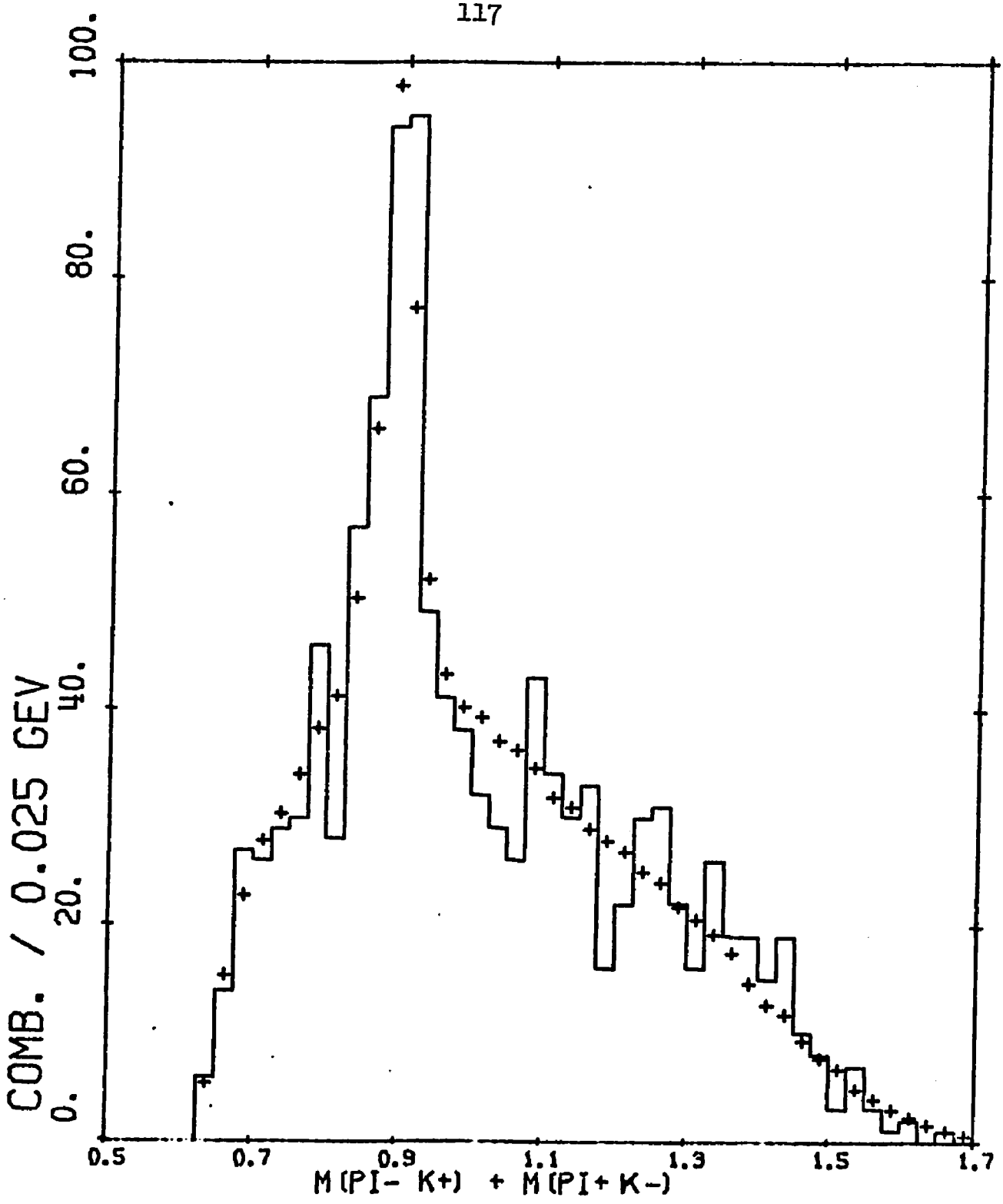


Figure 3.3-3. The $\pi^{\pm}K^{\mp}$ invariant mass distribution. (2 combinations/event)

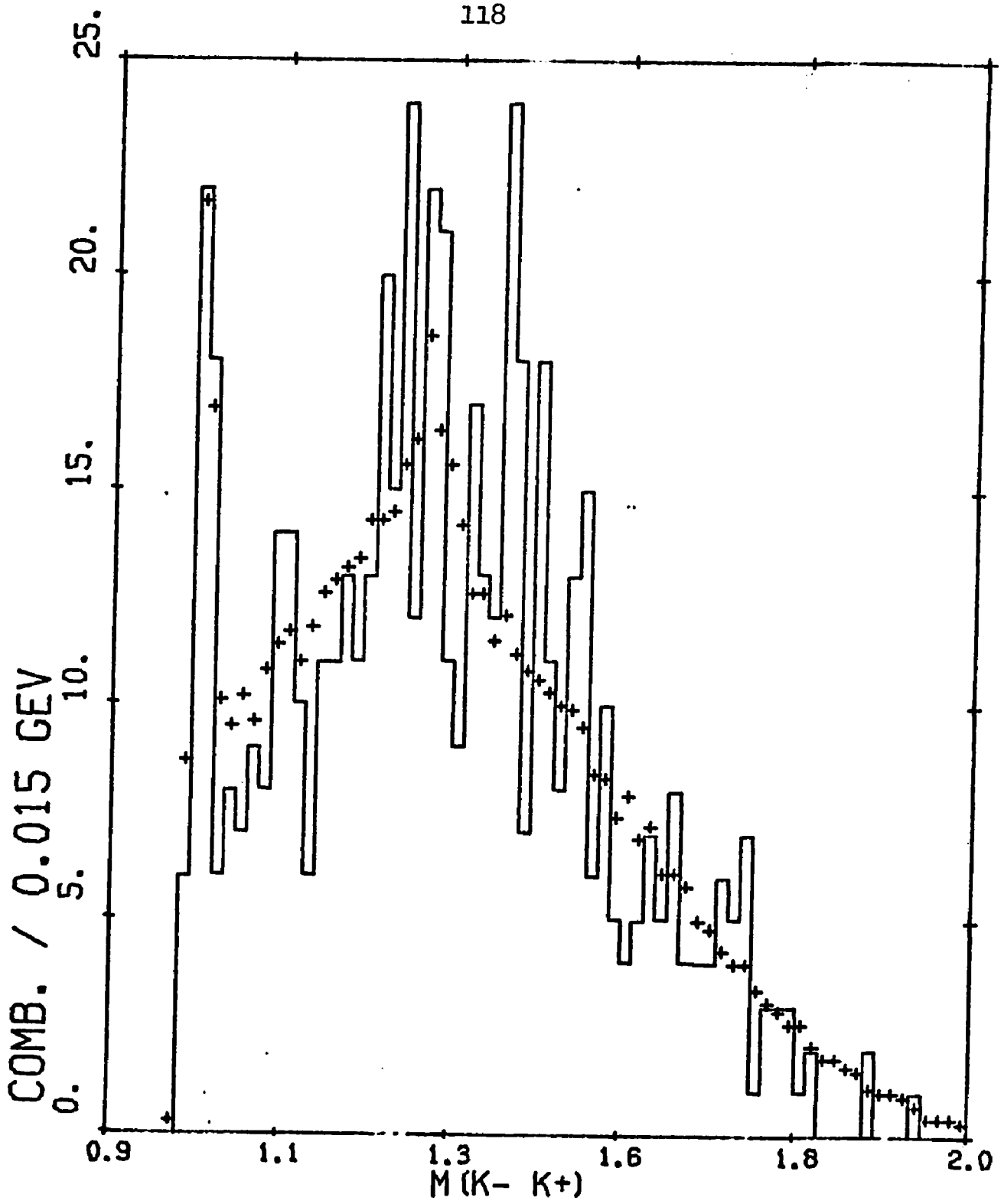


Figure 3.3-4. The K^-K^+ invariant mass distribution. (1 combination/event)

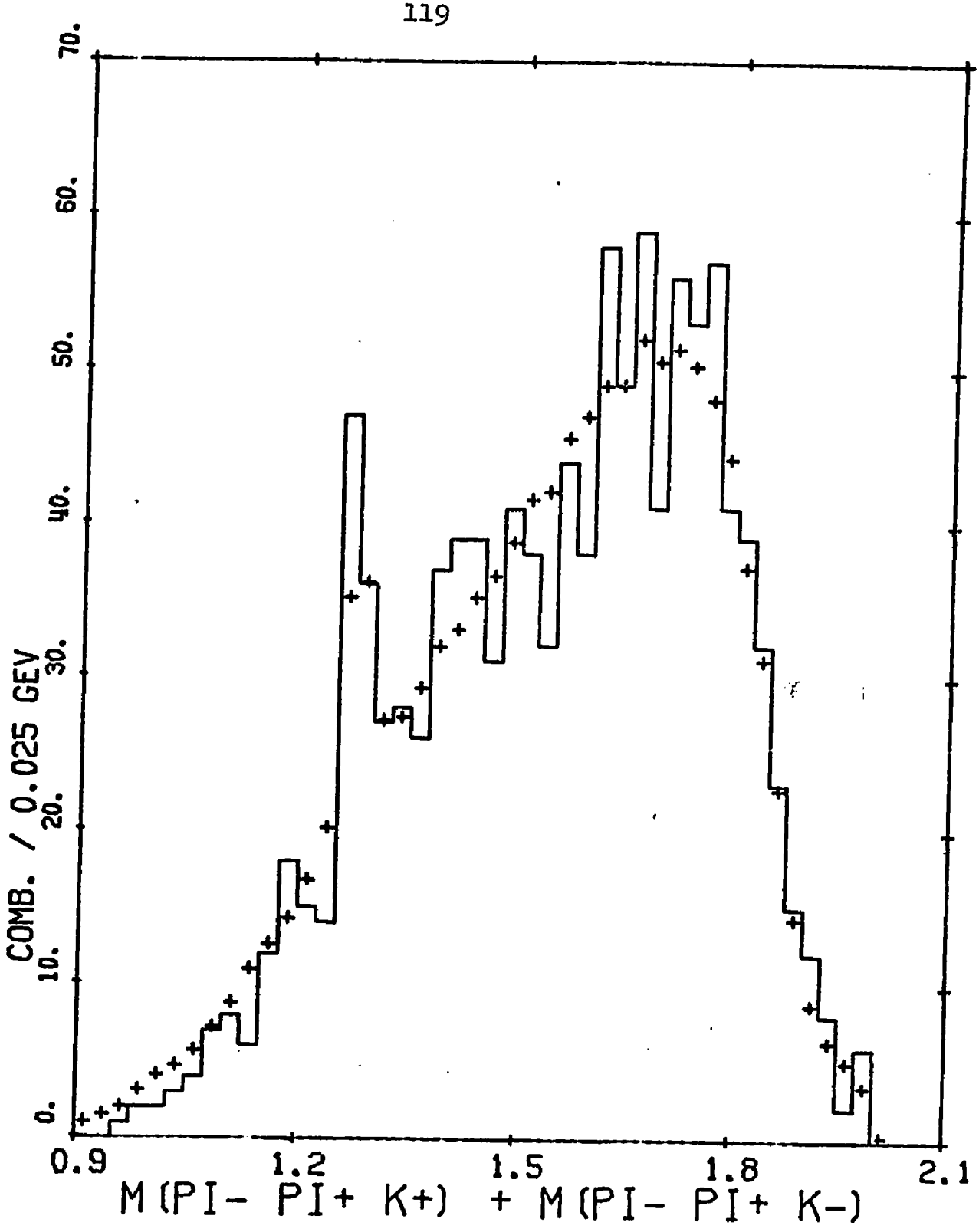


Figure 3.3-5. The $\pi^-\pi^+K^\pm$ mass distribution.
(2 combinations/event)

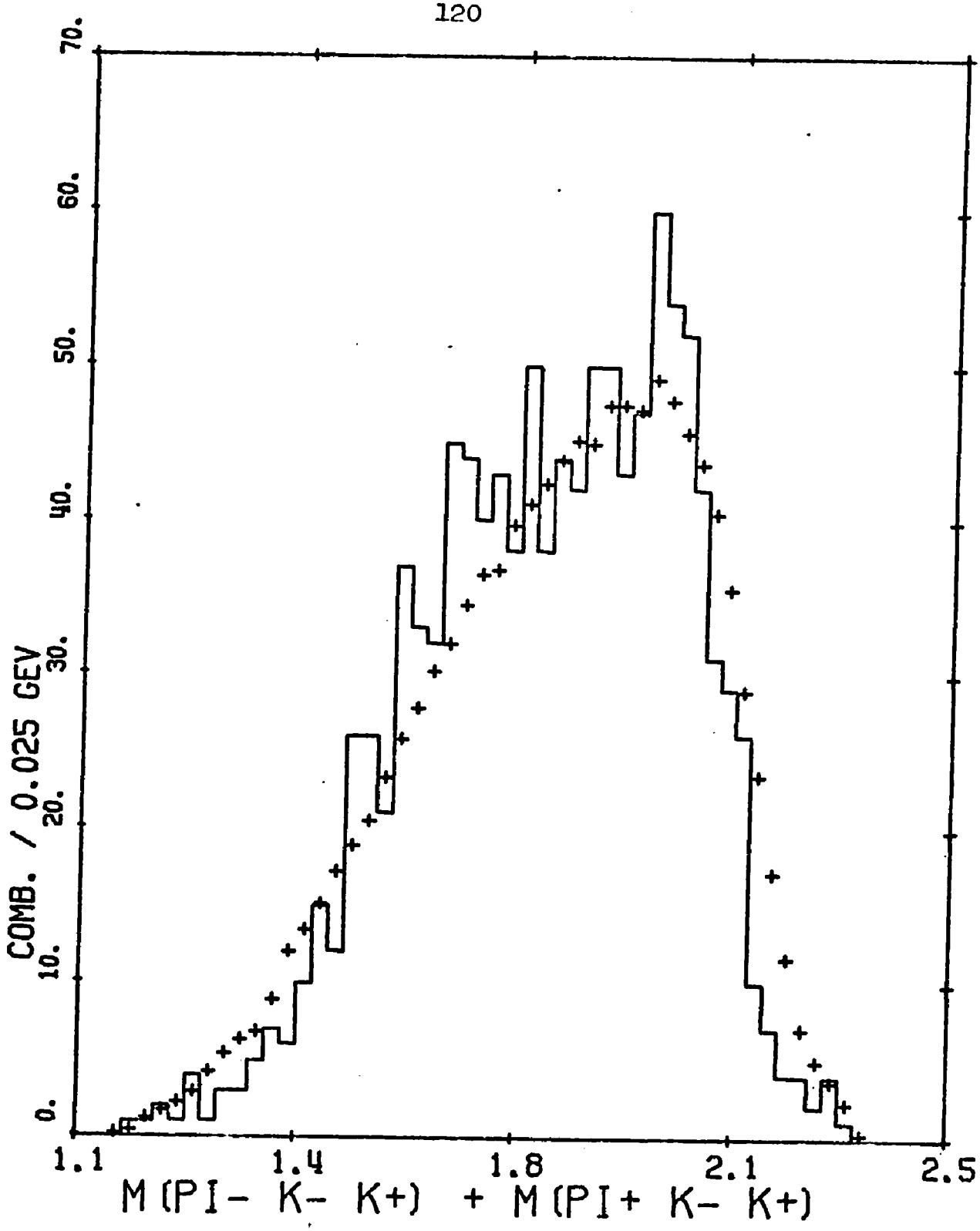


Figure 3.3-6. The $\pi^{\pm}K^{-}K^{+}$ invariant mass spectrum. (2 combinations/event)

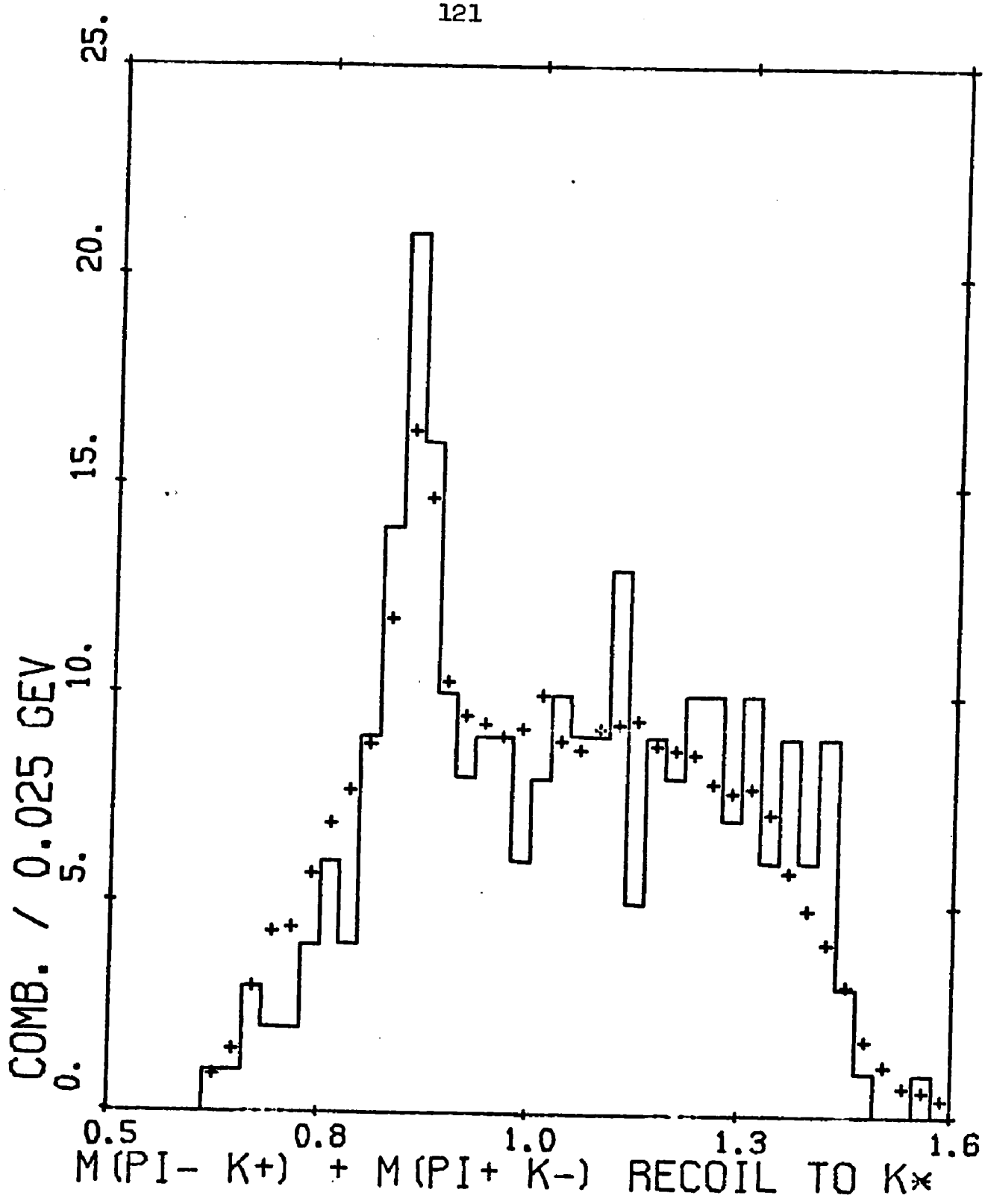


Figure 3.3-7. The $\pi^{\pm}K^{\pm}$ mass distribution when the recoil πK is in the K* region, 850 to 930 MeV.

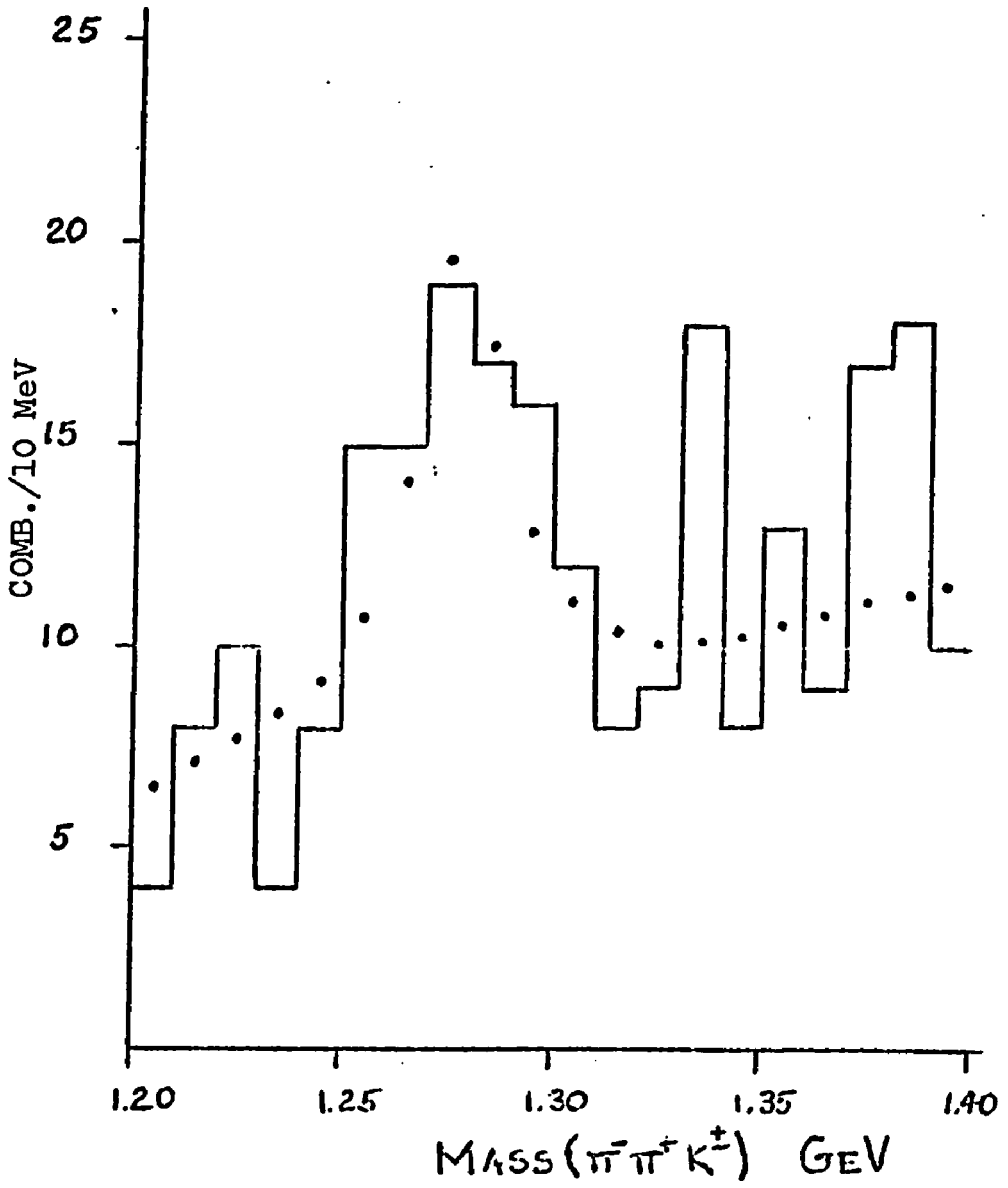


Figure 3.3-8. Part of the $\pi^-\pi^+K^\pm$ mass spectrum with Breit-Wigner fit--(see text).

interpretation is ambiguous, i.e. it may be a resonance or a threshold enhancement. The $K_A^*(1240)$ or "C" meson seems to be produced in $\bar{p}p$ capture at rest with a mass of 1242±9 MeV and a width of 120 MeV (Review of Particle Properties, 1971). Several other bumps in the $\pi\pi K$ mass distributions have been seen in K^+p interactions. A K^+p experiment at 2.0 GeV/c observed a signal at 1281 MeV with a FWHM of 51±22 MeV (J. Friedman, 1969).

Several additional plots were examined to see if the enhancement at 1278 MeV had some striking characteristic which might further indicate that it was a resonance rather than a statistical fluctuation. No essential difference was found. The CM angular distribution of the combinations within the enhancement did not differ significantly from the ones produced by the neighboring $\pi\pi K$ mass bands. Dalitz plots were made for the $\pi\pi K$ system using the same cuts. These plots had the same basic structure. Histograms were made of the ρK and $K^*\pi$ mass spectra to see if the enhancement was going through a particular quasi two-body state. The signal was found in both plots with about the same strength. Further, we would expect to see this enhancement in the $\pi\pi K$ mass of other final states, e.g. $K_1K_1\pi^-\pi^+$, $K^\circ K^+\pi^-\pi^+\pi^\circ$. Such plots were examined and no clear indication of a bump was found (H. Ring, 1970).

3.4 Sub-Channel Percentages

As was the case with the 4π events, the method of maximum likelihood was used to determine the percentages of resonance production. From a study of the various mass spectra the following channels were included in the fit:

(1) $K^*K\pi$,
(2) $\varphi\pi\pi$,
(3) ρKK,
(4) $A_2\pi\pi$,
(5) QK,
(6) K^*K^*,
(7) $\pi\pi KK$.

In channel (5) the symbol Q is to be understood simply as convenient notation for the enhancement at 1278 MeV.

Preliminary fits to the $\pi^{\mp}K^{\pm}$ mass spectrum gave a K^* mass of 891.8 MeV with an error of 3.4 MeV and a width of 50.8±5.7 MeV. These values were varied by as much as 8 MeV in the SHERLOCK fits to see how sensitive the results were to the exact value used. In all cases the percentages were consistent within the errors. The fits were also found to be insensitive to the masses and widths used for the other resonances. Monte Carlo generated mass distributions were compared to the experimental ones. The masses and widths which produced the lowest χ^2 were as follows:

Resonance	Mass MeV	Width MeV
K^*	891	45
φ	1014	20
A_2	1305	90
ρ	739	142
Q	1274	20

The results of using these values are presented in Table 3.4-1.

In order to examine these results in greater detail, maximum likelihood fits to the entire data sample were made assuming phase space plus resonance production according to the following hypotheses:

(a) $K^*K\pi$,

(b) $K^*K\pi + \varphi\pi\pi$,

(c) $K^*K\pi + \varphi\pi\pi + \rho KK$,

(d) $K^*K\pi + \varphi\pi\pi + \rho KK + A_2\pi\pi$,

(e) $K^*K\pi + \varphi\pi\pi + \rho KK + A_2\pi\pi + QK$,

(f) $K^*K\pi + \varphi\pi\pi + \rho KK + A_2\pi\pi + QK + K^*K^*$.

The mass and width parameters were left unchanged from the initial values. The results of fits (a) thru (f) are presented in Table 3.4-2. They are encouraging; we see the percentage of each resonance is quite stable. This gives

Table 3.4-1. Results of maximum likelihood fitting in percent of $\pi^-\pi^+K^-K^+$ cross section for various momentum sets.

Channel	Beam momentum (GeV/c) and number of events in each set. 1.63 1.77 (207)	1.83 1.88 (199)	1.95 2.20 (167)	1.77, 1.88 1.83, 1.95 (410)	All $2\pi 2K$ (573 events)
$K^*K\pi$	26±11	34±12	25±11	29±8	28±7
$\varphi\pi\pi$	$^{+4}_{6-3}$	$^{+4}_{6-3}$	$^{+5}_{9-3}$	$^{+3}_{6-2}$	7±2
ρKK	22±10	11±11	11±11	15±7	16±6
$A_2\pi\pi$	14±8	6±9	2±9	7±6	8±5
QK	1±5	7±5	9±6	8±4	6±3
K^*K^*	4±5	3±5	4±5	3±3	$^{+3}_{4-2}$
$\pi\pi KK$	27	33	40	32	31

Table 3.4-2. Results of maximum likelihood fits to all the 573 $2\pi 2K$ events in percent of the $2\pi 2K$ cross section using hypotheses (a) thru (f)--(see text).

Channel	Fit					
	(a)	(b)	(c)	(d)	(e)	(f)
$K^*K\pi$	33±6	35±6	35±6	35±6	33±6	28±7
$\varphi\pi\pi$	-	6±2	6±2	7±2	7±2	7±2
ρKK	-	-	19±6	18±6	16±6	16±6
$A_2\pi\pi$	-	-	-	8±5	8±5	8±5
QK	-	-	-	-	6±3	6±3
K^*K^*	-	-	-	-	-	4±3
$\pi\pi KK$	67	59	40	32	30	31

us confidence the percentages do indeed reflect a reasonable description of the resonance production.

We note that the $K^*K\pi$ state is clearly the dominant channel for resonance production. It accounts for 28^{+8}_{-6} percent of the $2\pi 2K$ events. The ρKK state is next in importance, accounting for 16 ± 6 percent. The third significant resonance channel is φKK. Overall, it contributes 7 ± 2 percent to the cross section. The fits prefer to have nonzero values for the remaining three resonant states (K^*K^*, $A_2\pi\pi$, and QK). However, it is difficult to conclude these channels are established due to the large errors resulting from our relatively small sample of $2\pi 2K$ events. We find no significant dependence on beam momentum within errors, except for a general decrease in resonance production with a increase in energy.

The mass distributions predicted by these fits were generated using Monte Carlo techniques. Seven spectra were chosen for comparison with the data (Figures 3.3-1 thru 3.3-7). Table 3.4-3 gives the χ^2 values for these simulations, as well as values for 100 percent phase space production. The results are not as good as we would like. For a total of 287 bins χ^2 ranges from 520 for one free parameter down to 395 for six parameters. This indicates that our description of the reaction is rather crude and incomplete. It appears that more theoretical work must be done in order to make a significant improvement. Predictions by multi-Regge models for $\bar{p}p$ annihilations (A. Frodesen, 1970) tend to over empha-

Table 3.4-3. χ^2 values from Monte Carlo generated distributions for fits (a) thru (f)--(see text). Histograms 1 thru 7 correspond to Figures 3.3-1 thru 3.3-7, respectively.

Fit	χ^2 for Histograms							
	(1)	(2)	(3)	(4)	(5)	(6)	(7)	Total
Phase Space	62	132	176	106	75	74	70	695
(a)	66	127	47	108	68	68	36	520
(b)	67	108	44	89	65	68	35	476
(c)	69	95	43	82	60	66	35	450
(d)	70	94	43	70	60	60	34	431
(e)	69	99	45	69	31	64	35	412
(f)	70	97	45	68	32	64	19	395
Bins:	41	38	39	55	40	42	32	287

size the resonances; they do not agree well with experiment.

From inspection of the experimental distribution, the $K^*K\pi$ and $\varphi\pi\pi$ states are considered to be well established. The decrease in χ^2 from 476 to 450 between fits (b) and (c) with the addition of one new parameter leads us to conclude the ρKK channel to be also established. The evidence for the remainning channels is not as compelling, but it is not insignificant. For instance, the addition of the K^*K^* channel reduces the χ^2 of histogram 3.3-7 from 35 to 19. The results of the distributions generated for fit (f) are shown in Figures 3.3-1 thru 3.3-7.

As noted in section 3.3, the initial fit to the $\pi\pi K$ spectrum gave a 3.7σ effect for the Q. However, we see from Table 3.4-1 the Q is only a 2σ effect. This discrepancy appears to be due to the fact the maximum likelihood fit naturally takes account of the reflections produced by a resonance. By comparing fits (d) and (e) in Table 3.4-3, we see the addition of the Q has decreased χ^2 for the $\pi\pi K$ spectrum from 60 to 31, but at the same time it has increased χ^2 for several other mass spectra.

The Monte Carlo generated $\pi^{\pm}K^{\pm}$ distributions in Figure 3.3-1 systematically predicts more events than is experimentally observed in the high mass end of the spectrum. This distortion carries over to the $\pi\pi K$ spectrum at a reduced level. A similar systematic difference was observed in the $\pi^{\pm}\pi^{\pm}$ histogram in the $\pi^-\pi^-\pi^+\pi^+$ channel (section 2.4) and also in the $\pi^-\pi^-\pi^+\pi^+\pi^\circ$ channel (R. Green,

1972). Because the particles are not identical in the $\pi^-\pi^+K^-K^+$ reaction, the effect due to Bose statistics (G. Goldhaber, 1960) should not be present. This suggests that some other dynamic process is occurring. It presumably is producing the "charge inertia" effect seen also in this channel in Figure 3.5-3, shifting the spectrum of the doubly charged mass combinations away from the high mass end. This conclusion is further supported by the observation that the addition of the Goldhaber effect does not produce a good fit in either of the pion channels (section 2.4; R. Green, 1972). It is interesting to note the χ^2 value for the $\pi^\pm K^\pm$ histogram increases from 62 for 100 percent phase space to 70 for fit (f).

3.5 Angular Distributions

The $\cos\theta$ distribution of the $\pi^\pm$ particles in the center of momentum (CM) frame is given in Figure 3.5-1. As in the $\pi^-\pi^-\pi^+\pi^+$ channel we see a forward peak. However, a backward peak is not apparent. Figure 3.5-2 presents the $K^\pm$ $\cos\theta$ distribution in the CM. Here, we see that the spectrum does have both forward and backward peaks which resemble quite closely the distribution for the $\pi^-\pi^-\pi^+\pi^+$ events. Figures 3.5-3 and 4 give the $\cos\theta$ distributions of the charged and neutral πK combinations respectively. The neutral distribution appears quite symmetric, even though this is not required by charge conjugation invariance. We looked at the $\cos\theta$ distribution in the K^* region (850-

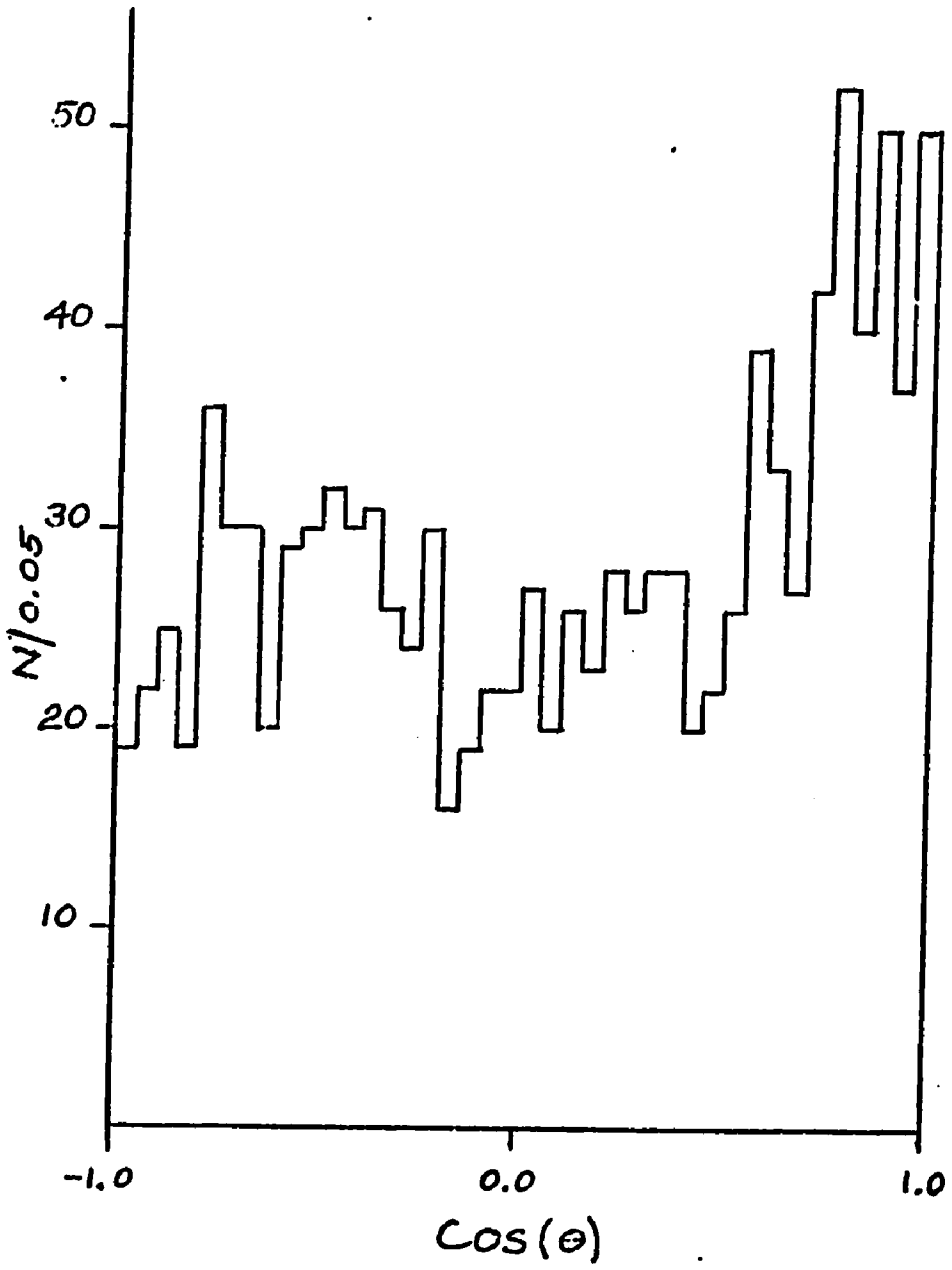


Figure 3.5-1. Cos(θ) distribution of $\pi^{\pm}$ from $2\pi^{\mp}2K$ final state in CM frame. The angle of the $\pi^{+}(\pi^{-})$ is measured relative to the p($\bar{p}$).

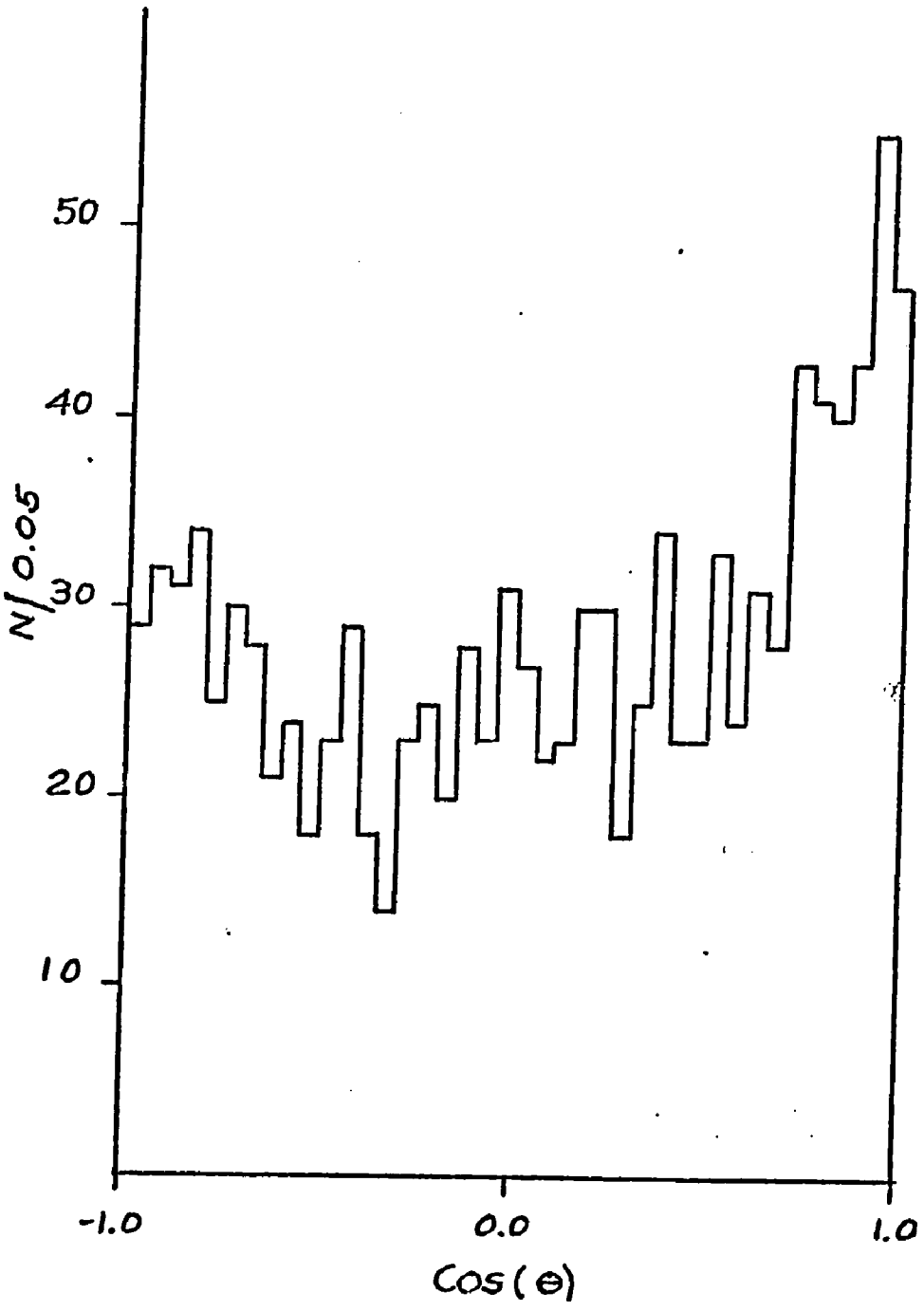


Figure 3.5-2. $\mathrm{Cos}(\theta)$ distribution of $K^{\pm}$ from $2\pi 2K$ final state in CM frame. The angle of the $K^{+}(K^{-})$ is measured relative to the $p(\bar{p})$.

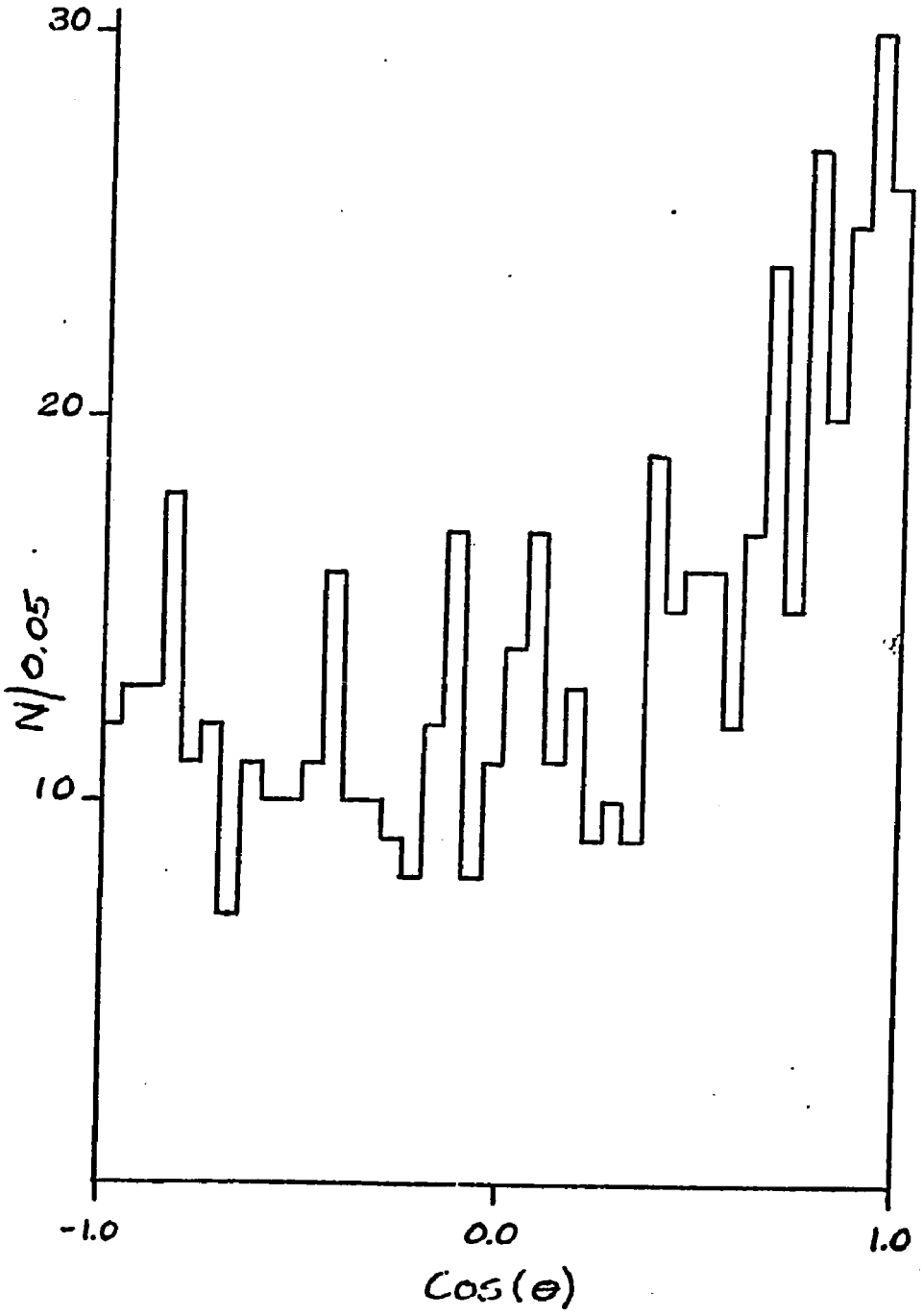


Figure 3.5-3. Cos(θ) distribution of π^-K^- combinations in the CM. The angle θ is measured with respect to the $\bar{p}$ direction.

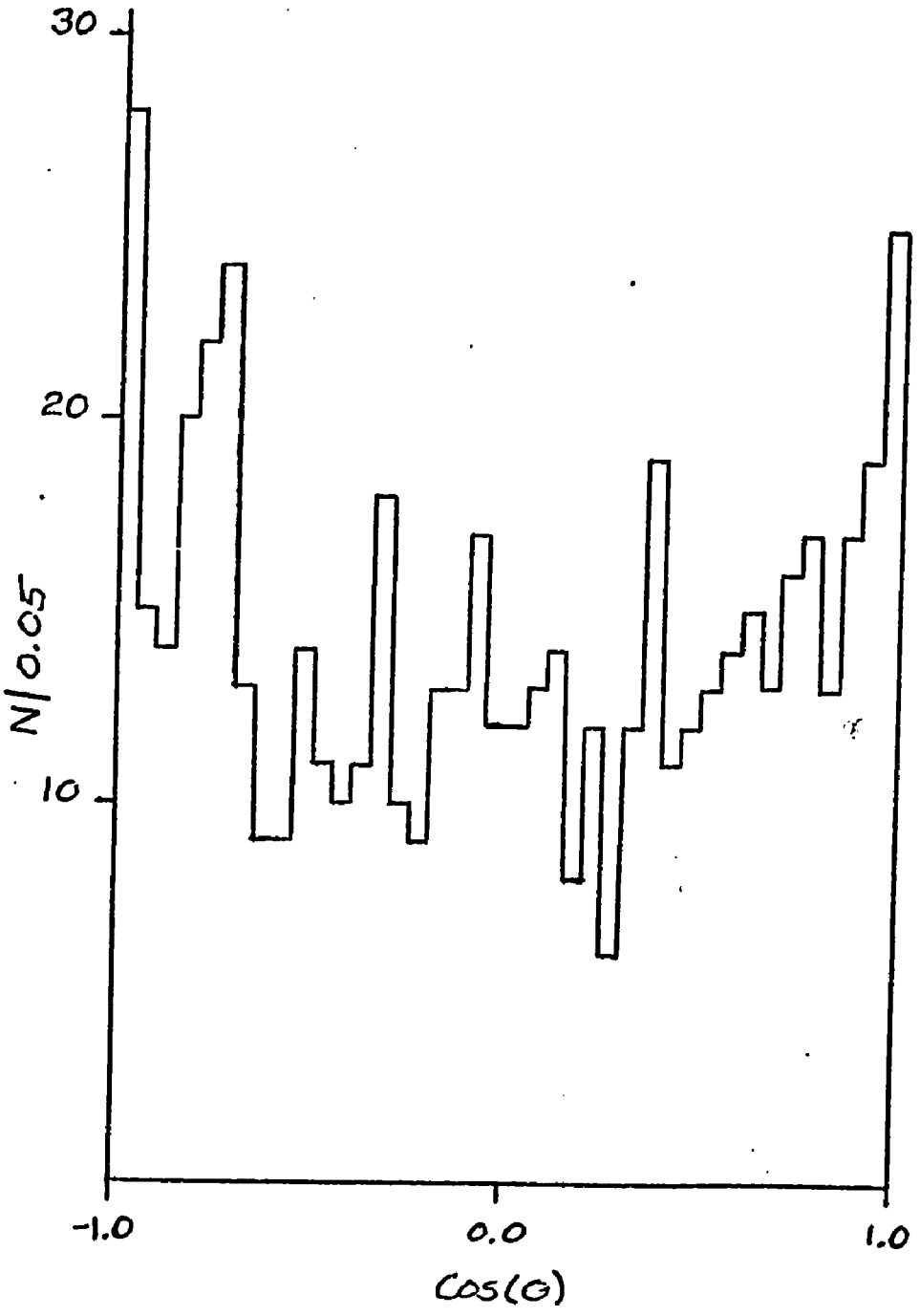


Figure 3.5-4. Cos(θ) distribution of the π^-K^+ combinations in the CM. The angle θ is measured with respect to the $\bar{p}$ direction.

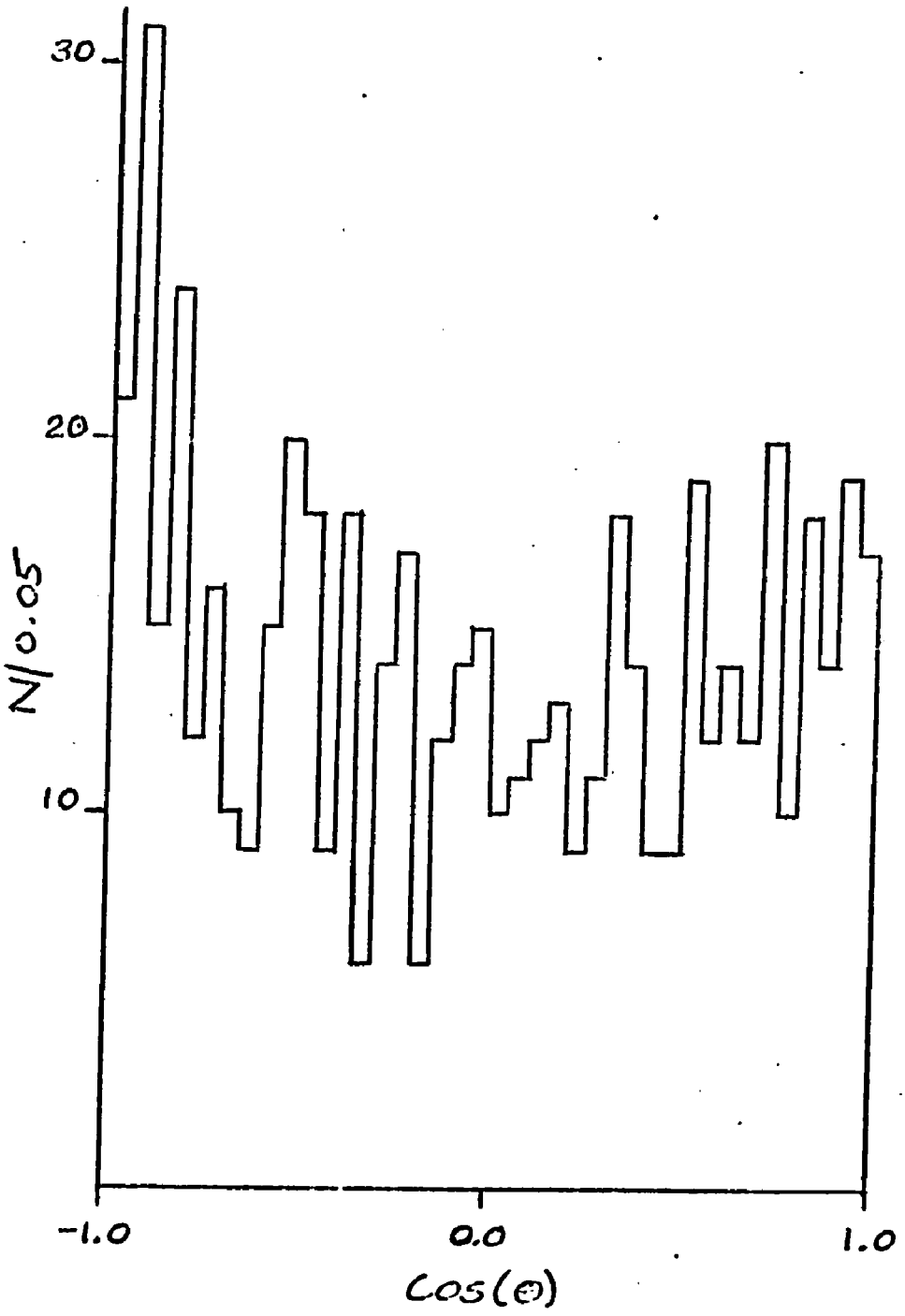


Figure 3.5-5. Cos(θ) distribution of the $\pi^-\pi^+$ combinations from the $2\pi 2K$ final state in the CM frame. The angle θ is measured with respect to the $\bar{p}$ direction.

930 MeV). It did not differ significantly from the entire spectrum. Figure 3.5-5 gives the cosθ distribution of the $\pi^-\pi^+$ combinations; charge conjugation invariance requires this distribution to be symmetric.

Chapter IV

THE REACTION $\bar{p}p \rightarrow K^-K^-K^+K^+$

4.1 Introduction

Little is known about the $\bar{p}p$ annihilation into four charged kaons. Experiments which have studied $\bar{p}p$ interactions have not reported on this channel to date. We have 42 events which fit the $K^-K^-K^+K^+$ final state with a confidence level $\geq 10^{-6}$ and have two or more constraints. All of these events were looked at in order to check for consistency with bubble density predictions. Only six were $K^-K^-K^+K^+$ events. The confidence level distribution for these events is shown in Figure 4.1-1. Within errors it is consistent with being flat.

4.2 Reaction Cross Section

The six events in this channel are evenly distributed over our momentum sets (2 at 2.20, 1 at 1.95, 1 at 1.83, and 2 at 1.63 GeV/c). Consequently, we combine them and calculate an average cross section. Using the same fiducial volume as in the $2\pi 2K$ reaction, we have a total of 41,889 events. The average four-prong cross section over our momentum range is 26.6±0.8 mb (see Table 1.5-1). From this data we calculate

$$\bar{\sigma}(\bar{p}p \rightarrow K^-K^-K^+K^+) = \frac{(6 \pm \sqrt{6})(26.6 \pm 0.8)}{41,889} \text{ mb}$$

$$= 3.8 \pm 0.8 \ \mu b$$

It is interesting to note that in order of magnitude terms

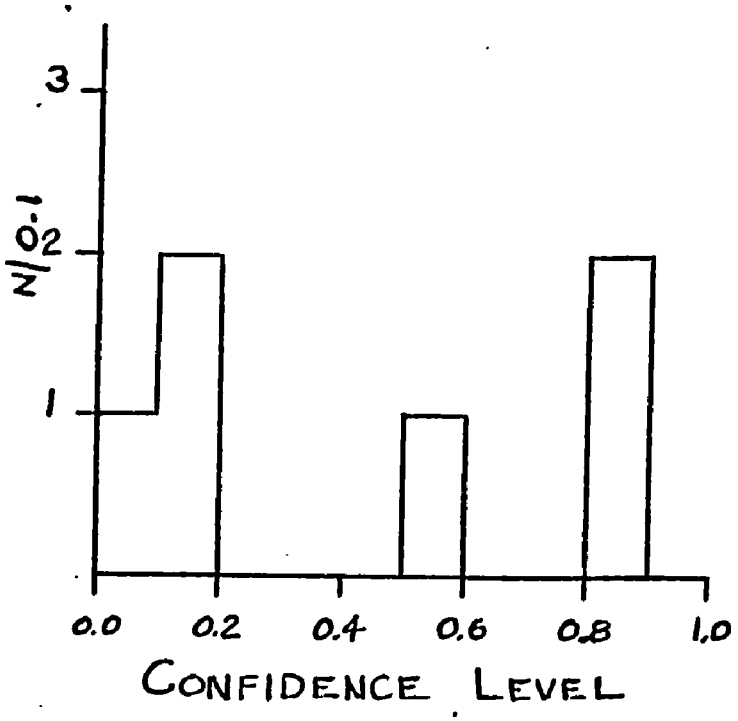


Figure 4.1-1. Confidence level distribution for $K^-K^-K^+K^+$ events.

$\bar{\sigma}(4K)$ is about 0.002 of our $\sigma(4\pi)$ while $\sigma(2\pi 2K)$ is roughly 0.2 of $\sigma(4\pi)$.

4.3 Mass distributions

Figure 4.3-1 shows the $K^{\pm}K^{\pm}$ mass distribution. As expected for the doubly charged combinations, there is not a statistically significant indication of any resonances. The $K^{+}K^{-}$ mass spectrum in Figure 4.3-2 is much more interesting. There is a strong φ signal, i.e. $K^{-}K^{+}$ mass combinations with a mass between 1015 and 1023 MeV. Only one of the six events does not have a φ meson associated with it; one event has a $\varphi\varphi$ pair. This gives a $\sigma(\varphi\varphi)$ of 0.6 μb. Two events are such that a K^{+} combines with each of the K^{-} particles to form combinations in the φ mass range. Using a phase space distribution, the probability for this is ~1%. This may be a new effect; hopefully, other experiments will report on this channel in the near future. The remaining two events have one φ associated with them. Thus we have four φKK enents giving $\sigma(\varphi KK)$ a value of 2.5 μb. The $K^{-}K^{+}K^{\pm}$ mass spectrum is shown in Figure 4.3-3. Within statistics, it is phase space.

4.4 Angular Distributions

The CM $\cos(\theta)$ distribution for the kaons is shown in Figure 4.4-1. The angle of a kaon is measured relative to the nucleon of like charge. We note there is little indication of the Forward-Backward peaking that was apparent in the 4π channel. Figure 4.4-2 gives the CM $\cos(\theta)$ distribution of the $K^{+}K^{+}$ combinations. Here the CM distribution is measured relative to p.

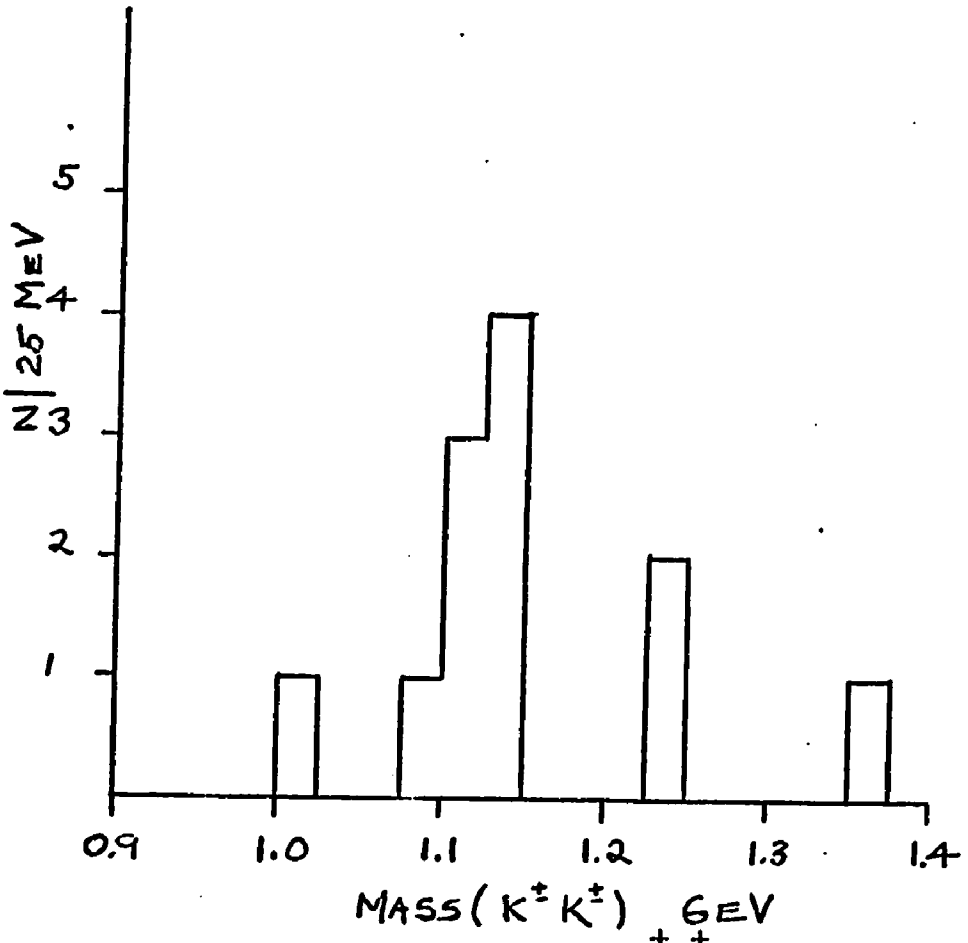


Figure 4.3-1. Mass spectrum for $K^{\pm}K^{\pm}$ combinations. (2 combinations/event)

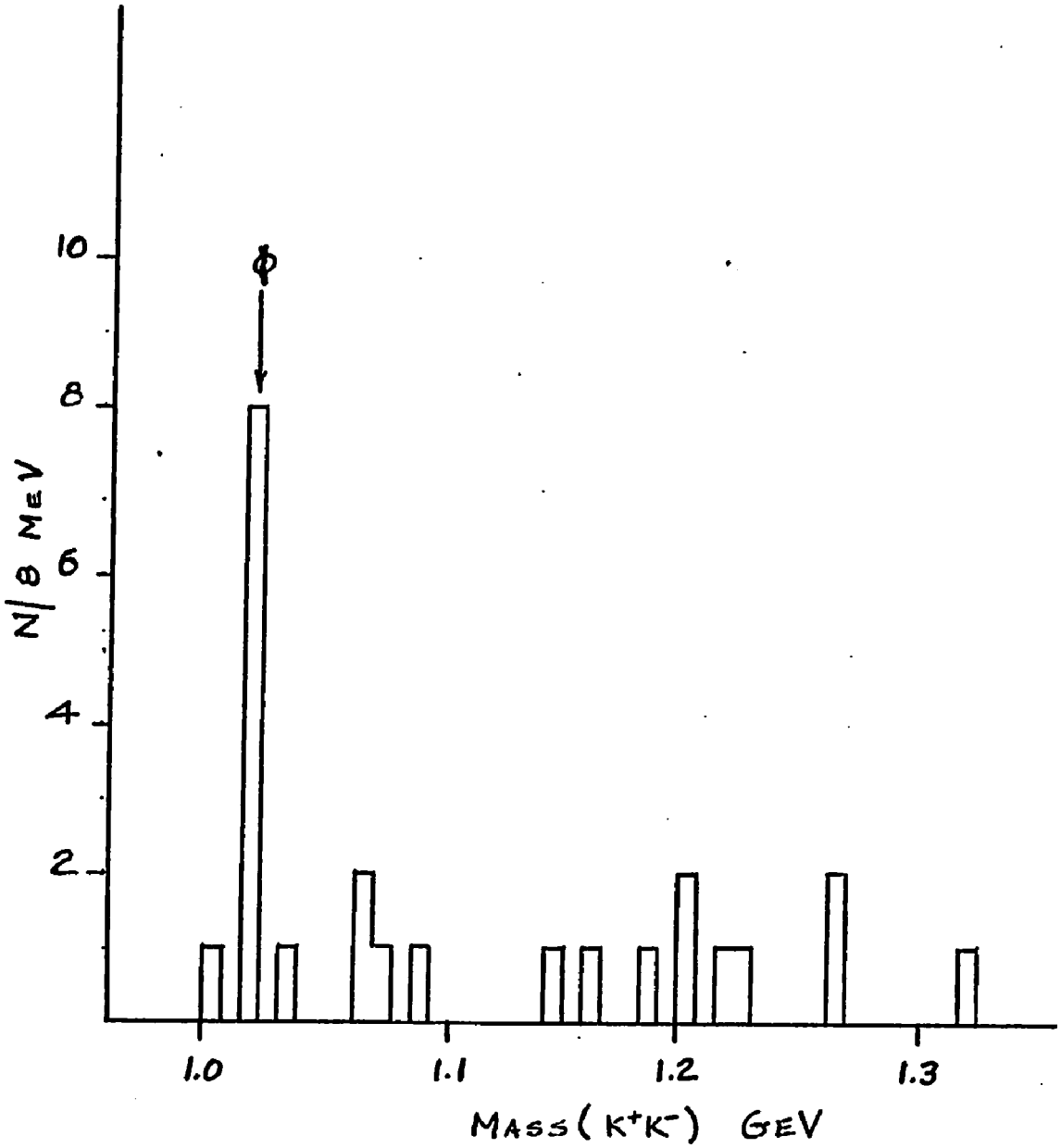


Figure 4.3-2. Mass spectrum for K^+K^- combinations. (4 combinations/event)

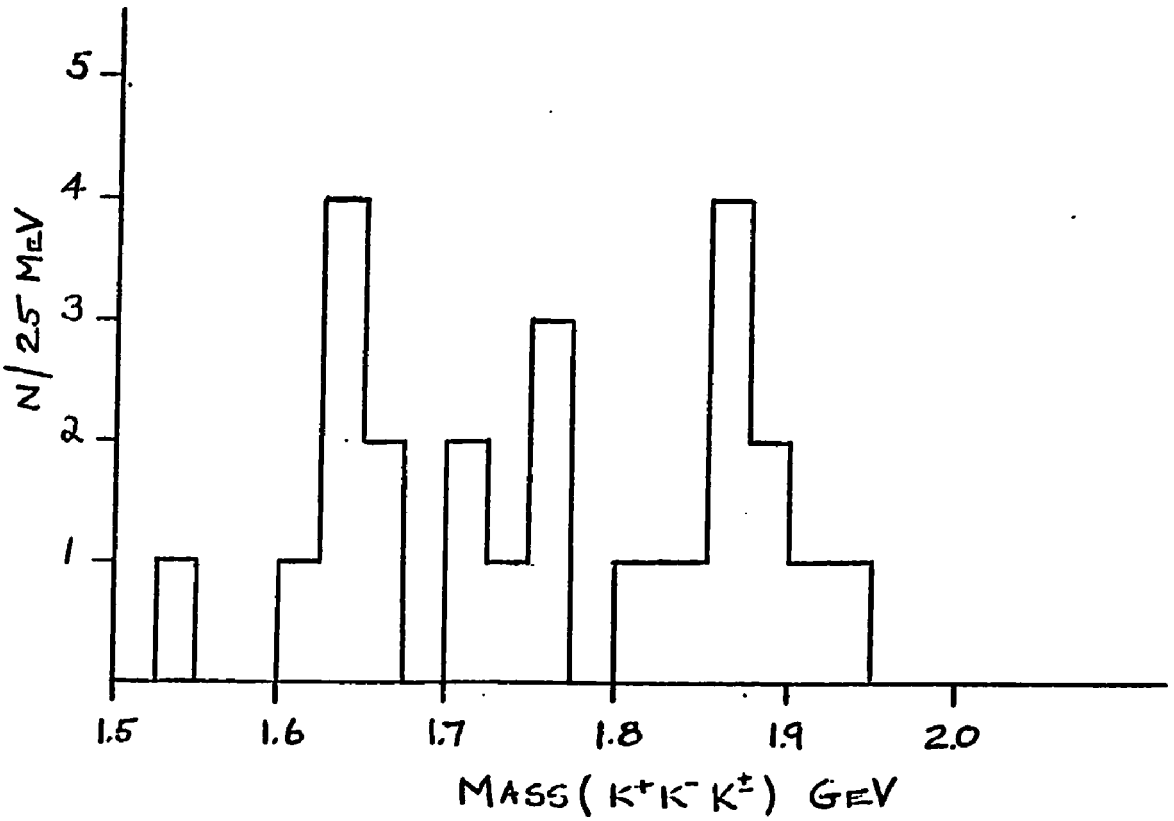


Figure 4.3-3. Mass spectrum for $K^+K^-K^{\pm}$ combinations. (4 combinations/event)

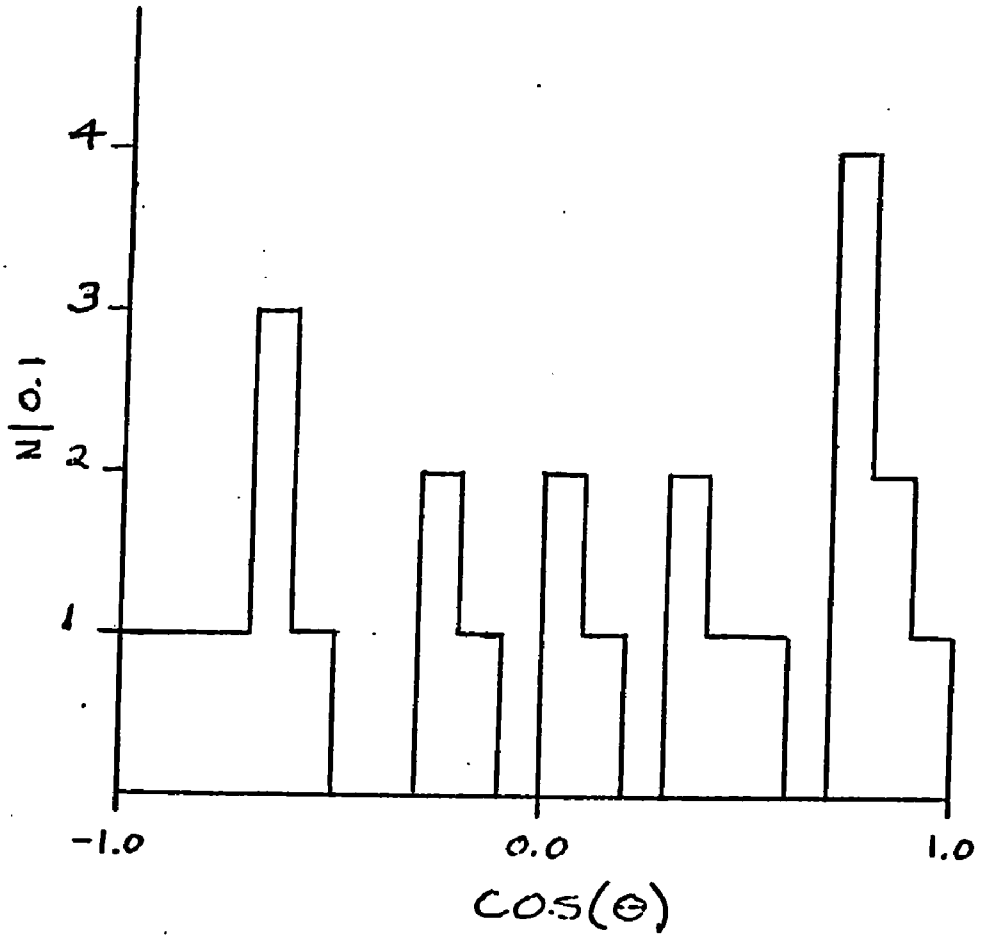


Figure 4.4-1. Angular distribution of the kaons in the CM frame. The angle of $K^+(K^-)$ is measured relative to $p(\bar{p})$. (4 combinations/event)

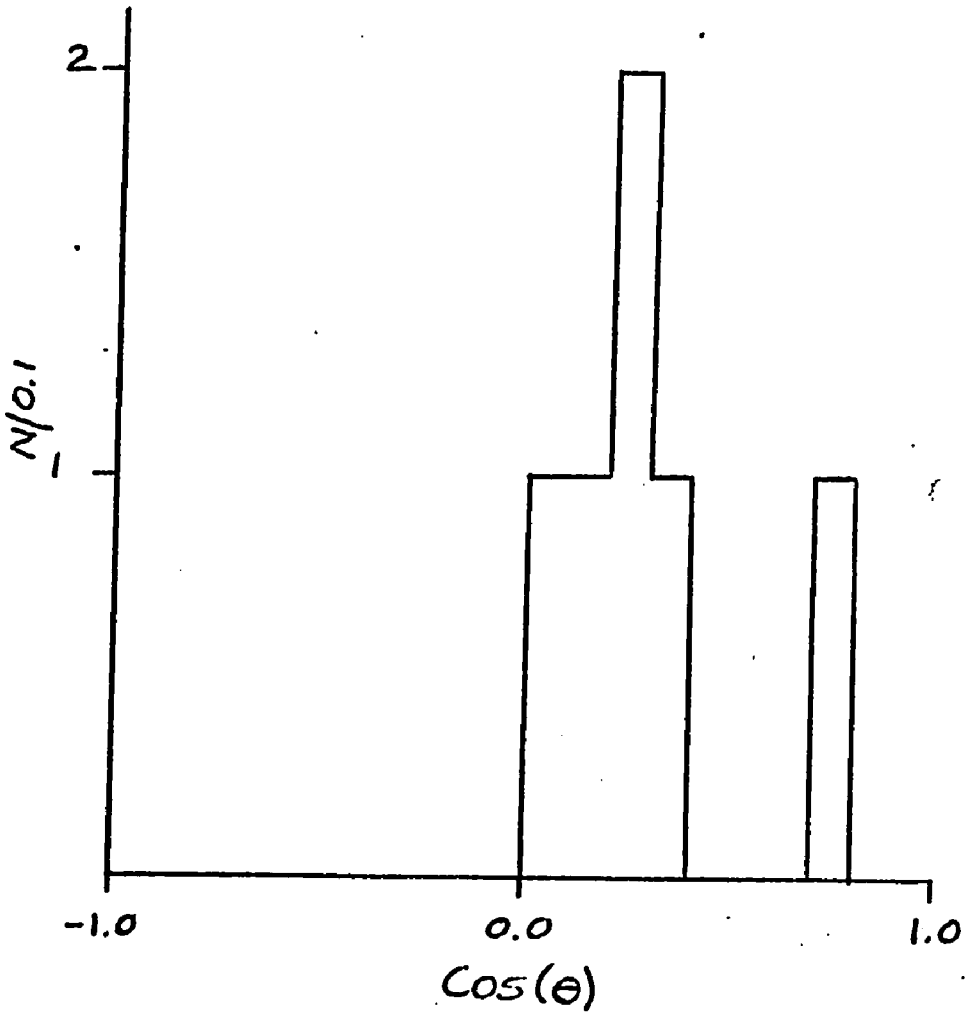


Figure 4.4-2. Angular distribution of K^+K^+ combination in CM frame. The angle of the system is measured with respect to p. (1 combination/event)

Chapter V

SUMMARY

The four prong cross section dropped from 29.5 to 23.1 mb as the $\bar{p}$ momentum ranged from 1.6 to 2.2 GeV/c. These values are compatible with the cross sections determined by earlier experiments. The four pion cross section was found to fall from 2.69 mb at 1.6 GeV/c $\bar{p}$ momentum to 1.28 mb at 2.2 GeV/c.

The percentages of resonance production in the 4π channel was examined using the maximum likelihood (ML) method. In our momentum range the 4π channel is dominated by $\rho\pi\pi$ and ρf production. The best fit also prefers a large amount of ff, but the percentage is very sensitive to the form of the parameterization; it is likely to be $f\pi\pi$. Monte Carlo simulations were used to evaluate the quality of the likelihood fits. The percentage of ρf decreases with $\bar{p}$ momentum, while the percentage of $\rho\pi\pi$ appears to increase. General agreement was observed when the ML fits are compared with earlier 4π experiments. The Goldhaber effect using Bose-Einstein Statistics was incorporated into the ML fits in an attempt to better simulate the $\pi^{\mp}\pi^{\mp}$ mass spectrum in particular and improve the overall χ^2 in general. The χ^2 values were not improved by this modification; however, the results do indicate the degree of sensitivity of the percentages to changes in the shape of the phase space background.

As with earlier studies, a forward-backward peaking,

("charge inertia") was seen in the cos(θ) distribution of the pions in the CM. The Forward-Backward and the Polar-Equatorial ratios increase with the pion momentum as expected from previous experiments. The spin density matrix elements were examined in both the Gottfried-Jackson and the Helicity Reference Frames. The distributions were fitted to a form that assumes (S,P) wave terms. The dependence on the mass and squared momentum transfer to the neutral dipion system was examined. No striking anomalies are found in the ρ or f regions. A fit assuming (S,P,D) wave terms was done in the f mass region. A study was made of ρ-ω interference in the $\pi^+\pi^-$ mass spectrum. Indications are seen for ρ-ω interference for $\bar{p}$ momentum 1.63 to 1.88 GeV/c consistent with being in the ρf channel.

A sample of $\pi^-\pi^+K^-K^+$ events was obtained by using bubble density information to select events consistent with the hypothesis. The cross section was determined for each momentum set. It is of the order of 350 μb; there is possible structure at $\sim$1.8 GeV/c. The errors are too large to be more definitive. Maximum likelihood fits were also done to this channel. The reaction is dominated by $K^*K\pi$, $\varphi\pi\pi$, and ρKK production. An enhancement is seen in the Q region of the $\pi\pi$K mass spectrum at 1278 MeV with a FWHM of 25 MeV. A distortion from phase space is seen in the doubly charged πK spectrum, similar to the doubly charged $\pi\pi$ spectrum from the 4π events. The Goldhaber effect should not be present, since the particles are not identical; this suggests

some other dynamic process is occuring. The CM $\cos(\theta)$ distributions were examined.

After bubble density selection, six events were found to be consistent with the $K^-K^-K^+K^+$ final state. The average cross section over the momentum range was found to be 3.8 μb. Mass spectra reveal that five of the six events have at least one φ meson produced; one of these is a $\varphi\varphi$ event.

List of References

Abramovich, M., H. Blumenfeld, F. Bruyant, V. Chaloupka, S. Chang, J. Diaz, F. Martin, L. Montanet, and J. Rubis, Nuclear Physics, Vol. B20, p. 209 (1970).

Abrams, R., R. Cool, G. Giacomelli, T. Kycia, B. Leontic, K. Li, and D. Michael, Physical Review Letters, Vol. 18, p. 1209 (1967).

Accensi, A., V. Alles-Borelli, B. French, Å. Frisk, J. Howie, W. Krischer, L. Michejda, W. Moorhead, B. Powell, P. Seyboth, P. Villemoes, Physics Letters, Vol. 20, p. 557 (1966).

Alles-Borelli, V., B. French, Å. Frisk, and L. Michejda, Nuovo Ciminto, Vol. 48A, p. 360 (1967).

Alvensleben, H., U. Becker, W. Bertram, M. Chen, K. Quinn, T. Knasel, R. Marshall, D. Quinn, M. Rohde, G. Sanders, H. Schubel, and S. Ting, International Symposium on Electron and Photon Interactions at High Energies, Liverpool, England, September 1969, edited by D. Braben (Daresbury Nuclear Physics Laboratory, Daresbury, England, 1970), Abstr. No. 163.

Allison, W., W. A. Cooper, T. Fields, and D. Rhines, Physical Review Letters, Vol. 24, p. 618 (1970).

Augustin, J., Physics Letters, Vol. 28B, p. 508 (1969).

Benson, G., Meson and Spectator Protons in $\pi^+ d \rightarrow \pi^+\pi^-\pi^\circ pp$ at 3.65 BeV/c, University Microfilms, Ann Arbor, Michigan (1966).

Bernstein, J. and G. Feinberg, Nuovo Cimento, Vol. 25, p. 1343 (1962).

Biggs, P., D. Kitching, and R. Rand, Physical Review Letters, Vol. 24, p. 1197 (1970).

Böckman, K., B. Nellen, E. Paul, B. Wagini, I. Borecka, J. Diaz, U. Heeren, U. Liebermeister, E. Lohrmann, E. Raubold, P. Söding, S. Wolff, J. Kidd, L. Mandelli, L. Mosca, V. Pelosi, S. Ratti, and L. Tallone, Nuovo Cimento, Vol. 42A, p. 954 (1966).

List of references(continued)

Borecka, I., G. Drews, W. Lenkeit, G. Comai, R. Santangelo, G. Comai, R. Santangelo, L. Bertanza, A. Bigi, R. Casali, P. Lariccia, R. Pazzi, R. Medves, and C. Petri, DESY 71/4 (1971).

Burns, R., P. Condon, J. Donahue, M. Mandelkem, and J. Schultz, Nuclear Physics, Vol. B27, p. 109, (1971).

Button, J., G. Kalbfleisch, G. Lynch, B. Maglic, A. Rosenfeld, and M. Stevenson, Physical Review, Vol. 126, p. 1858 (1962).

Chapman, J., F. Hess, J. Lys, C. T. Murphy, and J. Vander Velde, Physical Review Letters, Vol. 21, P. 1718 (1968).

Chapman, J., J. Davidson, R. Green, J. Lys, B. Roe, and J. Vander Velde, Nuclear Physics, Vol. B24, p. 445 (1970).

Chikovani, G., L. Dubel, M. Focacci, W. Kienzle, B. Levrot, B. Maglic, M. Martin, C. Nef, P. Sequinot, Physics Letters, Vol. 22, p. 233 (1966).

Clayton, J., P. Mason, H. Muirhead, D. Waldren, R. Rigopoulos, P. Tsilimigras, and A. Vayaki-Serafimidon, Nuclear Physics, Vol. B22, p. 85 (1970).

Lab. de Phys. Nucl. College de France, paper No. 241, Proceedings of Lund Int. Conf. on Elementary Particles, Lund, 1969.

Cooper, W., L. Hyman, W. Manner, B. Musgrave, L. Voyvodic, Physical Review Letters, Vol. 20, p. 1059 (1968).

Day, T., Transcribed Seminar on TVGP-SQUAW, Argonne National Laboratory (1967).

Donald, R., D. Edwards, R. Moore, E. Read, S. Reucroft, A. Frodesen, T. Jacobsen, S. Sire, O. Skjeggested, P. Saetre, H. Tøfte, A. Bettini, S. Limetani, L. Peruzzo, R. Santangels, and S. Sartori, Nuclear Physics, Vol. B6, p. 174 (1968).

Falconer, D., Large Angle Antiproton-Proton Elastic Scattering, University Microfilms, Ann Arbor, Michigan (1969).

List of References(continued)

Ferbel, T., A. Firestone, J. Sandweiss , H. Taft, M. Gailloud, T. Morris, W. Willis, A. Bachman, P. Baumel, and R. Lea, Physical Review, Vol. 143, p. 1096 (1966).

Ferbel, T., J. Johnson, H. Kraybill, J. Sandweiss, and H. Taft, Physical Review, Vol. 173, p. 1307 (1968).

Flatté, S., Physical Review, Vol. 1D, p. 1, (1970).

Firestone, A., The Q Region of $K\pi\pi$ Mass, Experimental Meson Spectroscopy, edited by C. Baltay and A. Rosenfeld, Columbia University Press, p. 229 (1970).

Foley, K., W. Love, S. Ozaki, E. Platner, A. Sanlys, E. Willen, and S. Lindenbaum, Physical Review Letters, Vol. 26, p. 413 (1971).

Friedman, J., R. Ross, Lawrence Radiation Laboratory Physics Notes P-102, (1964).

Friedman, J., Lawrence Radiation Laboratory Physics Notes P-156, (1966).

Friedman, J., Ph.D. Thesis, UCRL-18860, (1969).

Frodesen, A., O. Skeggestad, R. Moore, and S. Rencroft, Nuclear Physics, Vol. B10, p. 307 (1969).

Gatto, R., Nuovo Cimento, Vol. 28, p. 658 (1963).

Glashow, S., Physical Review Letters, Vol. 7, p. 469 (1961).

Goldhaber, G., W. Butler, D. Coyne, B. Hall, J. Mac Naughton, and G. Trilling, Physical Review Letters, Vol. 23, p. 1351 (1969).

Goldhaber, G., S. Goldhaber, W. Lee, A. Pais, Physical Review, Vol. 120, p. 300 (1960).

Gourdin, M., L. Stodolsky, and F. Renard, Physics Letters, Vol. 30B, p. 347 (1969).

Green, R., Resonance Production in $\bar{p}p \rightarrow \pi^+\pi^+\pi^-\pi^-\pi^\circ$ at 1.6 to 2.2 GeV/c, Ph.D. Thesis, University of Michigan (1972).

List of References(concluded)

Harte, J., and R. Sachs, Physical Review, Vol. 135B, p. 459 (1965).

James, F., M. Roos, CERN Computer Library D506, (1969).

Kalbfleisch, G., R. Strand, V. Vanderberg, Physics Letters, Vol. 29B, p. 259 (1969).

Kitagaki, T., K. Takahashi, S. Tanaka, T. Sato, A. Yamaguchi, K. Hasegawa, R. Suzawara, and K. Tamai, Physical Review Letters, Vol. 21, p. 175 (1968).

Lovell, L., Ph.D. Thesis, University of Michigan (1968).

Lys, J., J. Chapman, D. Falconer, C. T. Murphy, and J. Vander Velde, Physical Review Letters, Vol. 21, p. 1116 (1968).

Parker, D., Ph.D. Thesis, Michigan State University (1971).

Review of Particle Properties (particle Data Group), Reviews of Modern Physics, Vol. 43, Number 2, Supplement (1971).

Ring, H., Ph.D. Thesis, University of Michigan (1970).

Strand, D., private communication (1972).

Zemach, C., Physical Review, Vol. 133, p. 1201 (1964).

Zemach, C., Physical Review, Vol. 140, p. 97 (1965 a).

Zemach, C., Physical Review, Vol. 140, p. 109 (1965 b).